A TRANSLATIONAL APPROACH TO ASSESS THE RISK OF DIETARY SUBSTANCE-DRUG INTERACTIONS

Garrett Robert Ainslie

A dissertation submitted to the faculty at the University of North Carolina at Chapel Hill in partial fulfillment of the requirements for the degree of Doctor of Philosophy in the Curriculum in Toxicology in the School of Medicine.

Chapel Hill
2014

Approved by:

Mary F. Paine

Philip C. Smith

E. Claire Dees

Alexander Tropsha

Maciej Zamek-Gliszczynski

ABSTRACT

Garrett Robert Ainslie: A Translational Approach to Assess the Risk of Dietary Substance-Drug Interactions
(Under the direction of Mary F. Paine)

Myriad diet-derived substances, including foods, nutritional supplements, and exotic beverages are increasingly sought for their purported health benefits. These natural, seemingly safe, products can perpetrate pharmacokinetic/pharmacodynamic (PK/PD) interactions with conventional medications, placing the consumer at risk for potential adverse effects. Despite the ubiquitous nature of these products, there is a gap in the understanding of their drug interaction liability. This knowledge gap is due in part to the complex and variable chemical composition, prompting the need to characterize key constituents that contribute to perturbations in 'victim' drug PK/PD. Development of a framework to estimate the effect of the mixture using a single, or few, key constituents is principal to risk assessment.

Grapefruit juice (GFJ) is a well-studied beverage shown to inhibit pre-systemic (first-pass) drug metabolism in the gut, increasing systemic drug exposure and potential undesirable effects. GFJ acts by irreversible inhibition of cytochrome P450 3A (CYP3A) activity in the intestinal wall by a class of constituents termed furanocoumarins. 6'7'-Dihydroxybergamottin (DHB) is a well-studied and typically abundant furanocoumarin in GFJ, with inhibitory concentrations (1-5 μM) well below or within concentrations measured in GFJ (<60 μM or <5 mg / 240 mL serving). The relative abundance and

potent activity of DHB in GFJ makes it a promising candidate to serve as a marker constituent representative of the CYP3A-mediated effect of GFJ.

Anecdotal reports touting GFJ as a PK ‘booster’ raise concern that it may be used to increase systemic exposure to certain drugs. Loperamide is an over-the-counter opioid agonist that acts locally in the gut to slow motility. Incomplete absorption, extensive CYP3A-mediated first-pass metabolism, and active efflux by P-glycoprotein (P-gp) at the blood brain barrier prevent central nervous system opiate-like effects. The candidate marker constituent DHB and the exemplar victim drug loperamide were used to test the central hypothesis that an integrative approach involving in vitro assays, static and dynamic modeling, and proof-of-concept clinical testing can provide robust risk assessment of potential dietary substance-drug interactions. Results from this dissertation project demonstrated that the effects of GFJ on loperamide PK and PD could be predicted using PBPK/PD modeling and simulation. Furthermore, this work provides a refined framework to assess dietary substance-drug interaction risk in a time- and cost- efficient manner.

ACKNOWLEDGEMENTS

I am fortunate and grateful to have had great guidance and mentorship throughout my graduate career. First I would like to express my kind thanks to my research advisor, Mary F. Paine, and the members of my dissertation advisory committee, Philip Smith, Claire Dees, Alexander Tropsha and Maciej Zamek-Gliszczynski.

I wish to show my gratitude towards those who have contributed directly to the maturation of this work. I would like to acknowledge Yolanda Scarlett, Elizabeth Connolly, Yingxin Li and Kristina Wolf for their roles in the loperamide-grapefruit juice interaction study. I would like to thank Evan Kharasch for sharing the clinical data used to model alfentanil pharmacokinetics and pharmacodynamics. I am fortunate to have had the opportunity to work with a fantastic statistician and mentor, J. Heyward Hall. I thank Jeannie Padowski and Gary Pollack for sharing their expertise in pharmacokinetic and pharmacodynamic modeling. I would like to thank all of those have aided me in the naloxone clinical study, particularly. Matthew Layton, John White, Brandon Gufford, Debbie Weeks, Larissa Weeks and Abby Parsons.

I would like to thank my colleagues from the University of North Carolina at Chapel Hill, particularly Arlene Bridges and Nicole Zane, for their scientific support and personal guidance. I owe much gratitude to my former lab mates, in particular Scott Brantley, Christina Won and Catherine Denton whom all contributed significantly to my

training and research. I would like to share my appreciation for Harvey Clewell and Melvin Andersen for their roles in training me in physiologically-based pharmacokinetic modeling. I thank my friends and colleagues at Washington State University, particularly Kara R. Vogel and her three sons for their steadfast support and motivation. I thank Becky Gray for her administrative support, positive energy and motivation. I would like to thank the Curriculum in Toxicology and the supporting faculty for taking the 'chance' on me, supporting me, and fostering my professional development. Lastly, I thank my family for their support, patience and council. I thank my parents who have both pushed and supported me. I thank my brothers; Connell and Brett Ainslie, for their support in the times when I have most needed it.

PREFACE

The role of environmental factors such as diet in the disposition and metabolism of drugs is an aspect that has been long overlooked, although it is now well known that certain dietary substances can interact with drugs that result in untoward effects or reduced efficacy. A meeting by the National Toxicology Program in 1998 highlighted the importance of increased research in the field of dietary substances. However, over a decade later there remains no guidelines to systematically evaluate dietary substance-drug interaction risk. This project was undertaken to evaluate previously proposed translational frameworks to assess dietary substance-drug interaction risk. The key achievements of this work were (1) the identification of 6,'7-dihydroxybergamottin (DHB) as a promising marker constituent reflective of the CYP3A-mediated grapefruit juice effect; (2) the successful construction of physiologically-based pharmacokinetic/pharmacodynamic models capable of predicting a clinically relevant pharmacodynamic endpoint and; (3) the development of a human model to assess the opioid effect attenuation by naloxone. I conducted the majority of in vitro experiments described in this dissertation, and Maciej Zamek-Gliszczynski provided drug-tissue binding data for loperamide and DHB. My background in bioanalytical chemistry allowed me to conduct all LC-MS/MS analysis with the exception of that described in two clinical studies (loperamide and naloxone). In total, the work described within this dissertation included three clinical studies. The first study was a grapefruit juice-loperamide interaction study, which was conducted prior to my involvement in this project. This

study was conducted primarily by Elizabeth Connolly, Yolanda Scarlett, Yingxin Li, and Mary Paine. The quantification of loperamide and its metabolite was conducted by Kristina Wolf, and power calculations were conducted by J. Heyward Hull. A second clinical study described in this dissertation involved the determination of naloxone bioavailability for three extravascular formulations in six subjects. This pharmacokinetic study was led by John White and Mathew Layton and pharmacokinetic analysis was conducted by myself and Jeannie Padowski. I was involved in the study design along with Mary Paine and was the coordinator of the third clinical study described in Chapter 3. During this study I received extensive support from Brandon Gufford, Mathew Layton and John White, who were qualitied to administer medications and evaluate the health of and safety to study subjects. Furthermore, I received oversight and guidance from my research advisor, Dr. Mary Paine. Much of the work described in Chapter 2 involved advanced pharmacokinetic and pharmacodynamic modeling techniques. In the development of these, models I received constructive feedback from several key individuals, including Gary Pollack, Maciej Zamek-Gliszczynski, and Jeannie Padowski. J. Heyward Hull and Brandon Gufford advised on statistical analysis throughout this research. The achievements resulting from this work are those to be shared by all the great minds who contributed to the progress of this doctoral dissertation.

TABLE OF CONTENTS

List of figures xi

List of tables xiii

List of abreviations xv

Chapters

1 Introduction 1

2 Assessment of a candidate marker constituent predictive of a dietary substance-drug interaction: case study with grapefruit juice and CYP3A4 drug substrates 54

3 Characterizing the abuse potential of opioids using physiologically-based pharmacokinetic / pharmacodynamic modeling: case study with the grapefruit juice-loperamide interaction. 86

4 Evaluation of a novel human model to assess reversal of opioid effects by naloxone 117

5 Conclusions 138

Appendices

A Method development and validation of an HPLC-MS/MS method to quantify 6',7'-dihydroxybergamottin and other grapefruit juice constituents in human plasma. 160

B Characterization of furanocoumarin metabolites in human plasma and urine following grapefruit juice consumption. 169

C Recovery of in vitro kinetic parameters of loperamide and N-desmethylloperamide metabolism in human intestinal microsomes from individual donors. 173

D Recovery of in vitro kinetic parameters of loperamide metabolism and inhibitory kinetic parameters of DHB in rat. 178

E Inhibitory potency of supplements labeled to contain DHB and/or BG toward CYP3A activity. 185

F A physiologically-based pharmacokinetic model of loperamide..... 190

G Physiologically-based pharmacokinetic DHB-loperamide interaction model simulations. 200

H Physiologically-based pharmacokinetic/pharmacodynamic model simulations of alfentanil in healthy subjects. 204

LIST OF FIGURES

Chapter 1

Figure 1.1. Furanocoumarin structures.. 37

Figure 1.2. Loperamide metabolites in rat and human liver microsomes. 38

Chapter 2

Figure 2.1. Clinical study design and procedures..... 78

Figure 2.3. Time- and concentration-dependent inhibition of loperamide *N*-desmethylation by DHB in human intestinal microsomes 80

Figure 2.4. Relationship between the predicted and observed AUC_{GFJ}/AUC for 15 test drug substrates of the 'grapefruit juice effect' due to inhibition of intestinal CYP3A4 81

Figure 2.5. Relationship between the magnitude of a grapefruit juice-drug interaction for varying enterocyte concentrations of DHB and victim drug F_g. 82

Chapter 3

Figure 3.1. The general model structure of a physiologically-based pharmacokinetic/ pharmacodynamic model 107

Figure 3.2. Observed geometric mean and model-predicted mean plasma concentration-time profiles of loperamide taken with water or GFJ and of DHB. 108

Figure 3.3. Observed and model predicted alfentanil plasma concentration- and effect- time profiles after an intravenous or an oral dose. 109

Figure 3.4. Observed and model predicted methadone plasma concentration- and effect- time profiles. 110

Figure 3.5. Model-predicted maximum decrease in pupil diameter with increasing loperamide dose in the absence and presence of DHB..... 111

Chapter 4

Figure 4.1. Study design and procedures..... 131

Figure 4.2. Concentration-time profiles for naloxone following intravenous, intramuscular, or intranasal administration. 132

Figure 4.3. Mean pupil miosis-time profiles after administration of oral alfentanil. 133

Figure 4.4. Area under the effect-time curve and R_{max} following oral administration of alfentanil. 134

Appendices

Figure A.1. HPLC-MS/MS separation and detection of DHB..... 165

Figure A.2. DHB stability following storage at -80C..... 166

Figure A.3. DHB freeze-thaw stability in human plasma. 167

Figure B.1. Representative chromatograms following HPLC-MS/MS analysis of plasma from two subjects. 171

Figure C.1. Michaelis-Menten plot for *N*-desmethylation of loperamide by HIM. 176

Figure C.2. Parent disappearance of *N*-desmethylloperamide by HIMs and HLMs. 177

Figure D.1 Rat P450 enzymes catalyzing the formation of *N*-desmethylloperamide……182

Figure D.2. *N*-Desmethylloperamide formation at increasing loperamide concentrations in HLMs, RLMs, HIMs and RIMs. 183

Figure E.3. Comparison of the effects of supplements labeled to DHB..... 189

Figure F.1. Loperamide PBPK model structure. 192

Figure F.2. Model simulated plasma concentration-time profiles of loperamide and *N*-desmethylloperamide. 193

Figure G.1. Simulated loperamide hepatic fraction metabolized in the absence and presence of DHB 202

LIST OF TABLES

Chapter 1

Table 1.1. Phase I and II pathways and bioavailability (F) of common opioids. 31

Table 1.2. Models to predict perpetrator or victim substance specific parameters. 32

Table 1.3. Static models to assess drug interaction potential 33

Table 1.4. Software packages for PBPK modeling. 36

Chapter 2

Table 2.1. Pharmacokinetic outcomes of loperamide and *N*-desmethylloperamide in 16 healthy volunteers administered loperamide with 240 ml of water or grapefruit juice. 76

Table 2.2. Victim drug, F_g, F, and clinical study information for the IVIVE. 77

Chapter 3

Table 3.1. PBPK model input parameters. 104

Table 3.2. Pharmacodynamic model parameter input. 105

Table 3.3.Observed and model-predicted pharmacokinetic and pharmacodynamic outcomes following oral opioid administration. 106

Chapter 4

Table 4.1. Pharmacokinetics of naloxone after intravenous, intramuscular, and intranasal naloxone 129

Table 4.2. Clinical study inclusion and exclusion criteria. 130

Appendices

Table A.1. Precision (%CV) and accuracy (RE) inter- and intra-day variability of DHB in human plasma (n=3) 168

Table B.1. Individual DHB pharmacokinetic outcomes. 172

Table D.1. In vitro kinetic parameters for loperamide (K_m and V_{max}) and DHB (IC_{50}, k_{inact} and K_I) in human and rat microsomes. 184

Table G.1. Pharmacokinetic outcomes following oral loperamide and DHB..... 203

Table H.1. Model-predicted pharmacokinetic and pharmacodynamic outcomes following oral alfentanil administration in healthy volunteers..... 206

LIST OF ABREVIATIONS

ADAM	Advanced Dissolution, Absorption and Metabolism
AUC	area under the plasma concentration-time curve
AUC_m	AUC of the metabolite
AUC_p	AUC of the parent
AUEC	area under the effect-time curve
BG	bergamottin
B/P	blood to plasma ratio
bid	two times daily
CL/F	oral clearance
C_{last}	last measured concentration
Cl_{int}	intrinsic clearance
C_{max}	maximum concentration
CTRC	Clinical and Translational Research Center
CV	coefficient of variation
CYP	cytochrome P450
DHB	6',7'-dihydroxybergamottin
DDI	drug-drug interaction
DFB	3-[(3,4-difluorobenzyl)oxy]-5,5-dimethyl-4-[4-methylsulfonyl)phenyl] furan-2(5H)-one
DMSO	dimethyl sulfoxide
f_a	fraction absorbed
FDA	Food and Drug Administration

f_u	fraction unbound
GFJ	grapefruit juice
HIMs	human intestinal microsomes
HLMs	human liver microsomes
HTS	high throughput screening
IC_{50}	half-maximal inhibitory concentration
IM	intramuscular
IN	intranasal
IV	intravenous
IVIVE	in vitro-to-in vivo extrapolation
k_a	first-order rate constant for absorption
kg	kilogram
K_i	reversible inhibitory potency
K_I	concentration to achieve half the maximal inactivate rate
k_{inact}	maximal inactivation rate constant
K_m	concentration to achieve half the maximal metabolic rate
LC/MS/MS	liquid chromatography-tandem mass spectrometry
MAT	mean absorption time
MBI	mechanism-based inhibition
MDCK	Madin-Darby canine kidney
mg	milligram
mM	millimolar
mol	mole

NADPH	nicotinamide adenine dinucleotide phosphate
ND	not determined
nM	nanomolar
OATP	organic anion transporting polypeptide
PBPK	physiologically-based pharmacokinetic
PD	pharmacodynamic
P-gp	P-glycoprotein
pM	picomolar
PK	pharmacokinetics
RAF	Relative activity factor
RIMs	rat intestinal microsomes
RLMs	rat liver microsomes
rCYP	recombinant CYP
SD	standard deviation
SE	standard error
UDPGA	uridine diphosphate glucuronic acid
$t_{1/2}$	terminal elimination half-life
tid	three times daily
t_{max}	time to C_{max}
V_{max}	maximal metabolic rate
λ_z	terminal elimination rate constant
λ	first-order inactivation rate at a given I
µg	microgram

pM	picomolar
µM	micromolar
RAF	relative activity factor

CHAPTER 1 : INTRODUCTION

Dietary substance-drug interactions are a public health concern

The U.S. Environmental Protection Agency (EPA) implemented their ToxCast high throughput screening (HTS) initiative in 2007 (Dix et al., 2007). This project was designed to screen a bevy of failed pharmaceuticals, alternative plasticizers, pesticides, and food additives across 331 cell-free enzymatic and ligand-binding HTS assays (Haynes, 2010). These assays evaluated direct mechanisms of toxicity, such as those associated with carcinogenicity and neurotoxicity, and alterations in the activity of some cytochrome P450 (CYP) enzymes and transporters (Sipes et al., 2013). The ToxCast assays are demonstrating a potential to prioritize chemicals for more targeted risk assessment testing. The ToxCast approach parallels pharmaceutical discovery in certain ways; however, relative to drugs, little is understood about the quantitative influence of environmental exposures on the metabolism and transport of concurrent medications. Studies to determine the induction of certain CYPs by environmental agents have been reported. For example, heterocyclic aromatic amines, pro-carcinogens found in overcooked red meats, enhance their own metabolism *via* CYP1A and CYP3A gene induction (Kleman and Gustafsson, 1996; Fontana et al., 1999). St. John's wort *(Hypericum perforatum*), an herbal remedy for anxiety and depression, induces CYP3A and CYP2C9 (Di et al., 2008). While these observations are important, many drug metabolizing enzymes and transporters are overlooked, particularly with respect to dietary substances. There are documented interactions

between ‘victim’ drugs and ‘perpetrator’ herbs or foods when consumed concurrently (Won et al., 2012). Beverages, such as grapefruit juice (GFJ), are known to interact with >100 drugs through inhibition of intestinal CYP3A, P-glycoprotein (P-gp), or organic anion transporting polypeptide (OATP). Therefore, the result of consuming otherwise seemingly safe products with certain drugs may be detrimental and is concerning to public health.

The impact of certain dietary substances, including foods, nutritional supplements, and exotic juices on public health is increasing due to an increase in consumer popularity resulting from the purported health benefits and the misperception that “natural” equates with “safe”. The ever-growing market appearance of these substances raises concern when co-exposed with drugs, both prescription and non-prescription, potentially leading to untoward or toxic effects (Won et al., 2012). Both qualitative and quantitative assessment of dietary substance-enzyme/transporter interactions will provide more robust risk assessment of their combined intake.

Since dietary substances and many drugs are taken orally, mechanisms involving the inhibition of first-pass (*i.e.*, pre-systemic) elimination are most likely to be involved. Inhibition of the ‘first pass effect’ can result in substantial increases in victim drug systemic exposure, which may lead to untoward effects. The gut and the liver are the primary organs that mediate the first pass effect. CYP3A is a prominent enzyme subfamily in both the gut and liver and contributes to the metabolism of numerous marketed drugs and some dietary substances (Shimada et al., 1994; Paine et al., 2006). The human CYP3A family includes four genes: CYP3A4, CYP3A5, CYP3A7 and CYP3A43. CYP3A4/5 are the primary isoforms responsible for drug metabolism in

adults, whereas CYP3A7 is expressed in fetal and neonatal stages of life, and CYP3A43 has a role in steroid and cholesterol metabolism (Fanni et al., 2014). Given that CYP3A4/5 are responsible for the metabolism of >30% of marketed drugs (Zanger and Schwab, 2013), the liver and intestine are major sites of an interaction.

While the liver remains a major contributor to first-pass metabolism, the gut is also sensitive to enzyme or transporter inhibition. The gut, primarily the small intestine, is a critical portal for the absorption of ingested xenobiotics. Xenobiotic oxidative metabolism in the intestine is mediated primarily by CYP3A4/5 (Paine et al., 2006). The absorptive intestinal epithelial cells, enterocytes, provide active transport processes for the uptake and efflux of xenobiotics, including dietary substances and drugs. Organic anion transporting polypeptide (OATP) is one a family of uptake transporters expressed in the intestine, among other tissues, is and involved in the absorption of several drugs. A major apically located efflux transporter is P-glycoprotein (P-gp) and is expressed in a variety of other cell types, including endothelial cells in the liver and kidney and capillary cells constituting the blood-testis barrier and blood-brain barrier (BBB) (Ho and Kim, 2005). Perpetrator dietary substance constituents likely attain high concentrations in the enterocytes despite not achieving inhibitory concentrations in the liver.

The U.S. Food and Drug Administration (FDA) requires a comprehensive understanding of the drug interaction liability for new drug candidates prior to market approval. However, the FDA has limited jurisdiction regarding such characterization of dietary substances (US Food and Drug Administration, 2012a). Agencies in other countries, including the European Medicines Agency, Health Canada, and Therapeutic Goods Administration (Australia), have implemented more strict manufacturing

requirements for botanicals than in the US, although safety assessment of these products frequently lags behind that of drugs (Health Canada, 2011; European Medicines Agency: Committee for Human Medical Products, 2012). The FDA acknowledges the need for improved safety testing, and recent funding mechanisms offered by the National Center for Complementary and Alternative Medicines (division of the U.S. National Institute of Health) highlight this unmet need (de Lima Toccafondo Vieira and Huang, 2012).

Despite a change in the regulatory climate addressing the necessity for some standardization of products [European Medicines Agency (European Medicines Agency: Committee for Human Medical Products, 2012), Health Canada (Health Canada, 2011)] marketed as herbal products and dietary supplements, formal guidelines to assess the risk of dietary substance-drug interactions remain nonexistent. The study of dietary substances has certain challenges unique to those for drug development due to the highly variable biochemical makeup of dietary substances. A standard framework to assess these interactions without expensive clinical trials remains elusive. Since it would be extremely costly and time consuming to fully characterize all constituents of a given dietary substance, investigators have postulated that one or few constituents of the mixture, termed ‘marker constituents’, may be predictive of the effect of the whole mixture (Won et al., 2012; National Center for Complementary and Alternative Medicine, 2013; Ainslie et al., 2014). These marker constituents can be identified and used for testing. However, further work is needed using well-studied exemplar dietary substances and drugs to develop and substantiate a testing paradigm for dietary substance-drug interaction risk assessment.

Common mechanisms of enzyme inhibition

Reversible inhibition involves the rapid association and disassociation of an enzyme-inhibitor complex. Reversible inhibition frequently occurs by one of three specific mechanisms, including competitive, noncompetitive and uncompetitive (Shou et al., 2001; Walsh et al., 2011). Competitive inhibition is the result of a perpetrator substance binding to the active site of the enzyme preventing access by the victim substrate. The result in victim drug enzyme kinetics is an increase in the concentration needed for half-maximal rate of metabolism (K_m) with no change in maximal rate of metabolism (V_{max}) (Lin and Lu, 1998; Venkatakrishnan et al., 2003). Noncompetitive inhibition occurs when a perpetrator substance associates to a site of the enzyme other than the active site to attenuate enzyme activity. Noncompetitive inhibition is revealed by a decrease in V_{max} and no change in K_m. Uncompetitive inhibition occurs with the perpetrator substance binding to the enzyme-substrate complex, resulting in a decrease in both K_m and V_{max}. In the case of reversible inhibition enzyme activity is restored with removal of the perpetrator substance (Lin and Lu, 1998; Venkatakrishnan et al., 2003).

Reversible inhibition can initially be assed in the relevant enzyme system at a constant substrate concentration and a range of inhibitor concentrations. The inhibitor concentration required to inhibit enzyme activity by 50% (IC_{50}) can be recovered. The IC_{50} is dependent on substrate concentration and can be correlated to the reversible inhibitory potency constant (K_i) by the (Cheng and Prusoff, 1973). An inhibitor's K_i is a more definitive measure of reversible inhibitory potency and can be achieved by varying both substrate and inhibitor concentrations as covered in more detail below (Fowler and Zhang, 2008).

In general irreversible inhibition results from covalent or tight binding (quasi-irreversible) of a chemically reactive intermediate resulting in a loss of enzyme function (Grimm et al., 2009). This specific mode involving enzyme inactivation is known as mechanism-based inhibition (MBI). The MBI associated constant (K_I) and the rate of maximal enzyme inactivation (k_{inact}) are the parameters associated with MBI (Kalgutkar et al., 2007; Venkatakrishnan et al., 2010). The effects of irreversible inhibition can be prolonged after the inhibitor is removed, since transcription of new enzyme or cell regeneration is required to recover enzyme activity.

Grapefruit juice as an exemplar dietary substance and 6',7'-dihydroxybergamottin as a candidate marker constituent

Grapefruit juice (GFJ) is one of the most extensively studied dietary substances shown to perpetrate CYP3A-mediated inhibition of drug metabolism (Paine and Oberlies, 2007; Bailey et al., 2013). Many of these drugs undergo extensive first-pass metabolism by CYP3A. An extensive list of these medications has been reported elsewhere (Bailey et al. 2013). When consumed in usual volumes, GFJ elevates systemic concentrations of the victim drug by inhibiting enteric, but not hepatic, CYP3A. Despite that the juice inhibits only enteric CYP3A, the magnitude of the effect can be large enough to elicit untoward effects, such as severe muscle pain with some HMG-CoA reductase inhibitors (statins)(Dreier and Endres, 2004; Karch, 2004) and hypotension/dizziness with some calcium channel antagonists (Bailey and Dresser, 2004).

Myriad components in GFJ capable of inhibiting CYP3A *in vitro* have been identified, including furanocoumarins, several of which are potent reversible and

irreversible inhibitors of CYP3A (Paine and Oberlies, 2007). Using a “furanocoumarin-free” GFJ suitable for human consumption and the CYP3A probe substrate felodipine, furanocoumarins, in aggregate, were demonstrated unequivocally as major CYP3A inhibitors in vivo. In addition to their ability to inhibit enteric CYP3A, furanocoumarins have been shown to inhibit the P-gp in vitro (Eagling et al., 1999; Paine and Oberlies, 2007). Moreover, using the aforementioned furanocoumarin-free juice, GFJ/furanocoumarins were shown to inhibit the enteric P-gp-mediated translocation of the dual CYP3A/P-gp substrate cyclosporine in healthy volunteers, as well as in the human intestine-derived cell line Caco-2 (Paine et al., 2008). Parallel in vitro studies identified the furanocoumarins bergamottin (BG) and 6’,7’-dihydroxybergamottin (DHB) (Figure 1.1.) as mechanism based inhibitors of CYP3A (K_I, 1.6 and 0.7 μM, respectively) and P-gp activity (IC_{50}, 0.74 and 0.33 μM, respectively) (Eagling et al., 1999; Paine et al., 2004).

Despite the potent inhibitory activity of BG towards CYP3A in vitro, BG has high tissue binding properties and is less readily absorbed than DHB, indicating it may contribute less to the GFJ effect in vivo (Paine et al., 2004; Paine et al., 2005). The clinical role of BG is evidenced largely by two studies designed to evaluate the contribution of BG to CYP3A-mediated GFJ-drug interactions. Bailey et al. conducted the first in 2003, which compared lime juice, which is typically high in BG but not DHB (Wagner et al., 2002; Gorgus et al., 2010; Guth et al., 2011; Costa et al., 2014), with GFJ as a reference perpetrator of a felodipine interaction (Bailey et al., 2003). In this randomized crossover study, subjects were administered 250 ml of water, lime juice (100 μM BG and undetectable DHB) diluted 4-fold or GFJ (containing 25 μM BG; DHB

was not reported) prior to felodipine (10 mg). The lime juice was diluted such that the concentration of BG was the same as that in GFJ. Relative to water, GFJ increased felodipine area under the plasma concentration-time curve from time zero to infinite time ($AUC_{0\text{-}inf}$) and maximum observed plasma concentration (C_{max}) by 2- and 1.9-fold, respectively. In contrast, lime juice had no effect on the pharmacokinetics of felodipine despite an extract having both reversible and irreversible inhibitory activity in a microsomal CYP3A activity assay. In vitro activity assays were conducted using recombinant CYP3A4, increasing amounts of juice extracts, and testosterone 6β-hydroxylation as the index reaction. The observed in vitro-to-in vivo disconnect may be due to the slower absorption of BG compared to DHB in Caco-2 cells (Paine et al., 2005) and perhaps a delay in felodipine treatment following lime juice would have resulted in an interaction. Alternatively, there may have been components in the lime juice extract which did not attain high enough enteric concentrations.

Goosen and colleagues at North-West University in South Africa conducted the second benchmark clinical study evaluating BG as a causative constituent in GFJ in 2004 (Goosen et al., 2004). BG was obtained from a commercial source (Sigma Aldrich, ≥ 98% purity) and was administered to 11 healthy volunteers in a five-phase clinical study. Felodipine (5 mg) was tested as the victim drug and was given on each study day. On study days 1-2, subjects were randomized to receive either water or GFJ (containing 1.7 mg BG, DHB was not measured). On study days 3-5, subjects were randomized to receive capsules containing 2, 6 or 12 mg BG with water. Blood was drawn for 12 h following the felodipine dose, and plasma was quantified for felodipine, BG and DHB using HPLC-MS/MS. Relative to pre-treatment with water, BG doses of 6

and 12 mg increased felodipine $AUC_{0\text{-}12h}$ by 1.3-fold. The GFJ product containing 1.7 mg of BG resulted in a 1.5-fold increase, whereas 2 mg of BG had no significant effect. This study suggested that BG contributes to the GFJ effect but alone does not account for the effect of the mixture in vivo. Additionally, at the higher BG doses, DHB was detected in plasma, indicating that BG is biotransformed to DHB in vivo or the study product was contaminated with DHB.

In vitro assessment of other furanocoumarins, including dimers and trimers, have indicated that some of these constituents are highly potent as well (IC_{50}, 0.003-1 μM) (Guo et al., 2000b; Guo et al., 2000a; Tassaneeyakul et al., 2000; Row et al., 2006; Oda et al., 2007). Despite these data, such constituents have unknown/poor stability (light, pH, and metabolic), and their clinical relevance is unknown (Morliere et al., 1990; Kent et al., 2006). Improved methods to quantify these constituents in both the juice and biologic matrices are required to further understand their role in the CYP3A-mediated GFJ effect.

There are limitations to using furanocoumarin dimers or BG as marker constituents that include the known unfavorable physicochemical properties (high nonspecific binding affinities) (Paine et al., 2004) of BG and unknown physiochemical properties of dimers make these chemicals less desirable candidates as a marker constituent. In contrast, DHB has multiple desirable characteristics: (1) physicochemical properties in alignment with straightforward quantification in both GFJ and biologic matrices; (2) typically ample quantities in GFJ that exceed the reported MBI associated constant (K_I, 1-5 μM); (3) the onset of maximum loss of enteric CYP3A4 protein in human intestine-derived cell monolayers (Caco-2) (Paine et al., 2005) corresponds to

that in healthy volunteers administered GFJ (Lown et al., 1997); and (4) the existence of commercially available authentic standards that are not cost prohibitive.

Grapefruit juice as a 'pharmacokinetic boosting' agent

The discovery of GFJ as an irreversible inhibitor of intestinal CYP3A4 has spurred the marketing of dietary supplements labeled to contain BG, DHB and/or GFJ extracts. These products have been marketed as 'pharmacokinetic boosting' agents aimed towards body builders to increase the bioavailability of oral hormones and supplements. Many hormones (e.g., androgens) are metabolized by CYP3A (Hara and Nishiyama, 2014), and GFJ has been shown to increase systemic exposure to the sex hormone, 17 β-estradiol (Schubert et al., 1994), providing loose justification for the products marketed use. Even in conventional pharmacotherapy, GFJ has been proposed as a means to increase the exposure to expensive and poorly bioavailable drugs as a cost-savings strategy, including some immunosuppressive and anticancer agents (Reif et al., 2002; Liu et al., 2009; Kimura et al., 2011; Cohen et al., 2012). Similarly, the role of GFJ as a pharmacokinetic booster has been implicated in anecdotal reports as a means to increase the systemic exposure to certain opioids (e.g., methadone, morphine, oxycodone, hydrocodone and loperamide) (Bluelight, 2014b; Bluelight, 2014a).

Loperamide as a candidate GFJ victim drug with abuse potential

Loperamide is a peripherally acting μ-opioid receptor agonist, which, despite having a high affinity towards its target receptor, is not associated with central nervous system effects due to an extremely low oral bioavailability (0.3%) (Yu et al., 2004) and active P-gp-mediated efflux at the blood brain barrier (Skarke et al., 2003; Zamek-

Gliszczynski et al., 2012). The low bioavailability is in part due to the high first pass effect mediated primarily by CYP2C8 and CYP3A4 (Figure 1.2) (Kim et al., 2004). Anecdotal reports and case studies have implicated the potential for loperamide abuse when taken concomitantly with CYP3A4 or dual CYP3A/P-gp inhibitors (Daniulaityte et al., 2013). A limited number of case studies have also signified that high doses of loperamide can result in abuse or death (Langlitz et al., 2001; Sklerov et al., 2005). In contrast, clinical evaluations in healthy volunteers have shown that increases in loperamide plasma exposure do not translate to a central opiate-like effect (Tayrouz et al., 2001; Skarke et al., 2003; Niemi et al., 2006). Although supratherapeutic doses of loperamide have been examined (up to 24 mg) in non-addict populations, these doses are much lower than those from anecdotal reports of abuse (70-200 mg) (Daniulaityte et al., 2013). Due to ethical and safety concerns, an alternative approach must be taken to evaluate the validity of these claims and to assess the abuse potential of loperamide.

The in vivo impact of grapefruit juice on various clinically used opioids

Naturally-occurring opiates and synthetic opioids are metabolized predominately by CYP3A, CYP2B6, CYP2D6, and the UDP-glucuronosyltransferases (UGTs), particularly UGT2B7 (Iribarne et al., 1997; Iribarne et al., 1998; Benetton et al., 2004; Hutchinson et al., 2004; Yasar et al., 2005; Kharasch et al., 2007; Klimas and Mikus, 2014). Some of these opioids are presented in table 1.1; however, of the many opioids metabolized by CYP3A, only five (i.e., alfentanil, methadone, morphine, oxycodone, and tilidine) have been evaluated in vivo as victims of the GFJ effect. As certain opioids have a narrow therapeutic window, when given acutely, an examination of these GFJ-

opioid interaction studies is warranted. A common limitation of the following studies is lack of measured constituents in the study juice (Overholser and Foster, 2011).

ALFENTANIL

Alfentanil is a short-acting ($t_{1/2}$ = 1.5 h) (Egan et al., 1996) synthetic opioid used in anesthesia for surgical procedures (Scholz et al., 1996). Clinically, alfentanil is administered intravenously, although it has been administered both orally and intravenously as a 'probe' of intestinal and hepatic CYP3A (Kharasch et al., 2004a; Klees et al., 2005a; Klees et al., 2005b; Kharasch et al., 2007; Kharasch et al., 2011). A decade ago, GFJ was shown to increase oral alfentanil (23 μg/kg) plasma exposure (AUC) by 1.7-fold relative to water in healthy volunteers (Kharasch et al., 2004a). In this study, a pharmacodynamic endpoint (pupil diameter) was measured, resulting in a 1.4-fold increase in the area under the effect curve (AUEC).

METHADONE

Methadone is a long-acting opioid ($t_{1/2}$ = 40 h) administered orally to treat opioid withdrawal symptoms in opioid-addicted patients and abusers (Nilsson et al., 1982). Since methadone is given both orally and chronically, a GFJ-methadone interaction would be concerning, as unforeseen accumulation of the drug would result in overdose. However, a clinical study conducted in 12 healthy volunteers with no history of drug abuse revealed a low risk of a GFJ-methadone interaction (1.2-fold increase in AUC) (Kharasch et al., 2004b). Pupil diameter also was measured in this study and was reflective of the minimal increase in total methadone plasma exposure (1.1-fold increase in AUEC). However, plasma exposure to the primary metabolite, 2-ethyl-1,5-dimethyl-3,3-diphenylpyrrolinium, decreased by 43% with no change in C_{max}. Results from this

study suggested that the role of intestinal CYP3A, in methadone metabolism, is minimal compared to that in the liver and of CYP2B6 (Kharasch et al., 2004b).

In a second GFJ-methadone interaction study, the racemic components were examined (Benmebarek et al., 2004). Subjects (n=8) undergoing methadone maintenance therapy consumed water or GFJ (200 mL) 30 minutes prior to and in conjunction with their methadone dose for 5 days. Blood was collected for 24 hours following the methadone dose and quantified for total methadone and the individual enantiomers (R and S). A mean increase in AUC of 17% was observed for both enantiomers, with a similar increase in C_{max}. However, the maximal increase in plasma AUC of R-methadone, the most potent enantiomer, was 29%. This study in methadone patients confirmed that reported in healthy volunteers, which indicated a low magnitude of effect by GFJ.

MORPHINE

Morphine is perhaps the most historically significant opioid agonist. It was first used in opium-derived elixirs hundreds of years ago and later isolated and identified in 1804. The discovery of morphine spurred synthetic development of many of the opioids currently used in pain management. Morphine is primarily metabolized by hepatic UGT2B7, forming a 6-glucuronide conjugate that is a more potent μ-opioid receptor agonist than morphine, and the 3-glucuronide conjugate that is inactive and possibly antagonistic (Osborne et al., 1992; Handal et al., 2007; Klimas and Mikus, 2014).

The affinity for CYP3A4 and the low oral bioavailability (Table 1.1) makes morphine a possible candidate for a GFJ interaction. A CYP3A-mediated interaction with morphine, in theory, could reduce enteric elimination of parent, resulting in further

UGT2B7-mediated glucuronide formation by hepatic UGT2B7 (Groer et al., 2014). Okura and colleagues studied the GFJ-morphine interaction in rats, by, demonstrating that a GFJ preparation could increase antinociception by 50% (Okura et al., 2008). This interaction has not been confirmed in humans.

OXYCODONE

Oxycodone is one of the most frequently prescribed oral opioids to treat pain. A clinical evaluation of the GFJ-oxycodone interaction detected a 70% increase in oxycodone (10 mg dose) plasma AUC in the presence of GFJ (200 ml t.i.d. x 5 days). Effect was measured using the cold compression test, visual analog scale and the self-reported performance test of which only the self-reported performance test detected a significant albeit modest increase in response (20%) in the presence of GFJ (Nieminen et al., 2010). These findings may raise the concern of an alternative means of oxycodone abuse.

TILIDINE

Tilidine is an orally administered prodrug, given as a racemic mixture, which is believed to be primarily bioactivated by CYP3A *via N*-desmethlyation in the gut to form the active metabolite nortidine (Grun et al., 2012; Wustrow et al., 2012; Eichbaum et al., 2014). Nortidine is further desmethylated and inactivated by the liver, forming bisnortilidine. Inhibition of intestinal CYP3A could reduce pharmacologic response, prompting clinical evaluation with GFJ (Wustrow et al., 2012). This was conducted in a randomized, open-label, placebo-controlled, cross-over study in 12 healthy volunteers administered tilidine (100 mg p.o.) with and without GFJ (250 mL q 12 hr x 3). GFJ did not augment the AUC or C_{max} of tilidine or its metabolites (nortilidine and bisnortilidine),

suggesting that intestinal CYP3A does not contribute to the first-pass metabolism of tilidine. The authors concluded that enzymes other than CYP3A might be involved in tilidine metabolism; however, the study juice was not quantified for furanocoumarin content, precluding definitive interpretation. The lack of measured marker constituents in study products is a common limitation of GFJ-drug interaction studies (Won et al., 2012).

IN VIVO OPIOID INTERACTION SUMMARY

Despite the limited number of GFJ-opioid interaction studies conducted to date, those existing provide important evidence to clinicians regarding the safety and efficacy of these dietary substance-drug combinations. While the interaction reported with alfentanil occurs, the clinical impact is likely minimal, whereas that with oxycodone may be concerning. The GFJ-oxycodone interaction may elicit accidental overdose or promote intentional opioid abuse and deserves further investigation. Assessing the abuse and interaction potential of opioids clinically is accompanied by certain ethical concerns. (1) Opioids are often associated with abuse, dependence and overdose; therefore, studies investigating dietary substance-opioid interaction potential in opioid naïve subjects require more careful consideration than with relatively safer medications. (2) Despite the addictive properties of opioids, they remain important in pain management. Recruiting patients undergoing pain management regimens would be a natural alternative to healthy subjects, yet there is a responsibility by the investigator to minimize potential harm to these patients who may experience excruciating pain with decreasing opioid exposures or develop dependence with elevated opioid exposures. (3) To avoid the risk of developing dependence in a non-addict population, or to study

treatments for addicts, human studies have utilized opioid addict populations. Studies in these populations raise even more issues, which have been extensively reviewed, and include considerations of coercion and exploitation in subject recruit concerns (Smith, 2008; Timmermans and McKay, 2009). Finally, the Declaration of Helsinki provides a statement that, “In advance of a clinical trial, sponsors, researchers and host country governments should make provisions for post-trial access for all participants who still need an intervention identified as beneficial in the trial” (World Medical, 2013; Fletcher, 2014). As the ethical apprehensions are daunting, such clinical evaluation of a dietary substance-opioid interaction should be preceded with careful preclinical evaluation and considerations of risk. Preparation for such studies would be well-informed from preclinical modeling and simulation approaches.

Preclinical models for assessing dietary substance-drug interaction potential

In vitro-to-in vivo extrapolation (IVIVE) of dietary substance-drug interaction liability has been conducted using several techniques, which span a spectrum of cost, complexity and accuracy. Methods may be as straightforward as direct extrapolation of in vitro inhibition assay data to predict clinical interactions, to the application of simple or complex algebraic equations from in vitro data, to the use of more complex models comprised of differential equations.

Historically, due to the high cost and lack of regulatory requirements to conduct clinical studies, dietary substance-drug interactions have been predominantly examined in both in vitro systems and preclinical animal models. Several groups have investigated the use of rodents as a useful screening tool to evaluate these interactions early in early drug discovery (Okura et al., 2008; Song et al., 2014; Zhao et al., 2014). The advantage

of using live animals is that they can be administered a test beverage or extract in the presence of a victim drug with relative ease, by generally accepted oral administration routes (*e.g.* oral gavage, dietary supplementation), resulting in a moderate throughput assay. However, these models are limited by differences in metabolism and enzyme expression that is differentially distributed in humans. Despite limited reports of a reasonable assessment of CYP3A-mediated interactions in rats (Kosugi et al., 2012; Vuppugalla et al., 2012; Rioux et al., 2013), this approach has been generally unsuccessful but remains in practice and may gain in popularity with the refinement of humanized rodent models (Jaiswal et al., 2014).

A second 'direct extrapolation' technique has been the use of human cell fractions (microsomes, S9 or recombinantly expressed enzyme) as an enzyme source to determine inhibitory potency of dietary substances. This is a high throughput technique involving the incubation of human microsomes (*e.g.* liver, intestine and kidney) (Al Saabi et al., 2013; Gufford et al., 2014) with cofactor (*e.g.* NADPH, UDGPA), and a probe substrate (*e.g.* midazolam, 4-methylumbelliferone) in the absence and presence of inhibitor. The test inhibitor may be added to the mixture as a crude extract, semi-purified extract or isolated constituent. To assess reversible inhibition, experiments may be conducted in this manner over a range of inhibitor concentrations at a constant substrate concentration and incubation time. The reaction velocity in the absence of inhibitor in conjunction with that in the presence of inhibitor may be used to extrapolate the IC_{50}, using eq. 1, for a test perpetrator substance (Grime et al., 2009). The values recovered from this assay are dependent on substrate concentration and may not translate from assay to assay (Cheng and Prusoff, 1973). To obtain more robust

parameters of inhibitory potency, the K_i can be determined with a matrix of substrate and inhibitor concentration spanning, ideally, 5-fold below and above the estimated inhibitor K_i (e.g., based on IC_{50}) and substrate K_m (eq. 2). To assess MBI of an enzyme, a common approach analogous to the IC_{50} recovery is to determine the "IC_{50} shift". The IC_{50} shift assay includes a pre-incubation of varying inhibitor concentrations in the presence of enzyme source (with and without) the appropriate cofactor, followed by enzyme activity measurements with the probe substrate of interest (Grimm et al., 2009). The fold change in the apparent IC_{50} is a widely used measure of time-dependent inhibition (TDI). MBI, a specific mechanism of TDI, can be further characterized by recovering the k_{inact} and K_I (Riley et al., 2007). Incubations containing crude extracts, a conventional approach, at times result in challenging data interpretation due to the unknown composition and often existence of fatty acids and lipids. These constituents have unknown clinical relevance due to poor cell membrane permeability of high molecular weight lipids and extensive metabolism of fatty acids by gut microflora (Clarke et al., 2014; Trier et al., 2014). Single constituents have been postulated to be ideal if in vitro kinetic parameters are to be incorporated into static models or dynamic models (National Center for Complementary and Alternative Medicine, 2013).

$$v = \frac{v_0}{1 + \frac{I}{IC_{50}}} \qquad \text{eq. 1}$$

where v denotes the measured reaction velocity; v_0, initial reaction velocity; I, inhibitor concentration.

$$v = \frac{V_{max} \bullet S}{K_m \bullet \left(1 + \frac{I}{K_i}\right) + S} \qquad \text{eq. 2}$$

where V_{max} denotes maximum reaction velocity; S, substrate concentration.

$$k_{inact,app} = \frac{k_{inact} \bullet I}{K_I + I} \qquad \text{eq. 3}$$

where $k_{inact,app}$ denotes the apparent inactivation rate constant at each inhibitor concentration, determined by the slope of the monoexponential decline in activity.

Mathematical methods to extrapolate in vitro data to humans vary in complexity and can be categorized into two classes: those to predict parameters for victim drugs and inhibitors (*e.g.*, inhibitor/drug plasma concentration; fraction of dose escaping intestinal extraction, F_g; or intrinsic clearance) (Table 1.2) and those to evaluate the interaction potential. The latter can be further divided into to three types of models: simple static, mechanistic static, and physiologically-based pharmacokinetic (PBPK). Simple static models (Table 1.3) allow for a quantifiable estimate of the interaction liability using as little as a single experimentally recovered parameter (e.g. K_i). Kinetic parameters for reversible (K_i) or irreversible (K_I and k_{inact}) inhibition can be used along with estimated inhibitor concentrations in humans to determine the likelihood of an interaction. These models are often used to justify further investigation or to declare the likelihood of an interaction to be low (US Food and Drug Administration, 2012a). Simple static models exist to predict both reversible and time-dependent inhibition; however, some lack the ability to predict the magnitude of interaction and do not account for the location of the interaction (*i.e.,* intestine, liver, kidney). Lastly, these models are not typically robust enough to accurately predict the magnitude of a clinical interaction directly.

Mechanistic static models have been applied to account for interactions limited to specific tissues (*e.g.*, gut or liver) and predict clinically important outcomes (*e.g.*,

changes in AUC, intrinsic clearance or F_g). Success by the pharmaceutical industry has been seen in many cases, justifying the continued use of mechanistic static models (Obach et al., 2006; Obach et al., 2007; Gertz et al., 2010). Popularity of mechanistic static models should grow in early assessment of dietary substance-drug interactions because the requisite data can be readily obtained from reversible inhibition or time dependent assay data (IC_{50} shift, K_I/k_{inact}). One differentiating characteristic of simple versus mechanistic static models is that the latter requires more information (*i.e.*, more experimentally derived parameters) about the victim drug, such as the F_g, which may not be known in early drug discovery, precluding dietary substance interaction risk at this early stage. Mechanistic static models (Table 1.3) may also be combined or refined to include additional modes of action or routes/modes of elimination/inhibition. The application of mechanistic static models to dietary substances as perpetrators is limited, due to the gap in human pharmacokinetic knowledge of perpetrator substances and/or the lack of isolated constituents for in vitro parameter recovery.

The use of either a simple or mechanistic static model remains limited with their inability to account for varying dose and dose frequency of test perpetrator substances. These limitations can be accounted for with PBPK models, which utilize physiological parameters to account for anatomy, enzyme expression and transporter activity among others.

The first report of a PK model with a physiologically relevant structure was by Torsten Teorell in 1937 (Teorell, 1937b; Teorell, 1937a). It was not until the 1970s and 1980s that PBPK modeling began to mature and find purpose in drug discovery and in environmental risk assessment (Dedrick et al., 1973; Huffman et al., 1973; Andersen et

al., 1977; Andersen et al., 1979; Clewell and Andersen, 1985). Ever since, these types of models have been used by pharmaceutical, cosmetic and chemical industries (Charnick et al., 1995; Sinha et al., 2012; Rowland, 2013; Bachler et al., 2014; Chen et al., 2014; Cristofoletti and Dressman, 2014; Schuhmacher et al., 2014; Suemizu et al., 2014).

This growth has been catalyzed in part by the increased computing power of the modern era and available software packages. Programs available to construct and use PBPK models can be categorized as either 'free form coding' or 'preassembled'. Free form coding programs such as Matlab®, Berkeley Madonna™, acslX, and ModelMaker® allow the user complete control of model structure and parameterization, limited only by the user's ability and data availability. Preassembled programs include BioDMET, Gastroplus™, Simbiology® (Matlab), PK Sim and Simcyp® (Table 1.4) (Schmitt and Willmann, 2005; Graf et al., 2012). These packages comprise built-in model structures and physiological parameters. Some allow for modification and customization but are typically limited to the manufacturer's specifications, which are ever evolving to meet the customer's expectations and needs.

A second reason for the interest in PBPK modeling is the availability of certain physiological data previously not known (e.g. transporter tissue expression, polymorphic enzymes, disease specific changes to physiology) (Prasad et al., 2014). With these tools, modelers are armed with the ability to estimate drug-tissue concentrations and to predict nonlinear pharmacokinetics, xenobiotic-drug interactions and efficacy/toxicity, particularly in special populations and disease states (Jiang et al., 2013; Lin et al., 2013; Abduljalil et al., 2014; Li et al., 2014; Lu et al., 2014).

Physiologically based pharmacokinetic/pharmacodynamic models

Publications including simulated PK of drugs using PBPK models have exploded during the past several years. Clinical investigation of dietary substance-drug interactions with both pharmacokinetic and effect endpoints has increased (Sugimoto et al., 2006; Misaka et al., 2013; Chakraborty et al., 2014; Ide et al., 2014). Following this trend, the next innovative step would be to incorporate pharmacodynamic endpoints into interaction simulations using PBPK/ PD models. As with the initial resurgence of PBPK models in the 1970s, contemporary environmental toxicologists have taken the lead on examining PBPK/PD models for exposure risk assessment. Models have been applied to assess the risk of arsenic, carbonyl, chlorpyrifos, methyl-parathion and methyl-diazion exposure (Ling and Liao, 2009; Foxenberg et al., 2011; Hinderliter et al., 2011; Tan et al., 2011; Knaak et al., 2012; Wason et al., 2012; Poet et al., 2014; Smith et al., 2014; Yoon et al., 2014). PBPK/PD modeling is entering pharmaceutical assessment as embodied in recent work aimed at predicting the bioequivalence of generic ibuprofen formulations (Cristofoletti and Dressman, 2014). In this study, the authors used the PBPK/PD modeling and simulation software, Simcyp®, and two reference studies where ibuprofen was given at 400 mg and 10 mg/kg. These outcomes were compared to test formulations at 280 mg and 7 mg/kg, where bioequivalence was archived based on effect but not on pharmacokinetic outcomes.

A requisite of PBPK/PD modeling as an approach will be the availability of a meaningful and understood pharmacodynamic endpoint for which to model. The effect of pain medications, for example, can be measured in humans with subjective surveys, or in some cases objective measurements. The available measures of centrally-acting

opioid effect lend toward the ability to construct such PBPK/PD models with this class of drugs. Namely, pupil diameter (miosis) offers a sensitive and relatively precise measure of effect of centrally-acting opioid agonists.

Clinical assessment of dietary substance-opioid interactions and reversal of opioid effect

Despite maturation of the abovementioned predictive models, clinical evaluation remains the only absolute measure of dietary substance-opioid interaction risk. Clinical studies can be used to validate predictive models or to gain mechanistic insight following an in silico-to-in vivo disconnect. Either outcome may be informative. Once model simulations conducted in virtual healthy subjects are successfully validated with a healthy volunteer (*i.e.,* 'proof-of-concept') clinical study, the PBPK or PBPK/PD model may be applied to special populations (pediatrics, geriatrics, patients). In a recent publication, Li et al. applied this PBPK modeling and simulation strategy to seven drugs (antipyrine, nisoldipine, repaglinide, glibenclamide, glimepiride, chlorzoxazone, and metformin) (Li et al., 2014). PBPK models of all seven drugs were individually constructed, and model simulations were compared to outcomes observed in healthy volunteer studies. After confirming model robustness, the plasma concentration-time profiles for each drug were simulated in diabetic patients. The resulting model-predicted AUCs all lay within 50% of those observed in diabetic patients. Sensitivity analysis of key disease specific parameters was conducted, identifying gut transit time, altered hepatic enzyme activity and impaired renal function as disease specific alterations most responsible to changes in drug exposure in diabetic patients. This

synergy between PBPK modeling and clinical evaluation may also be applied to dietary substance-opioid interactions.

In many cases, the primary obstacles to conducting clinical studies are time, cost, personnel and materials (The National Academies Collection: Reports funded by National Institutes of Health, 2010). Each of these barriers is interconnected with one another. While the time to obtain Institutional Review Board approval can vary greatly depending on the sponsoring institution and host country, the study duration is dependent on the availability of personnel/facilities and speed of sample analysis (frequently quantification of drug in blood or plasma). Increased study complexity may benefit the scientific merit, yet detriments the cost-efficiency, as additional study phases or long collection time-periods accelerate expenditures.

While these challenges apply to all clinical studies, those designed to evaluate dietary substance-opioid interaction risk could readily address each of these hurdles. In a market where contract research organizations charge $40-65 per sample for plasma LC/MS/MS analysis, testing measures of opioid effect would eliminate the associated blood collection and bioanalytical costs and time. Specific measures of central opioid effect, such as respiratory rate, blood oxygen saturation, and pupil diameter are readily obtained by less skilled personnel and data analysis is in real time. This approach liberates the more highly trained medical professionals and allows insertion of trainees in the clinical environment. While the FDA has preferred CYP3A probe substrates for drug-drug interaction risk assessment, there are no guidelines specific to dietary substance-drug interaction risk assessment in vivo. To facilitate or prioritize this risk assessment, additional probes, where opioid effect can be measured, should be

considered. A short-acting and well-studied opioid would reduce the duration of a study day, and associated monetary burden of staff and subject compensation. A sensitive, noninvasive measurement of opioid effect would decrease analytical time and cost and at minimum help prioritize more thorough and complex studies.

The short-acting μ-opioid receptor agonist, alfentanil ($t_{1/2}$, ~1.5 h), is a CYP3A specific substrate and candidate to assess dietary substance-opioid interactions mediated by CYP3A. Kharasch et al. have proposed alfentanil as a probe to assess CYP3A phenotypes in humans and has utility in assessing dietary substance-drug interactions mediated by CYP3A (Kharasch et al., 2004a; Kharasch et al., 2007; Kharasch et al., 2011). The promise of using this probe is that it can be administered both orally and intravenously in the absence and presence of a test dietary substance, and pupil diameter can be measured in lieu of plasma drug concentrations. This less invasive approach would require less medically trained staff, would decrease time and costs associated with plasma analysis and decrease the risk infectious disease transmission.

As described earlier, the clinical application of opioids is challenged with the potential of adverse events, mainly respiratory depression. The definitive treatment for opioid overdose is the opioid antagonist, naloxone, approved for intravenous (IV) and intramuscular (IM) administration (Dowling et al., 2008). Oral delivery of naloxone results in poor absolute bioavailability (≤2%) due to extensive pre-systemic glucuronidation in both the gut and liver (Gill et al., 2012; Smith et al., 2012). The high first-pass extraction of naloxone has been exploited in new tamper resistant formulations of oxycodone (Remoxy® and *Targiniq™ ER*), buprenorphine (Suboxone®)

and morphine (Embeda®; withdrawn from the market due to production issues) (Johnson et al., 2010; Stanos et al., 2012). When naloxone-containing combinatorial medications are used as intended, systemic naloxone concentrations to reverse the effects of the active opioid are not achieved. Conversely, if the formulation is altered (*i.e.,* crushed) for intravenous use, naloxone is expected to attenuate opioid effects. A liability of these orally administered drugs is the potential for a complex dietary substance-drug interaction. Naloxone is metabolized by primarily by UGT2B7 and therefore inhibition of these enzymes by perpetrator dietary substances could increase naloxone exposure sufficiently for it to act systemically and potentially elicit withdrawal symptoms (Gill et al., 2012; Gufford et al., 2014).

While the low oral bioavailability of naloxone is beneficial in tamper resistant medications, it is problematic for its use in emergency medicine. Until the recent FDA approval of a single-dose naloxone, product, Evizio™, intravenous and intramuscular (IM) naloxone were the only available naloxone formulations and required medically trained personal to administer this lifesaving drug. Evzio™, which allows for the lay bystander to administer naloxone IM naloxone. Production of this device is a step in the right direction but is cost-prohibitive (>$200/dose) and invasive, risking the transmission of infectious diseases (The Medical Letter, 2014). Intranasal (IN) naloxone would be an alternative formulation that could be readily administered. Several programs across the U.S. support IN naloxone for in-field treatment of opioid overdose by lay persons, who typically are the first responders (Barton et al., 2002; Glaser et al., 2005; Heard et al., 2009). These programs use the parenteral formulations and an atomization device. Although rescue rates are relatively high, the absolute bioavailability of this formulation

(4%) does not support widespread use or FDA approval (Barton et al., 2002; Dowling et al., 2008). Development of novel IN naloxone products will continue following a call by the FDA (US Food and Drug Administration, 2012b) and support by the Australian government (Lenton et al., 2014).

The recent development and market appearance of these new naloxone-containing products is challenged with a lack of a human model to measure the efficacy (*i.e.,* reversal of opioid effects) of naloxone formulations. Ideally, early stage clinical evaluation with such a model would facilitate the production of noninvasive naloxone products or help evaluate the dietary substance-drug interaction potential of naloxone-containing products. Taken together, there is an urgency for a noninvasive cost- and time- effective human model to (1) assess dietary substance-opioid interactions, (2) determine dietary substance-drug interaction potential of combinatorial naloxone products, and (3) develop novel antidotes to treat opioid overdose.

Summary and project aims

Certain dietary substances can perpetrate alterations in the absorption, distribution, and elimination of victim drugs, resulting in altered systemic exposure and, potentially, untoward effects. Regulatory agencies are acknowledging this public health concern, yet there are no guidelines to assess dietary-substance-drug interaction risk. It has been postulated that, despite the complex mixtures of most dietary substances, one or a few marker constituents can be identified to serve as 'marker constituent(s)' reflective of the whole mixture. The ideal marker constituent would be readily measurable in the test product and in biological matrices and would not be cost-prohibitive. An exemplar dietary substance (GFJ) and test marker constituent (DHB) can

be evaluated using approaches taken from the pharmaceutical industry. Some of these methodologies include rodent models, in vitro testing and in silico predictions. While clinical evaluation is the definitive assessment of a dietary substance-drug interaction, certain measures should be taken to reduce the burden on sponsoring agencies to increase the throughput of dietary substance testing clinically. Despite the well-studied nature of GFJ in both the clinical and preclinical setting, there remain some gaps in current interaction risk knowledge and in methods to predict GFJ-drug interaction *a priori*. Recent restrictions on opioid prescribing may promote an alternate means of abuse, including pharmacokinetic boosting with GFJ. Methods to assess GFJ-opioid interaction potential are critical, since clinical studies with these drugs may be particularly challenging due to ethical concerns. As such, in vitro studies and IVIVE techniques must be well developed to accurately inform clinical studies. Furthermore, the trends of opioid abuse have prompted the need for tamper resistant opioids and novel naloxone formulations for which a human model to assess the reversal of opioids is lacking. Since dietary substances may promote the abuse of opioids or interact with the antidote (*i.e.,* naloxone), this dissertation will address these gaps in knowledge with the following specific aims:

Specific Aim 1: Develop robust in vitro methods to recover key kinetic parameters associated with DHB-mediated inhibition of loperamide metabolism.

Hypothesis: Human-derived in vitro systems will provide requisite kinetic parameters associated with the metabolism of loperamide in the absence and presence of DHB.

1a. Develop a rapid and sensitive LC/MS/MS method for the quantification of loperamide, the major CYP3A-mediated metabolite, *N*-desmethylloperamide, and

DHB in biological matrices.

1b. Determine enzyme kinetic parameters (K_m, V_{max}) of loperamide *N*-demethylation using established human enzyme systems (human intestinal microsomes, recombinant CYP3A enzymes).

1c. Determine the reversible (K_i) and mechanism-based (K_I, k_{inact}) inhibition kinetics of DHB toward *N*-desmethylloperamide formation using human intestinal microsomes.

Specific Aim 2: Predict the interaction risk of a GFJ with loperamide using a single marker constituent.

Hypothesis: A robust PBPK/PD model can be used to predict the likelihood and magnitude of an interaction between a GFJ and loperamide.

2a. Develop a PBPK/PD interaction model using kinetic parameters derived from Aim 1 and from the literature.

2b. Evaluate the PBPK model using existing in-house clinical data from a GFJ-loperamide study in which DHB was measured in the GFJ product.

2c. Simulate the PK and PD outcomes of a DHB supplement/GFJ-loperamide interaction under various DHB doses to emulate the rage found in dietary supplements, as well as with the therapeutic and maximum tolerated doses of loperamide.

Specific Aim 3: Evaluate the performance of a human model to assess the reversal of opioid effect.

Hypothesis: A human model using the model opioid, alfentanil, and the exemplar antagonist, naloxone can be used to test novel naloxone formulations.

3a. Design a proof-of-concept clinical study to assess the reversal of opioid effect in the

absence and presence of grapefruit juice.

3b. Implement a clinical study to assess the reversal of opioid effect by a novel naloxone formulation.

Table 1.1. Phase I and II pathways and bioavailability (F) of common opioids.

Opioid	Phase I	Phase II	F (%)[a]
Alfentanil[b]	CYP3A		30[c]
Codeine[d]	CYP2D6	UGT2B7	50±7
	CYP3A		
Fentanyl[e]	CYP3A		~50[b]
	CYP3A		
Hydrocodone[d]	CYP2D6	UGT1A3	
	CYP3A	UGT2B7	
Hydromorphone[d]		UGT1A3	42±23
		UGT2B7	
Loperamide[f]	CYP2B6		0.3[g]
	CYP2C8		
	CYP2D6		
	CYP3A4		
Methadone[d]	CYP2B6		92±21
	CYP2D6		
	CYP3A		
Morphine[d]	CYP3A	UGT2B7	24±12
Oxycodone[d]	CYP2D6		ER: 60-87
	CYP3A		IR:42±7
Oxymorphone[d]		UGT2B7	10[h]
Sufentanil[e]	CYP3A		
Tramadol[d]	CYP2D6		70-75[i]
Tropendtanol[i]	CYP2C9	UGT2B7	32[i]
	CYP2C19		
	CYP2D6		
	CYP3A		

IR, immediate release formulation;
ER, extended release formulation;
[a] Bioavailability reported in Goodman and Gilman's unless otherwise denoted (Brunton et al., 2010).
[b] Transdermal administration
[c] Bioavailability reported by Klees et al. (2005a)
[d] Metabolic pathway reported by Overholser and Foster (2011)
[e] Metabolic pathway reported by Guitton et al. (1997)
[f] Metabolic pathway reported by Kim et al. (2004)
[g] Bioavailability reported by Yu et al. (2004)
[h] Bioavailability reported by Davis (2005)
[I] Bioavailability reported by Brayfield (2011)

Table 1.2. Models to predict perpetrator or victim substance specific parameters.

Parameter	Site	Equation	Ref.
[I]			
	Intestinal	$I_g = \frac{D \times k_a \times f_a}{Q_{ent}}$	(Obach et al., 2006)
	Liver	$I_h = fu\left(I_{\max} \times \frac{D \times k_a \times f_a}{Q_h}\right)$	(Obach et al., 2006)
$Cl_{int,g}$	Intestine	$Cl\,\mathrm{int}_g = CLu_{\mathrm{int}} \times Content_{Enzyme}$	
F_g	Intestine	$F_g = \frac{Q_{villi}}{Q_{villi} + fu_g \times CLu_g\left(1 - \frac{Q_{villi}}{CL_{perm}}\right)}$	(Yang et al., 2007)

I_g, inhibitor concentration in the enterocyte; I_h, inhibitor concentration in the hepatocyte the hepatocyte; D, the oral dose of inhibitor; k_a, the first-order oral absorption rate constant of inhibitor; f_a, the fraction of dose of inhibitor absorbed into enterocytes; Q_{ent}, the enteric blood flow (may be interchanged with villous blood flow); f_u, fraction unbound in plasma or tissue; Q_h, hepatic blood flow; F_g, fraction of dose of drug/inhibitor escaping intestinal extraction; Q_{villi}, villous blood flow; $Clint_g$, intrinsic metabolic clearance in the gut; Fu_g, fraction of drug unbound in the enterocyte; CLu_g, the net intrinsic metabolic clearance in the gut based on unbound drug concentration; CL_{perm}, permeability clearance.

Table 1.3. Static models to assess drug interaction potential.

Model type	Mechanism of inhibition	Site of inhibition	Equation	Notes	Ref.
Simple static					
	Reversible	Liver	$R = \frac{I}{K_i} + 1$	R>1.1, possible	a
	Reversible	Liver	$R_i = \frac{I}{K_i}$ OR $R_i = \frac{C_{\max}}{K_i}$	R_i > 1, likely 1>R_i>0.1, possible R_i<0.1, unlikely	b
	Irreversible	Liver	$R_2 = \frac{\lambda}{k_{\deg}}$	R_2>1, likely 1>R_2>0.1, possible R_3<0.1, unlikely	c
	Irreversible	Liver	$R_3 = k_{inact} / K_I$	Assumes F_m = 1	
Mechanistic static					
	Reversible	Intestine	$\frac{AUC_i}{AUC} = \frac{1}{A_g \times (1 - F_g) + F_g}; A_g = \frac{1}{1 + \frac{I_g}{K_i}}$		f
	Reversible	Liver	$\frac{AUC_i}{AUC} = \frac{1}{A_h \times (1 - F_m) \times F_m}; A_h = \frac{1}{1 + \frac{I_h}{K_i}}$		f
	Irreversible	Intestine	$\frac{AUC_i}{AUC} = \frac{1}{B_g \times (1 - F_g) + F_g}; B_g = \frac{K_{\deg,g}}{K_{\deg,g} + \frac{I_g \times k_{inact}}{I_g + K_I}}$		f

Irreversible	Liver	$\frac{AUC_i}{AUC} = \frac{1 + \left(1 + \frac{\left(1 + \frac{IC_{50}^{-}}{IC_{50}^{+}} \right)}{k_{\deg} \times t} \right) \times Ln\left(\frac{2}{\left(1 + \frac{IC50_{50}^{+}}{IC_{50}^{-}} \right)} \right) \times \frac{I}{IC_{50}^{-}}}{1 + \frac{1}{IC_{50}^{-}}}$	From IC_{50} shift data	d
Irreversible	Liver	$\frac{AUC_i}{AUC} = \frac{1}{B_h \times (1 - F_m) \times F_m}; B_h = \frac{K_{\deg,h}}{K_{\deg,h} + \frac{I_h \times k_{inact}}{I_h + K_I}}$		
Irreversible	Intestine	$\frac{AUC_i}{AUC} = \frac{1}{\left(\frac{(1 - F_m)}{1 + \frac{I_g}{t_{inc} \times IC_{50}}} \right) + F_g}$	From IC_{50} shift data	E

Irreversible	Liver	$\frac{AUC_i}{AUC} = \frac{1}{\left(\frac{F_m}{1+\frac{I_h}{t_{inc} \times IC_{50}}}\right) + (1 - F_m)}$	From IC_{50} shift data	e
Combined	Combined	$\frac{AUC_i}{AUC} = \frac{1}{\left(\frac{F_m}{1+\frac{I_h}{t_{inc} \times IC_{50}}}\right) + (1 - F_m)} \times \frac{1}{F_g \times \left(\frac{(1-F_{g)}}{1+\left(\frac{I_g}{t_{inc} \times IC_{50}}\right.}\right.}$	From IC_{50} shift data	e
Combined	Intestine	$\frac{AUC_i}{AUC} = C_g = \frac{1}{[A_g \times B_g] \times (1 - F_g) + F_g}$		f
Combined	Liver	$\frac{AUC_i}{AUC} = C_h = \frac{1}{[A_h \times B_h] \times (1 - F_m) \times F_m}$		F
Combined	Combined	$\frac{AUC_i}{AUC} = C_g \times C_h$		F

R, value associated with drug interaction probability; I, inhibitor concentration; C_{max}, maximal observed or predicted inhibitor concentration; λ, first-order inactivation rate at a given MBI concentration; k_{deg}, degradation rate of enzyme; k_{inact}, maximal enzyme inactivation rate; K_I, concentration to elicit half-the maximal rate of enzyme inactivation; AUCi/AUC, the area under the victim drug plasma concentration-time curve in the presence of inhibitor over that in the absence of inhibitor; F_g, fraction of drug escaping intestinal extraction; f_m, fraction of victim drug metabolized; K_i, the reversible inhibition constant;IC_{50}, inhibitor concentration to elicit 50% of the maximal inhibition; the subscript 'h' denotes the term corresponds to the liver (hepatocyte); the subscript 'g' denotes the term refers to the gut (intestine); [a] US Food and Drug Administration (2012a); [b] Bjornsson et al. (2003); [c] Fujioka et al. (2012); [d] Sekiguchi et al. (2009); [e] (Obach et al., 2005; Obach et al., 2006; Obach et al., 2007); [f] Fahmi et al. (2009)

Table 1.4. Software packages for PBPK modeling.

Program	Provider	Link	Cost ($)
Free form			
acslX	AEgis Technologies Group	http://www.acslx.com	500-7,500
Berkeley Madonna		www.berkeleymadonna.com	69-299
Matlab (Simulink)	MathWorks®	www.mathworks.com	3,250
ModelMaker	ModelKinetix©	www.modelkinetix.com	233-770
Powersim Studio	PowerSim Software	http://www.powersim.com	99+
Preassembled			
BioDMET	General Electric	http://pdsl.research.ge.com	Beta is free
Gastroplus™	SimulationPlus, Inc	www.simulations-plus.com/Products	[a]
PK Sim®	Bayer Technology Services	www.systems-biology.com/products/pk-sim.html	[a]
Simbiology®	MathWorks®	http://www.mathworks.com/products/simbiology	3,250
Simcyp®	Certara	http://www.simcyp.com	[a]

[a] Quote available upon request; Cost varies on academic/industry and the number of licenses purchased.

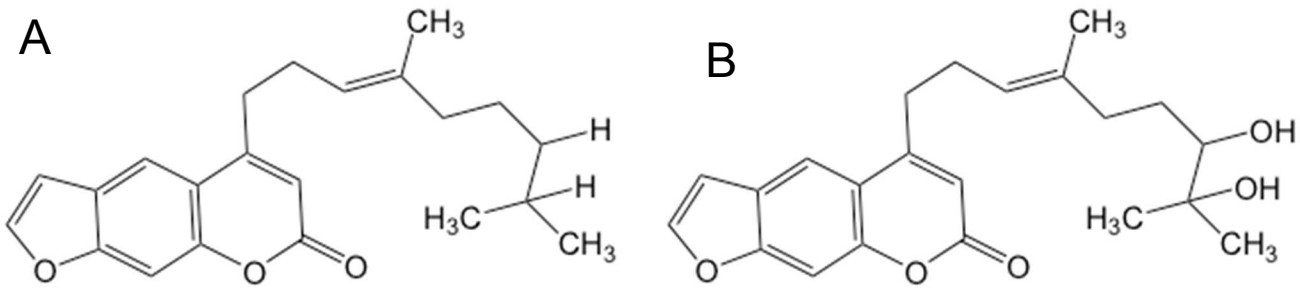

Figure 1.1. Furanocoumarin structures. Bergamottin (A) and 6',7'-dihydroxybergamottin (B).

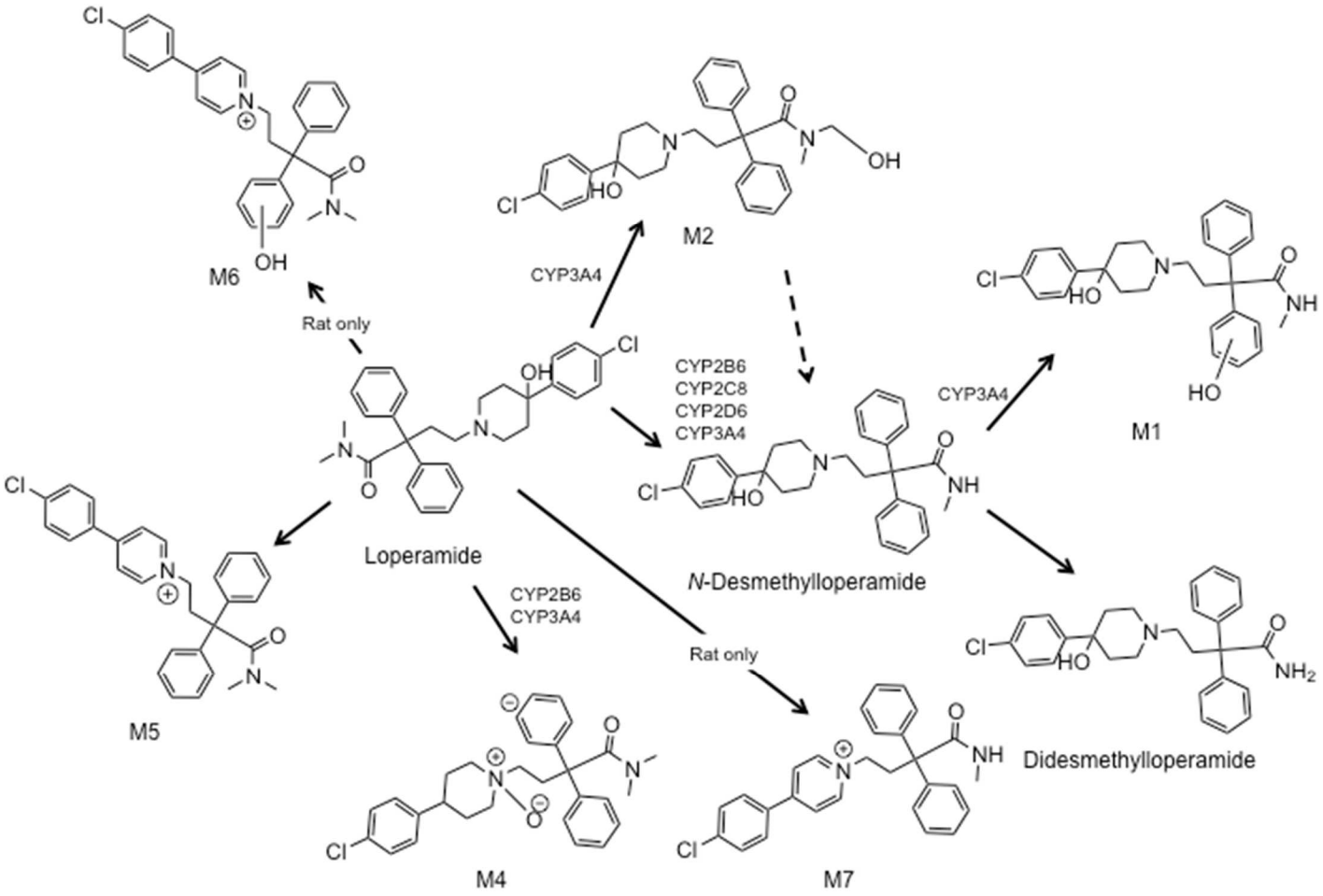

Figure 1.2. Loperamide metabolites in rat and human liver microsomes. Modified from Kalgutkar and Nguyen (2004) with additional evidence from Yoshida et al. (1979), Yu et al. (2004) and Kim et al. (2004).

REFERENCES

Abduljalil K, Jamei M, Rostami-Hodjegan A and Johnson TN (2014) Changes in individual drug-independent system parameters during virtual paediatric pharmacokinetic trials: introducing time-varying physiology into a paediatric PBPK model. *The AAPS journal* **16**:568-576.

Ainslie GR, Wolf KK, Li Y, Connolly EA, Scarlett YV, Hull JH and Paine MF (2014) Assessment of a Candidate Marker Constituent Predictive of a Dietary Substance-Drug Interaction: Case Study with Grapefruit Juice and CYP3A4 Drug Substrates. *J Pharmacol Exp Ther*.

Al Saabi A, Allorge D, Sauvage FL, Tournel G, Gaulier JM, Marquet P and Picard N (2013) Involvement of UDP-glucuronosyltransferases UGT1A9 and UGT2B7 in ethanol glucuronidation, and interactions with common drugs of abuse. *Drug Metab Dispos* **41**:568-574.

Andersen ME, Jones RA and Jenkins LJ, Jr. (1977) Enhancement of 1,1-dichloroethylene toxicity by pretreatment of fasted male rats with 2,3-epoxypropan-1-ol. *Drug and chemical toxicology* **1**:63-74.

Andersen ME, French JE, Gargas ML, Jones RA and Jenkins LJ, Jr. (1979) Saturable metabolism and the acute toxicity of 1,1-dichloroethylene. *Toxicol Appl Pharmacol* **47**:385-393.

Bachler G, von Goetz N and Hungerbuhler K (2014) Using physiologically based pharmacokinetic (PBPK) modeling for dietary risk assessment of titanium dioxide (TiO) nanoparticles. *Nanotoxicology*:1-8.

Bailey DG, Dresser GK and Bend JR (2003) Bergamottin, lime juice, and red wine as inhibitors of cytochrome P450 3A4 activity: comparison with grapefruit juice. *Clin Pharmacol Ther* **73**:529-537.

Bailey DG and Dresser GK (2004) Interactions between grapefruit juice and cardiovascular drugs. *Am J Cardiovasc Drugs* **4**:281-297.

Bailey DG, Dresser G and Arnold JM (2013) Grapefruit-medication interactions: Forbidden fruit or avoidable consequences? *CMAJ* **185**:309-316.

Barton ED, Ramos J, Colwell C, Benson J, Baily J and Dunn W (2002) Intranasal administration of naloxone by paramedics. *Prehospital emergency care : official journal of the National Association of EMS Physicians and the National Association of State EMS Directors* **6**:54-58.

Benetton SA, Borges VM, Chang TK and McErlane KM (2004) Role of individual human cytochrome P450 enzymes in the in vitro metabolism of hydromorphone. *Xenobiotica* **34**:335-344.

Benmebarek M, Devaud C, Gex-Fabry M, Powell Golay K, Brogli C, Baumann P, Gravier B and Eap CB (2004) Effects of grapefruit juice on the pharmacokinetics of the enantiomers of methadone. *Clin Pharmacol Ther* **76**:55-63.

Bjornsson TD, Callaghan JT, Einolf HJ, Fischer V, Gan L, Grimm S, Kao J, King SP, Miwa G, Ni L, Kumar G, McLeod J, Obach RS, Roberts S, Roe A, Shah A, Snikeris F, Sullivan JT, Tweedie D, Vega JM, Walsh J, Wrighton SA, Pharmaceutical R, Manufacturers of America Drug Metabolism/Clinical Pharmacology Technical Working G, Evaluation FDACfD and Research (2003) The conduct of in vitro and in vivo drug-drug interaction studies: a Pharmaceutical Research and Manufacturers of America (PhRMA) perspective. *Drug Metab Dispos* **31**:815-832.

Bluelight (2014a) in, vBulletin.

Bluelight (2014b) What is it in grapfruit juice tht potentiates opioids?, in, vBulletin.

Brayfield A (2011) Martindale: The Complete Drug Reference, in *Tapentadol hydrochloride: a novel analgesic* (Brayfeild A ed), Pharmaceutical Press.

Brunton LL, Chabner BA and Knollmann BC (2010) Appendix II, in *Goodman & Gilman's: The Pharmalogical Basis of Therapeutics* (Brunton L ed), McGraw Hill Medical.

Chakraborty M, Kamath JV and Bhattacharjee A (2014) Pharmacodynamic Interaction of Green Tea Extract with Hydrochlorothiazide against Cyclophosphamide-Induced Myocardial Damage. *Toxicology international* **21**:196-202.

Charnick SB, Kawai R, Nedelman JR, Lemaire M, Niederberger W and Sato H (1995) Perspectives in pharmacokinetics. Physiologically based pharmacokinetic modeling as a tool for drug development. *J Pharmacokinet Biopharm* **23**:217-229.

Chen Y, Mao J and Hop CE (2014) Physiologically Based Pharmacokinetic Modeling to Predict Drug-Drug Interactions Involving Inhibitory Metabolite - A Case Study of Amiodarone. *Drug Metab Dispos*.

Cheng Y and Prusoff WH (1973) Relationship between the inhibition constant (K1) and the concentration of inhibitor which causes 50 per cent inhibition (I50) of an enzymatic reaction. *Biochem Pharmacol* **22**:3099-3108.

Clarke G, Stilling RM, Kennedy PJ, Stanton C, Cryan JF and Dinan TG (2014) Minireview: Gut microbiota: the neglected endocrine organ. *Molecular endocrinology* **28**:1221-1238.

Clewell HJ, 3rd and Andersen ME (1985) Risk assessment extrapolations and physiological modeling. *Toxicology and industrial health* **1**:111-131.

Cohen EE, Wu K, Hartford C, Kocherginsky M, Eaton KN, Zha Y, Nallari A, Maitland ML, Fox-Kay K, Moshier K, House L, Ramirez J, Undevia SD, Fleming GF, Gajewski TF and Ratain MJ (2012) Phase I studies of sirolimus alone or in combination with pharmacokinetic modulators in advanced cancer patients. *Clinical cancer research : an official journal of the American Association for Cancer Research* **18**:4785-4793.

Costa R, Russo M, De Grazia S, Grasso E, Dugo P and Mondello L (2014) Thorough investigation of the oxygen heterocyclic fraction of lime (Citrus aurantifolia (Christm.) Swingle) juice. *Journal of separation science* **37**:792-797.

Cristofoletti R and Dressman JB (2014) Use of physiologically based pharmacokinetic models coupled with pharmacodynamic models to assess the clinical relevance of current bioequivalence criteria for generic drug products containing Ibuprofen. *J Pharm Sci* **103**:3263-3275.

Daniulaityte R, Carlson R, Falck R, Cameron D, Perera S, Chen L and Sheth A (2013) "I just wanted to tell you that loperamide WILL WORK": a web-based study of extra-medical use of loperamide. *Drug Alcohol Depend* **130**:241-244.

Davis MG, PA; Hardy, J (2005) *Opioids in Cancer Pain* Oxford, UK: Oxford University Press.

de Lima Toccafondo Vieira M and Huang SM (2012) Botanical-drug interactions: a scientific perspective. *Planta Med* **78**:1400-1415.

Dedrick RL, Forrester DD, Cannon JN, el-Dareer SM and Mellett LB (1973) Pharmacokinetics of 1-beta-D-arabinofuranosylcytosine (ARA-C) deamination in several species. *Biochem Pharmacol* **22**:2405-2417.

Di YM, Li CG, Xue CC and Zhou SF (2008) Clinical drugs that interact with St. John's wort and implication in drug development. *Current pharmaceutical design* **14**:1723-1742.

Dix DJ, Houck KA, Martin MT, Richard AM, Setzer RW and Kavlock RJ (2007) The ToxCast program for prioritizing toxicity testing of environmental chemicals. *Toxicological sciences : an official journal of the Society of Toxicology* **95**:5-12.

Dowling J, Isbister GK, Kirkpatrick CM, Naidoo D and Graudins A (2008) Population pharmacokinetics of intravenous, intramuscular, and intranasal naloxone in human volunteers. *Therapeutic drug monitoring* **30**:490-496.

Dreier JP and Endres M (2004) Statin-associated rhabdomyolysis triggered by grapefruit consumption. *Neurology* **62**:670.

Eagling VA, Profit L and Back DJ (1999) Inhibition of the CYP3A4-mediated metabolism and P-glycoprotein-mediated transport of the HIV-1 protease inhibitor saquinavir by grapefruit juice components. *Br J Clin Pharmacol* **48**:543-552.

Egan TD, Minto CF, Hermann DJ, Barr J, Muir KT and Shafer SL (1996) Remifentanil versus alfentanil: comparative pharmacokinetics and pharmacodynamics in healthy adult male volunteers. *Anesthesiology* **84**:821-833.

Eichbaum C, Mathes K, Burhenne J, Markert C, Blank A and Mikus G (2014) Presystemic Elimination of Tilidine: Localisation and Consequences for the Formation of the Active Metabolite Nortilidine. *Basic Clin Pharmacol Toxicol*.

European Medicines Agency: Committee for Human Medical Products (2012) Guidline on the Investigation of Drug Interactions.

Fahmi OA, Hurst S, Plowchalk D, Cook J, Guo F, Youdim K, Dickins M, Phipps A, Darekar A, Hyland R and Obach RS (2009) Comparison of different algorithms for predicting clinical drug-drug interactions, based on the use of CYP3A4 in vitro data: predictions of compounds as precipitants of interaction. *Drug Metab Dispos* **37**:1658-1666.

Fanni D, Ambu R, Gerosa C, Nemolato S, Castagnola M, Van Eyken P, Faa G and Fanos V (2014) Cytochrome P450 genetic polymorphism in neonatal drug metabolism: role and practical consequences towards a new drug culture in neonatology. *International journal of immunopathology and pharmacology* **27**:5-13.

Fletcher J (2014) Canada in breach of ethical standards for clinical trials. *CMAJ* **186**:11.

Fontana RJ, Lown KS, Paine MF, Fortlage L, Santella RM, Felton JS, Knize MG, Greenberg A and Watkins PB (1999) Effects of a chargrilled meat diet on expression of CYP3A, CYP1A, and P-glycoprotein levels in healthy volunteers. *Gastroenterology* **117**:89-98.

Fowler S and Zhang H (2008) In vitro evaluation of reversible and irreversible cytochrome P450 inhibition: current status on methodologies and their utility for predicting drug-drug interactions. *The AAPS journal* **10**:410-424.

Foxenberg RJ, Ellison CA, Knaak JB, Ma C and Olson JR (2011) Cytochrome P450-specific human PBPK/PD models for the organophosphorus pesticides: chlorpyrifos and parathion. *Toxicology* **285**:57-66.

Fujioka Y, Kunze KL and Isoherranen N (2012) Risk assessment of mechanism-based inactivation in drug-drug interactions. *Drug Metab Dispos* **40**:1653-1657.

Gertz M, Harrison A, Houston JB and Galetin A (2010) Prediction of human intestinal first-pass metabolism of 25 CYP3A substrates from in vitro clearance and permeability data. *Drug Metab Dispos* **38**:1147-1158.

Gill KL, Houston JB and Galetin A (2012) Characterization of in vitro glucuronidation clearance of a range of drugs in human kidney microsomes: comparison with

liver and intestinal glucuronidation and impact of albumin. *Drug Metab Dispos* **40**:825-835.

Glaser A, Arakaki D, Chan GM and Hoffman RS (2005) Randomised trial of intranasal versus intramuscular naloxone in prehospital treatment for suspected opioid overdose. *The Medical journal of Australia* **182**:427; author reply 427, 429.

Goosen TC, Cillie D, Bailey DG, Yu C, He K, Hollenberg PF, Woster PM, Cohen L, Williams JA, Rheeders M and Dijkstra HP (2004) Bergamottin contribution to the grapefruit juice-felodipine interaction and disposition in humans. *Clin Pharmacol Ther* **76**:607-617.

Gorgus E, Lohr C, Raquet N, Guth S and Schrenk D (2010) Limettin and furocoumarins in beverages containing citrus juices or extracts. *Food and chemical toxicology : an international journal published for the British Industrial Biological Research Association* **48**:93-98.

Graf JF, Scholz BJ and Zavodszky MI (2012) BioDMET: a physiologically based pharmacokinetic simulation tool for assessing proposed solutions to complex biological problems. *Journal of pharmacokinetics and pharmacodynamics* **39**:37-54.

Grime KH, Bird J, Ferguson D and Riley RJ (2009) Mechanism-based inhibition of cytochrome P450 enzymes: an evaluation of early decision making in vitro approaches and drug-drug interaction prediction methods. *European journal of pharmaceutical sciences : official journal of the European Federation for Pharmaceutical Sciences* **36**:175-191.

Grimm SW, Einolf HJ, Hall SD, He K, Lim HK, Ling KH, Lu C, Nomeir AA, Seibert E, Skordos KW, Tonn GR, Van Horn R, Wang RW, Wong YN, Yang TJ and Obach RS (2009) The conduct of in vitro studies to address time-dependent inhibition of drug-metabolizing enzymes: a perspective of the pharmaceutical research and manufacturers of America. *Drug Metab Dispos* **37**:1355-1370.

Groer C, Busch D, Patrzyk M, Beyer K, Busemann A, Heidecke CD, Drozdzik M, Siegmund W and Oswald S (2014) Absolute protein quantification of clinically relevant cytochrome P450 enzymes and UDP-glucuronosyltransferases by mass spectrometry-based targeted proteomics. *J Pharm Biomed Anal* **100**:393-401.

Grun B, Merkel U, Riedel KD, Weiss J and Mikus G (2012) Contribution of CYP2C19 and CYP3A4 to the formation of the active nortilidine from the prodrug tilidine. *Br J Clin Pharmacol* **74**:854-863.

Gufford BT, Chen G, Lazarus P, Graf TN, Oberlies NH and Paine MF (2014) Identification of diet-derived constituents as potent inhibitors of intestinal glucuronidation. *Drug Metab Dispos* **42**:1675-1683.

Guitton J, Buronfosse T, Desage M, Lepape A, Brazier JL and Beaune P (1997) Possible involvement of multiple cytochrome P450S in fentanyl and sufentanil metabolism as opposed to alfentanil. *Biochem Pharmacol* **53**:1613-1619.

Guo LQ, Taniguchi M, Xiao YQ, Baba K, Ohta T and Yamazoe Y (2000a) Inhibitory effect of natural furanocoumarins on human microsomal cytochrome P450 3A activity. *Japanese journal of pharmacology* **82**:122-129.

Guo LQ, Fukuda K, Ohta T and Yamazoe Y (2000b) Role of furanocoumarin derivatives on grapefruit juice-mediated inhibition of human CYP3A activity. *Drug Metab Dispos* **28**:766-771.

Guth S, Habermeyer M, Schrenk D and Eisenbrand G (2011) Update of the toxicological assessment of furanocoumarins in foodstuffs (Update of the SKLM statement of 23/24 September 2004)--Opinion of the Senate Commission on Food Safety (SKLM) of the German Research Foundation (DFG). *Molecular nutrition & food research* **55**:807-810.

Handal M, Ripel A, Aasmundstad T, Skurtveit S and Morland J (2007) Morphine-3-glucuronide inhibits morphine induced, but enhances morphine-6-glucuronide induced locomotor activity in mice. *Pharmacology, biochemistry, and behavior* **86**:576-586.

Hara N and Nishiyama T (2014) Androgen Metabolic Pathway Involved in Current and Emerging Treatment for Men with Castration Resistant Prostate Cancer: Intraprostatic Androgens as Therapeutic Targets and Endocrinological Biomarkers. *Current drug targets*.

Haynes RC (2010) ToxCast on target: in vitro assays and computer modeling show promise for screening chemicals. *Environmental health perspectives* **118**:A172.

Health Canada (2011) Guidance Document for Industry- Reporting Adverse Reactions to Marketed Health Products. Health Canada, Ottawa, Ontario., in.

Heard C, Creighton P and Lerman J (2009) Intranasal flumazenil and naloxone to reverse over-sedation in a child undergoing dental restorations. *Paediatric anaesthesia* **19**:795-797; discussion 798-799.

Hinderliter PM, Price PS, Bartels MJ, Timchalk C and Poet TS (2011) Development of a source-to-outcome model for dietary exposures to insecticide residues: an example using chlorpyrifos. *Regul Toxicol Pharmacol* **61**:82-92.

Ho RH and Kim RB (2005) Transporters and drug therapy: implications for drug disposition and disease. *Clin Pharmacol Ther* **78**:260-277.

Huffman DH, Wan SH, Azarnoff DL and Hogstraten B (1973) Pharmacokinetics of methotrexate. *Clin Pharmacol Ther* **14**:572-579.

Hutchinson MR, Menelaou A, Foster DJ, Coller JK and Somogyi AA (2004) CYP2D6 and CYP3A4 involvement in the primary oxidative metabolism of hydrocodone by human liver microsomes. *Br J Clin Pharmacol* **57**:287-297.

Ide K, Park M and Yamada H (2014) The effect of green tea with exceptionally high catechin content on nadolol plasma concentration. *Clin Pharmacol Ther* **95**:588.

Iribarne C, Picart D, Dreano Y, Bail JP and Berthou F (1997) Involvement of cytochrome P450 3A4 in N-dealkylation of buprenorphine in human liver microsomes. *Life sciences* **60**:1953-1964.

Iribarne C, Berthou F, Carlhant D, Dreano Y, Picart D, Lohezic F and Riche C (1998) Inhibition of methadone and buprenorphine N-dealkylations by three HIV-1 protease inhibitors. *Drug Metab Dispos* **26**:257-260.

Jaiswal S, Sharma A, Shukla M, Vaghasiya K, Rangaraj N and Lal J (2014) Novel pre-clinical methodologies for pharmacokinetic drug-drug interaction studies: spotlight on "humanized" animal models. *Drug metabolism reviews*:1-19.

Jiang XL, Zhao P, Barrett JS, Lesko LJ and Schmidt S (2013) Application of physiologically based pharmacokinetic modeling to predict acetaminophen metabolism and pharmacokinetics in children. *CPT Pharmacometrics Syst Pharmacol* **2**:e80.

Johnson FK, Stark JG, Bieberdorf FA and Stauffer J (2010) Relative oral bioavailability of morphine and naltrexone derived from crushed morphine sulfate and naltrexone hydrochloride extended-release capsules versus intact product and versus naltrexone solution: a single-dose, randomized-sequence, open-label, three-way crossover trial in healthy volunteers. *Clinical therapeutics* **32**:1149-1164.

Kalgutkar AS and Nguyen HT (2004) Identification of an N-methyl-4-phenylpyridinium-like metabolite of the antidiarrheal agent loperamide in human liver microsomes: underlying reason(s) for the lack of neurotoxicity despite the bioactivation event. *Drug Metab Dispos* **32**:943-952.

Kalgutkar AS, Obach RS and Maurer TS (2007) Mechanism-based inactivation of cytochrome P450 enzymes: chemical mechanisms, structure-activity relationships and relationship to clinical drug-drug interactions and idiosyncratic adverse drug reactions. *Curr Drug Metab* **8**:407-447.

Karch AM (2004) The grapefruit challenge: the juice inhibits a crucial enzyme, with possibly fatal consequences. *Am J Nurs* **104**:33-35.

Kent UM, Lin HL, Noon KR, Harris DL and Hollenberg PF (2006) Metabolism of bergamottin by cytochromes P450 2B6 and 3A5. *J Pharmacol Exp Ther* **318**:992-1005.

Kharasch ED, Walker A, Hoffer C and Sheffels P (2004a) Intravenous and oral alfentanil as in vivo probes for hepatic and first-pass cytochrome P450 3A activity: noninvasive assessment by use of pupillary miosis. *Clin Pharmacol Ther* **76**:452-466.

Kharasch ED, Hoffer C, Whittington D and Sheffels P (2004b) Role of hepatic and intestinal cytochrome P450 3A and 2B6 in the metabolism, disposition, and miotic effects of methadone. *Clin Pharmacol Ther* **76**:250-269.

Kharasch ED, Walker A, Isoherranen N, Hoffer C, Sheffels P, Thummel K, Whittington D and Ensign D (2007) Influence of CYP3A5 genotype on the pharmacokinetics and pharmacodynamics of the cytochrome P4503A probes alfentanil and midazolam. *Clin Pharmacol Ther* **82**:410-426.

Kharasch ED, Vangveravong S, Buck N, London A, Kim T, Blood J and Mach RH (2011) Concurrent assessment of hepatic and intestinal cytochrome P450 3A activities using deuterated alfentanil. *Clin Pharmacol Ther* **89**:562-570.

Kim KA, Chung J, Jung DH and Park JY (2004) Identification of cytochrome P450 isoforms involved in the metabolism of loperamide in human liver microsomes. *Eur J Clin Pharmacol* **60**:575-581.

Kimura S, Kako S, Wada H, Sakamoto K, Ashizawa M, Sato M, Terasako K, Kikuchi M, Nakasone H, Okuda S, Yamazaki R, Oshima K, Nishida J, Watanabe T and Kanda Y (2011) Can grapefruit juice decrease the cost of imatinib for the treatment of chronic myelogenous leukemia? *Leukemia research* **35**:e11-12.

Klees TM, Sheffels P, Dale O and Kharasch ED (2005a) Metabolism of alfentanil by cytochrome p4503a (cyp3a) enzymes. *Drug Metab Dispos* **33**:303-311.

Klees TM, Sheffels P, Thummel KE and Kharasch ED (2005b) Pharmacogenetic determinants of human liver microsomal alfentanil metabolism and the role of cytochrome P450 3A5. *Anesthesiology* **102**:550-556.

Kleman M and Gustafsson JA (1996) Interactions of procarcinogenic heterocyclic amines and indolocarbazoles with the dioxin receptor. *Biol Chem* **377**:741-762.

Klimas R and Mikus G (2014) Morphine-6-glucuronide is responsible for the analgesic effect after morphine administration: a quantitative review of morphine, morphine-6-glucuronide, and morphine-3-glucuronide. *British journal of anaesthesia*.

Knaak JB, Dary CC, Zhang X, Gerlach RW, Tornero-Velez R, Chang DT, Goldsmith R and Blancato JN (2012) Parameters for pyrethroid insecticide QSAR and PBPK/PD models for human risk assessment. *Reviews of environmental contamination and toxicology* **219**:1-114.

Kosugi Y, Hirabayashi H, Igari T, Fujioka Y, Hara Y, Okuda T and Moriwaki T (2012) Evaluation of cytochrome P450-mediated drug-drug interactions based on the strategies recommended by regulatory authorities. *Xenobiotica* **42**:127-138.

Langlitz N, Schotte K and Bschor T (2001) [Loperamide abuse in anxiety disorder]. *Der Nervenarzt* **72**:562-564.

Lenton S, Dietze P, Olsen A, Wiggins N, McDonald D and Fowlie C (2014) Working together: Expanding the availability of naloxone for peer administration to prevent opioid overdose deaths in the Australian Capital Territory and beyond. *Drug and alcohol review*.

Li J, Guo HF, Liu C, Zhong Z, Liu L and Liu XD (2014) Prediction of Drug Disposition in Diabetic Patients by Means of a Physiologically Based Pharmacokinetic Model. *Clin Pharmacokinet*.

Lin JH and Lu AY (1998) Inhibition and induction of cytochrome P450 and the clinical implications. *Clin Pharmacokinet* **35**:361-390.

Lin Z, Fisher JW, Wang R, Ross MK and Filipov NM (2013) Estimation of placental and lactational transfer and tissue distribution of atrazine and its main metabolites in rodent dams, fetuses, and neonates with physiologically based pharmacokinetic modeling. *Toxicol Appl Pharmacol* **273**:140-158.

Ling MP and Liao CM (2009) A human PBPK/PD model to assess arsenic exposure risk through farmed tilapia consumption. *Bulletin of environmental contamination and toxicology* **83**:108-114.

Liu C, Shang YF, Zhang XF, Zhang XG, Wang B, Wu Z, Liu XM, Yu L, Ma F and Lv Y (2009) Co-administration of grapefruit juice increases bioavailability of tacrolimus in liver transplant patients: a prospective study. *Eur J Clin Pharmacol* **65**:881-885.

Lown KS, Bailey DG, Fontana RJ, Janardan SK, Adair CH, Fortlage LA, Brown MB, Guo W and Watkins PB (1997) Grapefruit juice increases felodipine oral availability in humans by decreasing intestinal CYP3A protein expression. *J Clin Invest* **99**:2545-2553.

Lu C, Suri A, Shyu WC and Prakash S (2014) Assessment of cytochrome P450-mediated drug-drug interaction potential of orteronel and exposure changes in patients with renal impairment using physiologically based pharmacokinetic modeling and simulation. *Biopharm Drug Dispos*.

Misaka S, Miyazaki N, Yatabe MS, Ono T, Shikama Y, Fukushima T and Kimura J (2013) Pharmacokinetic and pharmacodynamic interaction of nadolol with itraconazole, rifampicin and grapefruit juice in healthy volunteers. *Journal of clinical pharmacology* **53**:738-745.

Morliere P, Huppe G, Averbeck D, Young AR, Santus R and Dubertret L (1990) In vitro photostability and photosensitizing properties of bergamot oil. Effects of a cinnamate sunscreen. *Journal of photochemistry and photobiology B, Biology* **7**:199-208.

National Center for Complementary and Alternative Medicine (2013) Dietary Supplement-Drug Interaction Expert Panel Meeting. *9000 Rockville Pike, Bethesda, Maryland 20892*.

Niemi M, Tornio A, Pasanen MK, Fredrikson H, Neuvonen PJ and Backman JT (2006) Itraconazole, gemfibrozil and their combination markedly raise the plasma concentrations of loperamide. *Eur J Clin Pharmacol* **62**:463-472.

Nieminen TH, Hagelberg NM, Saari TI, Neuvonen M, Neuvonen PJ, Laine K and Olkkola KT (2010) Grapefruit juice enhances the exposure to oral oxycodone. *Basic Clin Pharmacol Toxicol* **107**:782-788.

Nilsson MI, Meresaar U and Anggard E (1982) Clinical pharmacokinetics of methadone. *Acta anaesthesiologica Scandinavica Supplementum* **74**:66-69.

Obach RS, Walsky RL, Venkatakrishnan K, Houston JB and Tremaine LM (2005) In vitro cytochrome P450 inhibition data and the prediction of drug-drug interactions: qualitative relationships, quantitative predictions, and the rank-order approach. *Clin Pharmacol Ther* **78**:582-592.

Obach RS, Walsky RL, Venkatakrishnan K, Gaman EA, Houston JB and Tremaine LM (2006) The utility of in vitro cytochrome P450 inhibition data in the prediction of drug-drug interactions. *J Pharmacol Exp Ther* **316**:336-348.

Obach RS, Walsky RL and Venkatakrishnan K (2007) Mechanism-based inactivation of human cytochrome p450 enzymes and the prediction of drug-drug interactions. *Drug Metab Dispos* **35**:246-255.

Oda K, Yamaguchi Y, Yoshimura T, Wada K and Nishizono N (2007) Synthetic models related to furanocoumarin-CYP 3A4 interactions. comparison of furanocoumarin, coumarin, and benzofuran dimers as potent inhibitors of CYP3A4 activity. *Chemical & pharmaceutical bulletin* **55**:1419-1421.

Okura T, Ozawa T, Ito Y, Kimura M, Kagawa Y and Yamada S (2008) Enhancement by grapefruit juice of morphine antinociception. *Biological & pharmaceutical bulletin* **31**:2338-2341.

Osborne R, Thompson P, Joel S, Trew D, Patel N and Slevin M (1992) The analgesic activity of morphine-6-glucuronide. *Br J Clin Pharmacol* **34**:130-138.

Overholser BR and Foster DR (2011) Opioid pharmacokinetic drug-drug interactions. *The American journal of managed care* **17 Suppl 11**:S276-287.

Paine MF, Criss AB and Watkins PB (2004) Two major grapefruit juice components differ in intestinal CYP3A4 inhibition kinetic and binding properties. *Drug Metab Dispos* **32**:1146-1153.

Paine MF, Criss AB and Watkins PB (2005) Two major grapefruit juice components differ in time to onset of intestinal CYP3A4 inhibition. *J Pharmacol Exp Ther* **312**:1151-1160.

Paine MF, Hart HL, Ludington SS, Haining RL, Rettie AE and Zeldin DC (2006) The human intestinal cytochrome P450 "pie". *Drug Metab Dispos* **34**:880-886.

Paine MF and Oberlies NH (2007) Clinical relevance of the small intestine as an organ of drug elimination: drug-fruit juice interactions. *Expert Opin Drug Metab Toxicol* **3**:67-80.

Paine MF, Widmer WW, Pusek SN, Beavers KL, Criss AB, Snyder J and Watkins PB (2008) Further characterization of a furanocoumarin-free grapefruit juice on drug disposition: studies with cyclosporine. *Am J Clin Nutr* **87**:863-871.

Poet TS, Timchalk C, Hotchkiss JA and Bartels MJ (2014) Chlorpyrifos PBPK/PD model for multiple routes of exposure. *Xenobiotica* **44**:868-881.

Prasad B, Evers R, Gupta A, Hop CE, Salphati L, Shukla S, Ambudkar SV and Unadkat JD (2014) Interindividual variability in hepatic organic anion-transporting polypeptides and P-glycoprotein (ABCB1) protein expression: quantification by liquid chromatography tandem mass spectroscopy and influence of genotype, age, and sex. *Drug Metab Dispos* **42**:78-88.

Reif S, Nicolson MC, Bisset D, Reid M, Kloft C, Jaehde U and McLeod HL (2002) Effect of grapefruit juice intake on etoposide bioavailability. *Eur J Clin Pharmacol* **58**:491-494.

Riley RJ, Grime K and Weaver R (2007) Time-dependent CYP inhibition. *Expert Opin Drug Metab Toxicol* **3**:51-66.

Rioux N, Bellavance E, Bourg S, Garneau M, Ribadeneira MD and Duan J (2013) Assessment of CYP3A-mediated drug-drug interaction potential for victim drugs using an in vivo rat model. *Biopharm Drug Dispos* **34**:396-401.

Row E, Brown SA, Stachulski AV and Lennard MS (2006) Development of novel furanocoumarin dimers as potent and selective inhibitors of CYP3A4. *Drug Metab Dispos* **34**:324-330.

Rowland M (2013) Physiologically-Based Pharmacokinetic (PBPK) Modeling and Simulations Principles, Methods, and Applications in the Pharmaceutical Industry. *CPT Pharmacometrics Syst Pharmacol* **2**:e55.

Schmitt W and Willmann S (2005) Physiology-based pharmacokinetic modeling: ready to be used. *Drug discovery today Technologies* **2**:125-132.

Scholz J, Steinfath M and Schulz M (1996) Clinical pharmacokinetics of alfentanil, fentanyl and sufentanil. An update. *Clin Pharmacokinet* **31**:275-292.

Schubert W, Cullberg G, Edgar B and Hedner T (1994) Inhibition of 17 beta-estradiol metabolism by grapefruit juice in ovariectomized women. *Maturitas* **20**:155-163.

Schuhmacher M, Fabrega F, Kumar V, Garcia F, Nadal M and Domingo JL (2014) A PBPK model to estimate PCDD/F levels in adipose tissue: Comparison with experimental values of residents near a hazardous waste incinerator. *Environment international* **73**:150-157.

Sekiguchi N, Higashida A, Kato M, Nabuchi Y, Mitsui T, Takanashi K, Aso Y and Ishigai M (2009) Prediction of drug-drug interactions based on time-dependent inhibition from high throughput screening of cytochrome P450 3A4 inhibition. *Drug Metab Pharmacokinet* **24**:500-510.

Shimada T, Yamazaki H, Mimura M, Inui Y and Guengerich FP (1994) Interindividual variations in human liver cytochrome P-450 enzymes involved in the oxidation of drugs, carcinogens and toxic chemicals: studies with liver microsomes of 30 Japanese and 30 Caucasians. *J Pharmacol Exp Ther* **270**:414-423.

Shou M, Lin Y, Lu P, Tang C, Mei Q, Cui D, Tang W, Ngui JS, Lin CC, Singh R, Wong BK, Yergey JA, Lin JH, Pearson PG, Baillie TA, Rodrigues AD and Rushmore TH (2001) Enzyme kinetics of cytochrome P450-mediated reactions. *Curr Drug Metab* **2**:17-36.

Sinha VK, Snoeys J, Osselaer NV, Peer AV, Mackie C and Heald D (2012) From preclinical to human--prediction of oral absorption and drug-drug interaction potential using physiologically based pharmacokinetic (PBPK) modeling approach in an industrial setting: a workflow by using case example. *Biopharm Drug Dispos* **33**:111-121.

Sipes NS, Martin MT, Kothiya P, Reif DM, Judson RS, Richard AM, Houck KA, Dix DJ, Kavlock RJ and Knudsen TB (2013) Profiling 976 ToxCast chemicals across 331 enzymatic and receptor signaling assays. *Chemical research in toxicology* **26**:878-895.

Skarke C, Jarrar M, Schmidt H, Kauert G, Langer M, Geisslinger G and Lotsch J (2003) Effects of ABCB1 (multidrug resistance transporter) gene mutations on disposition and central nervous effects of loperamide in healthy volunteers. *Pharmacogenetics* **13**:651-660.

Sklerov J, Levine B, Moore KA, Allan C and Fowler D (2005) Tissue distribution of loperamide and N-desmethylloperamide following a fatal overdose. *J Anal Toxicol* **29**:750-754.

Smith JN, Hinderliter PM, Timchalk C, Bartels MJ and Poet TS (2014) A human life-stage physiologically based pharmacokinetic and pharmacodynamic model for chlorpyrifos: development and validation. *Regul Toxicol Pharmacol* **69**:580-597.

Smith K, Hopp M, Mundin G, Bond S, Bailey P, Woodward J and Bell D (2012) Low absolute bioavailability of oral naloxone in healthy subjects. *International journal of clinical pharmacology and therapeutics* **50**:360-367.

Smith LJ (2008) How ethical is ethical research? Recruiting marginalized, vulnerable groups into health services research. *Journal of advanced nursing* **62**:248-257.

Song IS, Kong TY, Jeong HU, Kim EN, Kwon SS, Kang HE, Choi SZ, Son M and Lee HS (2014) Evaluation of the transporter-mediated herb-drug interaction potential of DA-9801, a standardized dioscorea extract for diabetic neuropathy, in human in vitro and rat in vivo. *BMC complementary and alternative medicine* **14**:251.

Stanos SP, Bruckenthal P and Barkin RL (2012) Strategies to reduce the tampering and subsequent abuse of long-acting opioids: potential risks and benefits of formulations with physical or pharmacologic deterrents to tampering. *Mayo Clin Proc* **87**:683-694.

Suemizu H, Sota S, Kuronuma M, Shimizu M and Yamazaki H (2014) Pharmacokinetics and effects on serum cholinesterase activities of organophosphorus pesticides acephate and chlorpyrifos in chimeric mice transplanted with human hepatocytes. *Regul Toxicol Pharmacol* **70**:468-473.

Sugimoto K, Araki N, Ohmori M, Harada K, Cui Y, Tsuruoka S, Kawaguchi A and Fujimura A (2006) Interaction between grapefruit juice and hypnotic drugs: comparison of triazolam and quazepam. *Eur J Clin Pharmacol* **62**:209-215.

Tan YM, Clewell H, Campbell J and Andersen M (2011) Evaluating pharmacokinetic and pharmacodynamic interactions with computational models in supporting cumulative risk assessment. *International journal of environmental research and public health* **8**:1613-1630.

Tassaneeyakul W, Guo LQ, Fukuda K, Ohta T and Yamazoe Y (2000) Inhibition selectivity of grapefruit juice components on human cytochromes P450. *Archives of biochemistry and biophysics* **378**:356-363.

Tayrouz Y, Ganssmann B, Ding R, Klingmann A, Aderjan R, Burhenne J, Haefeli WE and Mikus G (2001) Ritonavir increases loperamide plasma concentrations without evidence for P-glycoprotein involvement. *Clin Pharmacol Ther* **70**:405-414.

Teorell T (1937a) Kinetic of distribution of substances administered to the body. II. *Arch Int Pharmacodyn Ther* **57**:226-2240.

Teorell T (1937b) Kinetics of distribution of substances adminstered to the body. I. *Arch Int Pharmacodyn Ther* **57**:205-225.

The Medical Letter (2014) In brief: a naloxone auto-injector (Evzio). *The Medical letter on drugs and therapeutics* **56**:45.

The National Academies Collection: Reports funded by National Institutes of Health (2010) in *Transforming Clinical Research in the United States: Challenges and Opportunities: Workshop Summary*, Washington (DC).

Timmermans S and McKay T (2009) Clinical trials as treatment option: bioethics and health care disparities in substance dependency. *Soc Sci Med* **69**:1784-1790.

Trier S, Linderoth L, Bjerregaard S, Andresen TL and Rahbek UL (2014) Acylation of glucagon-like Peptide-2: interaction with lipid membranes and in vitro intestinal permeability. *PloS one* **9**:e109939.

US Food and Drug Administration (2012a) Draft Guidance: Drug Interaction studies-study design, data analysis, implications for dosing, labeling recommendations. US Food and Drug Administration, Rockville, MD.

US Food and Drug Administration (2012b) Role of Naloxone in Opioid Overdose Fatality Prevention; Request for Comments; Public Workshop, in *Role of Naloxone in Opioid Overdose Fatality Prevention*, Silver Spring, MD.

Venkatakrishnan K, von Moltke LL, Obach RS and Greenblatt DJ (2003) Drug metabolism and drug interactions: application and clinical value of in vitro models. *Curr Drug Metab* **4**:423-459.

Venkatakrishnan K, Pickard MD and von Moltke LL (2010) A quantitative framework and strategies for management and evaluation of metabolic drug-drug interactions in oncology drug development: new molecular entities as object drugs. *Clin Pharmacokinet* **49**:703-727.

Vuppugalla R, Zhang Y, Chang S, Rodrigues AD and Marathe PH (2012) Impact of nonlinear midazolam pharmacokinetics on the magnitude of the midazolam-ketoconazole interaction in rats. *Xenobiotica* **42**:1058-1068.

Wagner AM, Wu JJ, Hansen RC, Nigg HN and Beiere RC (2002) Bullous phytophotodermatitis associated with high natural concentrations of furanocoumarins in limes. *American journal of contact dermatitis : official journal of the American Contact Dermatitis Society* **13**:10-14.

Walsh R, Martin E and Darvesh S (2011) Limitations of conventional inhibitor classifications. *Integrative biology : quantitative biosciences from nano to macro* **3**:1197-1201.

Wason SC, Smith TJ, Perry MJ and Levy JI (2012) Using physiologically-based pharmacokinetic models to incorporate chemical and non-chemical stressors into cumulative risk assessment: a case study of pesticide exposures. *International journal of environmental research and public health* **9**:1971-1983.

Won CS, Oberlies NH and Paine MF (2012) Mechanisms underlying food-drug interactions: inhibition of intestinal metabolism and transport. *Pharmacol Ther* **136**:186-201.

World Medical A (2013) World Medical Association Declaration of Helsinki: ethical principles for medical research involving human subjects. *JAMA* **310**:2191-2194.

Wustrow I, Riedel KD, Mikus G and Weiss J (2012) In vitro identification of the cytochrome P450 isozymes involved in the N-demethylation of the active opioid metabolite nortilidine to bisnortilidine. *Naunyn-Schmiedeberg's archives of pharmacology* **385**:633-639.

Yang J, Jamei M, Yeo KR, Tucker GT and Rostami-Hodjegan A (2007) Prediction of intestinal first-pass drug metabolism. *Curr Drug Metab* **8**:676-684.

Yasar U, Annas A, Svensson JO, Lazorova L, Artursson P and Al-Shurbaji A (2005) Ketobemidone is a substrate for cytochrome P4502C9 and 3A4, but not for P-glycoprotein. *Xenobiotica* **35**:785-796.

Yoon M, Kedderis GL, Yan GZ and Clewell HJ, 3rd (2014) Use of in vitro data in developing a physiologically based pharmacokinetic model: Carbaryl as a case study. *Toxicology*.

Yoshida K, Nambu K, Arakawa S, Miyazaki H and Hashimoto M (1979) Metabolites of loperamide in rats. *Biomedical mass spectrometry* **6**:253-259.

Yu JH, Kim HJ, Lee S, Hwang SJ, Kim W and Moon CJ (2004) LC-MS determination and bioavailability study of loperamide hydrochloride after oral administration of loperamide capsule in human volunteers. *J Pharm Biomed Anal* **36**:421-427.

Zamek-Gliszczynski MJ, Bedwell DW, Bao JQ and Higgins JW (2012) Characterization of SAGE Mdr1a (P-gp), Bcrp, and Mrp2 knockout rats using loperamide, paclitaxel, sulfasalazine, and carboxydichlorofluorescein pharmacokinetics. *Drug Metab Dispos* **40**:1825-1833.

Zanger UM and Schwab M (2013) Cytochrome P450 enzymes in drug metabolism: regulation of gene expression, enzyme activities, and impact of genetic variation. *Pharmacol Ther* **138**:103-141.

Zhao J, Gao B, Zhang Y, Zheng B, Liu H and Cao JL (2014) Effects of intrathecal opioids combined with low-dose naloxone on motilin and its receptor in a rat model of postoperative pain. *Life sciences* **103**:88-94.

CHAPTER 2 : ASSESSMENT OF A CANDIDATE MARKER CONSTITUENT PREDICTIVE OF A DIETARY SUBSTANCE-DRUG INTERACTION: CASE STUDY WITH GRAPEFRUIT JUICE AND CYP3A4 DRUG SUBSTRATES[1]

Introduction

Drug-drug interactions (DDIs) due to inhibition of drug metabolizing enzymes can lead to severe adverse effects, resulting in cautionary statements on drug labels or withdrawal of the drug from the market (Fujioka et al., 2012). Consequently, regulatory agencies recommend or require thorough characterization of new drug candidates as both DDI 'victims' and 'perpetrators' prior to marketing. Such characterization, spanning from discovery to clinical development, is well-defined and generally harmonized amongst the various agencies. In contrast, relevant guidelines are nonexistent for diet-derived products, including dietary supplements and certain beverages, which represent an ever-increasing share of the Western healthcare market. This deficiency reflects the relative lack of robust human-derived in vitro and in vivo data, precluding development of a systematic approach that would help identify dietary substances as potential perpetrators of interactions with drugs, as well as prioritize for clinical evaluation. As an initial step towards developing an aforementioned approach, methods used to predict and characterize metabolism-based DDIs can be extended to dietary substance-drug

[1] This chapter previously appeared as an article in the Journal of Pharmacology and Experimental Therapeutics. The original citation is as follows: Ainslie, GR, Wolf KK, Connolly EA, Scarlett YV, Hull JH, Paine MF. Assessment of a Candidate Marker Constituent Predictive of a Dietary Substance-Drug Interaction: Case Study with Grapefruit Juice and CYP3A4 Drug Substrates. *J Pharmacol Exp Ther*. 2014 Dec; 351(3):576-84.

interactions. DDI predictions using in vitro enzyme kinetic parameters have become increasingly more advanced in drug discovery (Vieira et al., 2014). Mechanistic static models have shown success for DDIs localized in the liver, the primary site of these interactions. However, because diet-derived constituents generally have a low systemic exposure (due to extensive pre-systemic metabolism) but high intestinal exposure, and most drugs are taken orally, the gut likely represents the primary interaction site for dietary substance-drug interactions. Accordingly, models that are tailored to processes exclusive to the gut may be more appropriate for predicting dietary substance-drug interactions.

Assessing dietary substance-drug interaction risk poses additional challenges compared to DDIs. Unlike drug products, dietary substances typically are complex mixtures that vary substantially in phytochemical composition, both between brands and batches of the same brand (Cancalon et al., 2011; Won et al., 2012). Accordingly, it has been postulated that ‘marker’ constituents can be identified and used to predict the effect of the mixture in vivo (Won et al., 2012; National Center for Complementary and Alternative Medicine, 2013). Such a constituent predictive of a mixture also would enable a simplified and cost-effective means to assess dietary substance-drug interaction liability.

Grapefruit juice is an extensively studied diet-derived perpetrator of dietary substance-drug interactions. When consumed in usual volumes, the ‘grapefruit juice effect’ is limited to the intestine, as evidenced by the general lack of an effect on the pharmacokinetics of intravenously administered drugs and on the terminal half-life of orally administered drugs. Most victim drugs share three requisite traits: orally

administered, a low to intermediate absolute bioavailability, and undergo cytochrome P450 3A4 (CYP3A4)-mediated first-pass metabolism in the intestine by (Bailey et al., 2013). Grapefruit juice contains a chemical class of constituents, furanocoumarins, which are potent mechanism-based inhibitors of CYP3A4 (Paine et al., 2006a), a prominent drug metabolizing enzyme expressed in both the intestine and liver (Paine et al., 2006b). One typically abundant furanocoumarin, 6',7'-dihydroxybergamottin (DHB), may represent a marker constituent predictive of the CYP3A4-mediated effect of grapefruit juice based on the following key properties/observations: the polarity relative to other furanocoumarins enables straightforward quantification in both grapefruit juice and biologic matrices; the mechanism-based inhibition (MBI) associated constant (K_I, 1-5 μM) is well below/within concentrations measured in the juice; the onset of peak effect, defined as the maximum loss of enteric CYP3A4 protein in human intestine-derived cell monolayers (Caco-2) (Paine et al., 2005), is predictive of that in healthy volunteers administered grapefruit juice (Lown et al., 1997); and authentic standard is commercially available that is not cost prohibitive.

In the present work, an in vitro to in vivo extrapolation (IVIVE) approach using DHB as a marker constituent of grapefruit juice was applied to a purported victim drug that had not been reported previously in the literature. Loperamide, a μ-opioid receptor agonist, was selected as the test victim drug based on the aforementioned criteria. In addition, anecdotal reports suggest an abuse potential when taken at supratherapeutic doses with grapefruit juice (Daniulaityte et al., 2013), substantiating investigation of the interaction liability. The aims of this study were to (1) confirm the grapefruit juice-loperamide interaction in healthy volunteers, (2) obtain MBI kinetic parameters for DHB

using loperamide *N*-desmethylation by human intestinal microsomes as the index reaction, (3) determine the accuracy of a mechanistic static model using DHB as a marker constituent predictive of the grapefruit juice-loperamide interaction, and (4) apply the model to previously reported grapefruit juice-drug interaction studies to evaluate the robustness of this IVIVE method. Results will aid in assessing the grapefruit juice interaction liability with candidate and marketed drugs and help prioritize for clinical evaluation.

Materials and Methods

Materials and Chemicals

Human intestinal microsomes (HIMs), pooled from 13 donors of mixed gender (7 male, 6 female), were purchased from Xenotech, LLC (Lenexa, KS). Plasma pooled from multiple donors (mixed gender, distribution unknown) was purchased from Biological Specialty Corporation (Colmar, PA). Loperamide hydrochloride, D_6-loperamide, *N*-desmethylloperamide, and D_3-*N*-desmethylloperamide were purchased from Toronto Research Chemicals, Inc. (North York, Ontario, Canada). DHB was purchased from Cayman Chemical (Ann Arbor, MI). Psoralen, NADPH, and dimethylsulfoxide (DMSO) were purchased from Sigma-Aldrich (St. Louis, MO). LC/MS/MS-grade acetonitrile, water, methanol, and formic acid were purchased from Thermo Fisher Scientific (Waltham, MA).

Human Subject Study

Preparation of Grapefruit Juice. Multiple cans of a single brand (Minute Maid®) and lot of frozen grapefruit juice concentrate were purchased from a local grocery store. The frozen juice concentrates were thawed and pooled, and an aliquot was saved for measurement of DHB by HPLC (Paine et al., 2006a). The pooled concentrate was reconstituted with water to achieve a 'double-strength' juice (DHB final concentration ~60 μM). The reconstituted juice was divided into 240 ml aliquots and stored at -20°C and protected from light until needed.

Clinical Protocol and Participants. The University of North Carolina Office of Human Research Ethics/Biomedical Institutional Review Board and Clinical and Translational Research Center (CTRC) Oversight Committee reviewed and approved

the protocol. Potential subjects provided written informed consent and Health Insurance Portability and Accountability Act authorization before screening at the CTRC, which consisted of a medical history, physical examination, liver function tests, and complete blood count. All women underwent a serum pregnancy test.

Study Design and Procedures. A prospective, randomized two-phase, open-label crossover study was conducted at the CTRC (Figure 2.1). Prior to the first study phase, the participants were asked to abstain from all fruit juices for one week before and during the study and from alcohol and caffeinated beverages the evening before each study day. Participants were admitted to the CTRC the evening before each study phase. Vital signs (blood pressure, temperature, pulse, respirations) and oxygen saturation were obtained upon admission and monitored periodically throughout the inpatient portion of each phase. All of the women underwent a repeat serum pregnancy test. After an overnight fast, each participant was administered 16 mg loperamide (Mylan Inc., Canonsburg, PA) with 240 ml of water or grapefruit juice. Blood (7 ml) was collected from an indwelling intravenous catheter before loperamide administration and at 0.5, 1, 2, 3, 4, 5, 6, 8, 10, and 12 h after loperamide administration. Blood was centrifuged within 1 h of collection; plasma was removed and stored at -80°C pending analysis for loperamide and the primary CYP3A4-mediated metabolite, *N*-desmethylloperamide, by LC/MS/MS (see below). Subjects continued to fast until after the 4-h blood collection, after which meals and snacks, devoid of fruit juices and caffeinated beverages, were provided. After the 12-h blood collection, subjects were discharged. Subjects returned to the CTRC as outpatients for blood draws at 24, 36, 48, and 72 h after loperamide administration.

Concurrent with the blood collections, dark-adapted pupil diameter, the most sensitive index of opioid effect (Grunberger et al., 1990), was measured using a NeurOptics VIP-200® pupillometer with a resolution of 0.1 mm (San Clemente, CA). Pupil diameter was obtained at least in triplicate, with coefficients of variation ≤2.8%. The light intensity of the room, measured by a Sper Scientific 840021 light meter (Scottsdale, AZ), was always <1 lux. As a positive control for the miotic effect, 9 subjects (5 men, 4 women) were administered a 'morphine challenge' on the evening of the first phase. Morphine sulfate (0.07 mg/kg; Hospira Inc., Lake Forest, IL) was administered as a 5-min intravenous infusion via a syringe pump. Pupil diameter was measured before and at 5, 10, 20, 30, 60, 90, and 120 min after infusion. Subjects were in the supine position and were monitored with an automated blood pressure cuff and pulse oximeter during the infusion and for 2 hours thereafter. Vital signs were monitored concurrent with pupil diameter measurement. Supplemental oxygen was available if oxygen saturation decreased to <94%. The opioid antagonist, naloxone (International Medication Systems Ltd, South El Monte, CA), and anti-emetic agent, promethazine (Goldline Laboratories, Inc., North Wales, PA), were available if needed.

Determination of Mechanism-Based Inhibition Kinetic Parameters for DHB

Time- and concentration-dependent inhibition of CYP3A4 activity by DHB in HIMs was assessed as described previously (Paine et al., 2004), only *N*-desmethylloperamide formation was used as the index reaction. Briefly, loperamide and DHB were dissolved in DMSO to yield working solutions of 5 and 2 mM, respectively. Primary incubation mixtures consisted of HIMs (5 mg/ml), DHB (0, 2.5, 5, 10, 30 μM), and potassium phosphate buffer (0.1 M, pH 7.4). The mixtures were equilibrated at

37°C for 5 min before initiating reactions with NADPH (1 mM final concentration), yielding a final volume of 80 µl; the final concentration of DMSO was ~1% (v/v). At designated times from 0-5 min, an aliquot (10 µl) was removed and diluted 20-fold into secondary incubation mixtures containing loperamide and NADPH (1 mM), yielding a final loperamide concentration of 60 µM. Secondary reactions were terminated after 20 min by transferring 100 µl to a 96-well plate containing 300 µl of acetonitrile/0.1% (v/v) formic acid and internal standard (0.5 µM D_3-*N*-desmethylloperamide). Plates were centrifuged at 2000 x g for 10 min, and 200 µl of supernatant were transferred to clean plates. The contents were dried under heated nitrogen (50°C), reconstituted in 200 µl of 95% water:5% acetonitrile:0.1% formic acid (v/v/v) (initial chromatographic conditions), and analyzed for *N*-desmethylloperamide by LC/MS/MS (see below).

Quantification of Loperamide and *N*-Desmethylloperamide

Human Plasma. Plasma (50 µl) was added to methanol (70 µl) containing internal standard (4.3 nM D_6-loperamide and D_3-*N*-desmethylloperamide) then precipitated with 360 µl of methanol. The mixtures were vortexed for 5 min and centrifuged (3000 g x 10 min at 4°C). Calibration (0.1-25 nM) and quality control (0.75, 4, 12 nM) solutions were prepared using authentic standards and blank human plasma. Sample (5 µl) was injected onto an Aquasil C18 (2.1 x 50 mm, 5 µm particle size) analytical column (Thermo Fisher Scientific). Analytes were eluted with a binary gradient consisting of water/0.1% (v/v) formic acid (mobile phase A) and acetonitrile/0.1% (v/v) formic acid (mobile phase B) at a total flow rate of 0.75 ml/min. Initially, mobile phase B was held at 20% for 0.4 min then increased linearly to 95% for 3.6 min. Mobile phase B was held at 95% for 0.5 min then returned to initial conditions

over 6 seconds and equilibrated. The total run time was 5 min. All eluted solvent was directed to an API4000 QTRAP® triple quadrupole mass spectrometer (AB Sciex, Framingham, MA). Loperamide (477.3→266.2 m/z), *N*-desmethylloperamide (463.2→252.2 m/z), D_6-loperamide (483.3→272.2 m/z), and D_3-*N*-desmethylloperamide (466.3→255.2 m/z) were quantified in multiple reaction monitoring mode; collision energy was set to 20 mV for all analytes. Analyte concentrations were quantified using Analyst software (v1.4.1) by interpolation from matrix matched calibration curves and quality controls with a linear range of 0.1-25 nM. The calibration standards and quality controls were judged for batch quality based on the 2013 FDA guidance for industry regarding bioanalytical method validation (US Food and Drug Administration, 2013).

Microsomal Incubations. Calibration (1-1000 nM) and quality control (2.5, 500, 800 nM) solutions were prepared using authentic *N*-desmethylloperamide standard and HIMs. Sample (5 µl) was injected onto an Aquasil C18 (2.1 x 50 mm, 5 µm particle size) analytical column. Chromatographic separation was achieved using the same HPLC system and mobile phases as for plasma. Due to the high buffer and salt content of the microsomal samples relative to plasma, the binary gradient method was modified. Initial conditions consisted of 10% mobile phase B, held for 1 minute, then increased linearly to 95% B over 1.5 min and held for 0.5 min. The gradient was returned to initial conditions over 0.1 min to equilibrate the column. The total run time was 4 min. The eluted solvent was directed to a Sciex API5600 triple quadrupole-time of flight mass spectrometer. Ionization was achieved with a turbo electrospray source operated in positive ion mode. The declustering potential and collision energy were set to 25 V and 30 mV, respectively. *N*-Desmethylloperamide was quantified using Multiquant™

software (v2.1.1), selecting the fragment ion range of 252.1-252.8 and 255.1-255.8 m/z for *N*-desmethylloperamide and D_3-*N*-desmethylloperamide, respectively. As with plasma analysis, all calibration standards and quality control samples were judged for batch quality based on the 2013 FDA guidance (US Food and Drug Administration, 2013).

Data Analysis

Pharmacokinetic and Pharmacodynamic Analysis. Pharmacokinetic and pharmacodynamic outcomes were recovered via noncompartmental methods using Phoenix® WinNonlin® (v6.3; Certara, St Louis, MO). *Pharmacokinetics.* The maximum concentration (C_{max}), time to reach C_{max} (t_{max}), and last measured concentration (C_{72h}) were obtained directly from the plasma concentration-time profiles. The terminal elimination rate constant (λ_z) was determined by linear regression of the terminal portion of the log-transformed concentration-time profile using at least three data points. The terminal half-life ($t_{1/2}$) was calculated as $\ln(2)/\lambda_z$. Area under the plasma concentration-time curve (AUC) from time zero to 72 h ($AUC_{0\text{-}72h}$) was determined using the trapezoidal method with linear up/log down interpolation. The AUC from time zero to infinity ($AUC_{0\text{-}inf}$) was calculated as the sum of $AUC_{0\text{-}72h}$ and C_{72h}/λ_z. The oral clearance of loperamide (Cl/F) was calculated as the ratio of dose to $AUC_{0\text{-}inf}$. The metabolite-to-parent AUC ratio [$(AUC_m/AUC_p)_{0\text{-}72h}$] was calculated as the ratio of the $AUC_{0\text{-}72h}$ of *N*-desmethylloperamide to that of loperamide. The primary pharmacokinetic outcome was the ratio of loperamide $AUC_{0\text{-}inf}$ in the presence to that in the absence of grapefruit juice (AUC_{GFJ}/AUC). *Pharmacodynamics.* Baseline pupil diameter was obtained at time zero, and miosis was determined as the decrease in pupil diameter from baseline. The area

under the effect (miosis)-time curve from 0-72 h ($AUEC_{0\text{-}72h}$) was calculated by the linear trapezoidal method with an adjustment from the baseline pupil diameter measurement. The maximum decrease in pupil diameter (R_{max}) was obtained directly from the miosis-time profile.

MBI Kinetic Parameters for DHB. K_I and k_{inact} were recovered using previously published methods (Paine et al., 2004; Obach et al., 2007; Brantley et al., 2013). Final parameter estimates were obtained by nonlinear least-squares regression using Phoenix® WinNonlin® and eq. 1:

$$k_{inact,app} = \frac{k_{inact} \cdot [DHB]}{K_I + [DHB]} \quad (1)$$

where $k_{inact,app}$ denotes the apparent inactivation rate constant at each inhibitor (DHB) concentration, determined by the slope of the mono-exponential decline in activity. Model fit was evaluated from visual inspection of the observed versus predicted data, randomness of the residuals, and standard errors of the parameter estimates. The efficiency of inactivation was calculated as the ratio of k_{inact} to K_I.

Grapefruit Juice-Loperamide Interaction Prediction Using DHB as a Marker Constituent. The grapefruit juice-mediated increase in AUC (AUC_{GFJ}/AUC) for loperamide was predicted using DHB as a marker constituent and a mechanistic static model (eq. 2) for intestinal MBI (Obach et al., 2006; Brantley et al., 2013):

$$\frac{AUC_{GFJ}}{AUC} = \frac{1}{F_g + (1 - F_g) \bullet \frac{1}{1 + \left(\frac{k_{inact} \bullet I_g}{k_{deg} \bullet (I_g + K_I)} \right)}} \quad (2)$$

where F_g denotes the fraction of the dose of victim drug (loperamide) escaping first-pass extraction in the intestine (0.62), I_g denotes the concentration of inhibitor

(DHB) in the enterocyte (5 μM), and k_{deg} denotes the degradation rate constant associated with intestinal CYP3A4 (0.000481 min^{-1}) (Obach et al., 2006). The Q_{gut} and Advanced Dissolution and Metabolism models in Simcyp® (v13; Certara, St. Louis, MO) were used to estimate loperamide F_g and DHB I_g using MDCK cell permeability (Tran et al., 2004) and recombinant CYP3A4 metabolism (Kim et al., 2004) data for loperamide and Caco-2 cell permeability data for DHB (Paine et al., 2005). The fraction of the dose of loperamide absorbed into enterocytes (F_{abs}) was assumed to remain unchanged in the presence of grapefruit juice.

Grapefruit Juice-Drug Interaction Predictions with Marketed Drugs Using DHB as a Marker Constituent. The utility of DHB as a marker constituent predictive of grapefruit juice-drug interactions was examined further with marketed drugs that have been evaluated in the clinic. Test victim drugs (Table 2.1) were selected based on the following criteria: intestinal CYP3A4 substrate, availability of human pharmacokinetic data, and availability of F_g. F_g was obtained from liver transplant recipients during the anhepatic phase of the operation, by the combined intravenous/oral administration method, or from in vitro-in vivo scaling techniques (Galetin et al., 2010). Drugs whose F_g were estimated by a third method, which involves grapefruit juice administration (Gertz et al., 2008), were excluded to avoid bias. Predictions were made using eq. 2. Predicted AUC_{GFJ}/AUCs were evaluated against observations from the literature. As the grapefruit juice-loperamide interaction study was powered to detect a 25% change in loperamide $AUC_{0\text{-}inf}$, predicted AUC_{GFJ}/AUCs were evaluated against observed ratios with a predefined cutoff of 25% to define a successful prediction (Vieira et al., 2014).

Sensitivity Analysis to Assess the Relationship between DHB I_g, Victim Drug F_g, and the Predicted AUC_{GFJ}/AUC. Due to the uncertainty in DHB I_g, the variability in grapefruit juice administration frequency in clinical studies, and the uncertainty in victim drug F_g predictions, AUC_{GFJ}/AUC ratios were simulated by increasing F_g and I_g. Simulations were conducted in Phoenix® WinNonlin® using eq. 2, with F_gs ranging from 0.1-0.9 and DHB concentrations from 0-5 μM in increments of 0.05 and 0.1 μM, respectively.

Statistical Analysis

Statistical analyses were conducted using SAS (v9.1.3; SAS Institute, Cary, NC). *Clinical study.* The sample size was based on 80% power to detect a 25% difference in the primary outcome of loperamide, AUC_{GFJ}/AUC, with an alpha of 0.05. Data are presented as the geometric mean [90% confidence interval] with the exception of t_{max}, which is reported as the median (range). The primary outcome was evaluated against the predefined no effect range of 0.75-1.33. The Wilcoxon signed-rank test was used to test for a difference in t_{max}. Differences in $AUC_{0\text{-}72h}$, $AUC_{0\text{-}inf}$, $C_{max,}$, $t_{1/2}$, Cl/F, and AUEC between treatment groups were analyzed by standard repeated-measures ANOVA (α = 0.05) using log-transformed data. *In vitro study.* Data are presented as the mean of duplicate incubations. MBI kinetic parameters are presented as estimates ± S.E.'s.

Results

All enrolled subjects completed the clinical study with negligible side effects. The mean (± S.D.) concentration of DHB in the test juice was 73.7 ± 4.0 μM, measured in triplicate. Of the 18 potential subjects screened, 8 men and 8 non-pregnant women were enrolled. The median [range] age was 29 [22-59] and 40 [29-53] years, respectively. Participants were self-identified as white (5 men, 4 women), African American (1 man, 4 women), Hispanic (1 man), or Asian (1 man). None of the subjects reported taking concomitant medications or dietary substances known to modulate the metabolism and transport of both loperamide and morphine. Concomitant medications included acetaminophen (two women) and promethazine (one woman). All subjects completed both phases of the study. Grapefruit juice and both test drugs were well-tolerated; one subject reported mild constipation with loperamide during the grapefruit juice phase that resolved within 24 h.

Grapefruit juice increased the systemic exposure of loperamide with no effect on pupil diameter. *Pharmacokinetics.* Loperamide and *N*-desmethylloperamide were detected readily in plasma in all subjects throughout the 72-h collection period. Relative to water, grapefruit juice elevated the plasma concentrations of loperamide but had no effect on those of *N*-desmethylloperamide (Fig. 2.1A). The percentage of loperamide $AUC_{0\text{-}inf}$ extrapolated from 72 h to infinite time was <25% in both the water and grapefruit juice phases. The primary outcome, AUC_{GFJ}/AUC, was outside the range associated with bioequivalence (0.75-1.33) (Table 1). Relative to water, grapefruit juice increased geometric mean loperamide C_{max}, $AUC_{0\text{-}72h}$, and $AUC_{0\text{-}inf}$ significantly, by ~60-70%; geometric mean Cl/F decreased significantly, by 43% (Table 2.1). Grapefruit juice

had no effect on geometric mean loperamide terminal $t_{1/2}$. Median loperamide t_{max} did not differ significantly between treatments. The percentage of *N*-desmethylloperamide $AUC_{0\text{-}inf}$ extrapolated from 72 h to infinite time was >40% in the water and grapefruit juice phases in 10 of the subjects, precluding accurate recovery of $AUC_{0\text{-}inf}$, as well as $t_{1/2}$, in these subjects. As such, geometric means for these outcomes are not reported. Grapefruit juice had no effect on *N*-desmethylloperamide geometric mean C_{max} and $AUC_{0\text{-}72h}$ and median t_{max}; $(AUC_m/AUC_p)_{0\text{-}72h}$ decreased by 40% (Table 2.1).

Pharmacodynamics. Relative to baseline, morphine, but not loperamide, decreased pupil diameter (Fig. 1B). The geometric mean [90% confidence interval] $AUEC_{0\text{-}2h}$ and R_{max} for morphine was 150 [115-195] mm*h and 1.9 [1.5-2.5] mm, respectively. The median (range) time to R_{max} was 1.0 (0.5-1.5) h. The geometric mean $AUEC_{0\text{-}72h}$ for loperamide in the absence and presence of grapefruit juice was 11.3 [9.2-13.9] and 11.8 [8.5-16.4] mm*h, respectively; geometric mean R_{max} was 0.38 [0.30-0.47] and 0.40 [0.33-0.51] mm, respectively.

DHB is a mechanism-based inhibitor of loperamide *N*-desmethylation in HIMs. DHB inhibited *N*-desmethylloperamide formation in a time- and concentration-dependent manner in HIMs (Fig. 2.2). The K_I and k_{inact} were 5.0 ± 0.9 μM and 0.38 ± 0.02 min^{-1}, respectively. The efficiency of inactivation (k_{inact}/K_I) was 76 μl/min/pmol.

DHB is predictive of interactions between grapefruit juice and loperamide and several marketed drugs. Using DHB as a marker constituent of grapefruit juice and a mechanistic static model, the predicted AUC_{GFJ}/AUC for loperamide was 1.6. The AUC_{GFJ}/AUC and F_g for other marketed drugs were obtained from the literature according to predefined criteria. The reported absolute bioavailability and F_g of these

drugs ranged from 0.12-0.94 and 0.14-0.94, respectively (Table 2.2). Application of the mechanistic static model to these marketed drugs predicted the AUC_{GFJ}/AUC of 12 of 15 interactions to within the pre-defined 25% criterion (Fig. 2.3).

Victim drug F_g is more sensitive than DHB (I_g) in the prediction of AUC_{GFJ}/AUC. At an F_g for loperamide of 0.62 (predicted using the Q_{gut} model in Simcyp®), incremental (0.1 μM) increases in I_g reached a maximum AUC_{GFJ}/AUC (1.6) at 1.2 μM (Fig. 2.4). The I_g required to achieve the maximum AUC_{GFJ}/AUC increased with decreasing F_g. An incremental decrease (0.05) in F_g from 0.90 to 0.45 at a constant I_g (1.2 μM) resulted in a nearly proportional increase in AUC_{GFJ}/AUC. Simulated F_gs less than 0.45 resulted in a greater than proportional increase in AUC_{GFJ}/AUC.

Discussion

Dietary substance-drug interaction risk assessment is fraught with challenges, adding to those encountered with DDIs. Dietary substances of plant-based origin have a more complex biochemical makeup compared to oral drug formulations. Identification of major constituents (chemical classes or single chemical entities) that contribute to inhibition of drug metabolizing enzymes, as well as transporters, in vivo would help overcome some of these challenges (Won et al., 2012; National Center for Complementary and Alternative Medicine, 2013). Ideally, a single phytochemical marker would be identified and evaluated using methods similar to those used in the pharmaceutical industry, including in vitro bioactivity assays, IVIVE, and clinical assessment. An approach involving a combination of these methods was evaluated using the exemplar perpetrator dietary substance grapefruit juice and the marker constituent DHB.

Loperamide was selected as the test victim drug because it meets the criteria for an interaction with grapefruit juice (Bailey et al., 2013), and a grapefruit juice-loperamide interaction study has not been reported. This purported interaction was confirmed with 16 healthy volunteers, in which the primary pharmacokinetic outcome, geometric mean loperamide AUC_{GFJ}/AUC, was 1.7. The lack of effect on loperamide terminal elimination half-life was consistent with an interaction limited to the gut, which is typical of grapefruit juice-drug interactions (Won et al., 2012; Bailey et al., 2013). In contrast to loperamide, the pharmacokinetics of the primary CYP3A4-mediated metabolite, *N*-desmethylloperamide, were unchanged in the presence of grapefruit juice, which may reflect elimination rate-limited kinetics and/or more rapid distribution into peripheral

tissues relative to loperamide (Sklerov et al., 2005). The pharmacokinetics of both loperamide and *N*-desmethylloperamide in the absence of grapefruit juice were consistent with those reported at an equivalent loperamide dose (16 mg) (Mukwaya, 2005) or lower (2-4 mg) after dose-normalization (Streel et al., 2005; Niemi et al., 2006).

Based on anecdotal reports describing abuse of loperamide when taken with grapefruit juice (Daniulaityte et al., 2013) and the ease of measuring pupil diameter as an index of central nervous system opiate-like effect, the opportunity was taken to assess a pharmacodynamic interaction. Compared to baseline, a relatively high dose of loperamide (16 mg), in both the absence and presence of grapefruit juice, did not decrease pupil diameter (i.e., produce miosis). The lack of miosis was consistent with previous healthy volunteer studies in which loperamide was administered at higher doses (≥24 mg) (Skarke et al., 2003) or with potent CYP3A4 or dual CYP3A4/P-glycoprotein (P-gp) inhibitors (Mukwaya et al., 2005; Niemi et al., 2006).

Confirmation of the grapefruit juice-loperamide interaction permitted evaluation of DHB as a marker constituent of whole juice. MBI kinetic parameters for DHB were recovered using HIMs and *N*-desmethylloperamide formation as the index reaction to inform a mechanistic static interaction model specific to the gut. The parameters, K_I and k_{inact} (5.0 μM and 0.38 min^{-1}, respectively), were comparable to those recovered using other CYP3A4-mediated reactions and HIMs, specifically testosterone 6β-hydroxylation (2.5 μM and 0.40 min^{-1}, respectively) and midazolam 1'-hydroxylation (3.5 μM and 0.31 min^{-1}, respectively) (Paine et al., 2004). The other parameters needed to inform the mechanistic static model, F_g and I_g, were estimated using literature data. The F_g for loperamide and the I_g for DHB were predicted using the Q_{gut} and Advanced Dissolution

and Metabolism models within Simcyp® (Yang et al., 2007), which were informed by permeability data (loperamide and DHB) (Tran et al., 2004; Paine et al., 2005), metabolic kinetic data (loperamide) (current work), and intestinal villous blood flow. The predicted AUC_{GFJ}/AUC agreed with the observed AUC_{GFJ}/AUC (1.6 versus 1.7) to within the 25% pre-defined criterion, supporting DHB as a marker constituent predictive of the effect of whole juice.

The successful IVIVE with the grapefruit juice-loperamide interaction prompted further evaluation with other previously tested drugs. Based on the availability of human pharmacokinetic data and F_gs, as well as the test drug being a CYP3A4 substrate, 15 grapefruit juice-drug interaction studies were identified. Although the absolute bioavailability of three of the drugs was relatively high (>70%), and thus not victim drugs per se, these drugs were included to provide a wide range of AUC_{GFJ}/AUCs. The F_gs of the test drugs, determined from liver transplant patients during the anhepatic phase of the operation, by combined intravenous and oral administration, or in vitro-in vivo scaling techniques, ranged from 0.14 to 0.94. Drugs whose F_g was determined using grapefruit juice as an inhibitor of intestinal metabolism were excluded to avoid bias. The same DHB I_g used for the loperamide interaction prediction was used for the other victim drugs. As with loperamide, DHB was predictive to within 25% of the observed AUC_{GFJ}/AUC for 10 of the interactions. The three outlier victim drugs were atorvastatin, simvastatin, and triazolam. The interaction with atorvastatin was over predicted by 3.3-fold (4.0 versus 1.2), which may reflect atorvastatin being a substrate for organic anion transporting polypeptide (OATP) 2B1 (K_m, 0.2 μM) (Kalliokoski and Niemi, 2009), an uptake transporter expressed on the apical membrane of enterocytes and other cell

types (Ito et al., 2005). Grapefruit juice has been shown to decrease systemic exposure to the OATP substrate fexofenadine via inhibition of intestinal OATP(s) (Dresser et al., 2002). As inhibition of intestinal OATP(s) and CYP3A4 decrease and increase systemic drug exposure, respectively, these two processes acting in concert would be expected to reduce the AUC_{GFJ}/AUC compared to CYP3A4 inhibition alone. Conversely, substrates of both CYP3A4 and the apically-located efflux transporter, P-gp, would be expected to increase AUC_{GFJ}/AUC compared to CYP3A4 inhibition alone. The AUC_{GFJ}/AUC of such dual CYP3A4/P-gp substrates (cyclosporine, methadone, quinidine, tacrolimus) were well-predicted despite implications that DHB inhibits P-gp (Eagling et al., 1999; de Castro et al., 2007) in addition to CYP3A4. This observation suggests that the contribution of intestinal CYP3A4 inhibition supersedes that of intestinal P-gp inhibition when grapefruit juice is co-administered with dual CYP3A4/P-gp substrates.

Unlike with atorvastatin, the interaction with simvastatin was underpredicted, by a factor of 2.4 (1.5 versus 3.6). Simvastatin was one of three drugs whose F_g was determined using an in vitro extrapolation technique, which may have overestimated F_g, resulting in the underprediction. The method used to derive the F_g for simvastatin (0.66) involved oral clinical pharmacokinetic data and in vitro microsomal clearance data. This estimate was used in lieu of that obtained with the Q_{gut} model (0.06) (Gertz et al., 2010), as the former was derived using at least some clinical data versus in vitro data alone. The F_g from the Q_{gut} model would have over predicted simvastatin AUC_{GFJ}/AUC by 9-fold. The disconnect between the two methods and between the observed and

predicted AUC_{GFJ}/AUC suggest that other unknown mechanisms/factors contribute to the grapefruit juice-simvastatin interaction.

As with simvastatin, the interaction with triazolam was under predicted, albeit modestly (1.5 versus 2.0). This underprediction may be due to ethnic and/or sex differences between subjects. The reference clinical study involved nine healthy Japanese men (Sugimoto et al., 2006), and the estimated F_g was derived from healthy Caucasians (10 men, 11 women) (Masica et al., 2004). In addition, the dose-normalized AUC in the absence of grapefruit juice was lower in the Japanese study compared to that reported for American men (11 Caucasians, 2 African Americans) (Greenblatt et al., 2005). Taken together, the extent of intestinal extraction of triazolam may be greater (i.e., F_g may be lower) in Japanese than American men, which would explain the greater AUC_{GFJ}/AUC in the Japanese cohort.

The aforementioned discrepancies highlight limitations of the IVIVE method used in the current work. First, the accuracy of this estimate is dependent on an accurate victim drug F_g, as the model is sensitive to this parameter, particularly when less than 0.45 (Fig. 4). Second, significant involvement of transporters in the disposition of the test drug would preclude the use of this model. Despite these limitations, this IVIVE approach, which is used routinely by the pharmaceutical industry, can be implemented readily into work streams in the drug discovery process upon the identification of candidate marker constituents.

In summary, the importance of dietary substance-drug interaction risk assessment has been recognized by regulatory agencies, yet relevant guidelines have not been established. A framework to identify causative constituents in dietary

substances has been proposed (National Center for Complementary and Alternative Medicine, 2013), which was applied in the current work using grapefruit juice as an exemplar perpetrator, DHB as a marker constituent, and loperamide as a test victim drug. A clinical study confirmed a pharmacokinetic interaction between grapefruit juice and loperamide. A mechanistic static model of intestinal CYP3A4 MBI incorporating DHB kinetic parameters was sufficient to predict the grapefruit juice-loperamide interaction, as well as 12 of 15 previously reported grapefruit juice-drug interaction studies, to within 25%. This approach has limitations when applied to victim drugs whose estimated F_g is inaccurate/uncertain and/or that are substrates for intestinal OATPs or other uptake transporters. This IVIVE method is a relatively simple and cost-effective means to assess grapefruit juice-drug interaction liability or to prioritize compounds for more advanced and resource heavy assessment, such as dynamic modeling approaches and/or clinical evaluation. In conclusion, this IVIVE method expands upon proposed frameworks to assess clinically relevant dietary substance-drug interactions, results of which will help guide dietary substance-drug interaction risk assessment.

Table 2.1. Pharmacokinetic outcomes of loperamide and N-desmethylloperamide in 16 healthy volunteers administered loperamide with 240 ml of water or grapefruit juice.

Outcome	Water	GFJ	GFJ/Water Ratio
Loperamide			
C_{max} (nM)	6.5 [5.3-8.1]	10 [8.2-13]	1.58 [1.33-1.88] [b]
$AUC_{0\text{-}72h}$ (nM · h)	105 [87-126]	180 [149-220]	1.72 [1.58-1.87] [b]
$AUC_{0\text{-}inf}$ (nM · h)	118 [96-145]	203 [165-250]	1.73 [1.58-1.89] [b]
Cl/F (L/h)	285 [232-351]	165 [134-203]	0.57 [0.53-0.62] [b]
Terminal $t_{½}$ (h)	23.3 [20.7-26.3]	23.2 [20.8-26.0]	1.04 [0.94-1.16]
t_{max} (h) [median (range)]	3.0 (0.5-12)	5.0 (2.0-6.0) [a]	
N-Desmethylloperamide			
C_{max} (nM)	7.9 [6.7-9.2]	7.7 [6.6-9.0]	0.98 [0.83-1.15]
$AUC_{0\text{-}72h}$ (nM · h)	271 [253-290]	290 [270-310]	1.04 [0.99-1.10]
t_{max} (h) [median (range)]	5.5 (2.0-12)	7.0 (4.0-26) [a]	
Metabolite/parent AUC ratio			
$(AUC_m/AUC_p)_{0\text{-}72h}$	2.6 [2.2-3.1]	1.6 [1.3-1.9]	

$AUC_{0\text{-}72h}$, area under the plasma concentration-time curve from 0 to 72 h; $AUC_{0\text{-}inf}$, AUC from 0 to infinite time; AUC_m, AUC of N-desmethylloperamide; AUC_p, AUC of loperamide; CL/F, oral clearance; C_{max}, maximum plasma concentration; $t_{1/2}$, terminal elimination half-life; t_{max}, time to C_{max}. Values denote the geometric mean [90% confidence intervals] unless indicated otherwise. [a]Not significant ($p<0.05$, Wilcoxon signed-rank test). [b]Outside the predefined no effect range (0.75-1.33).

Table 2.2. Victim drug, F_g, F, and clinical study information for the IVIVE.

Victim drug	F_g		F [a]	AUC_{GFJ}/AUC [b]	
	Estimate	Reference		Observed	Reference
Alfentanil	0.60 [c]	(Kharasch et al., 2008)	0.42 [d]	1.6	(Kharasch et al., 2004a)
Alprazolam	0.94 [e]	(Hirota et al., 2001)	0.88 ± 0.16	1.1	(Yasui et al., 2000)
Atorvastatin	0.24 [c]	(Lennernas, 2003)	0.12	1.2	(Reddy et al., 2011)
Buspirone	0.21 [e]	(Obach et al., 2005)	0.40 ± 0.04	4.3	(Lilja et al., 1998)
Cyclosporine	0.28-0.68 [c]	(Ducharme et al., 1995)	0.28 ± 0.18	1.4-1.9	(Schwarz et al., 2006; Paine et al., 2008)
Felodipine	0.45 [c]	(Lundahl et al., 1997)	0.15 ± 0.8	2.0	(Paine et al., 2006)
Methadone	0.78 [c]	(Kharasch et al., 2004b)	0.92 ± 0.21	1.1	(Kharasch et al., 2008)
Midazolam	0.57 [f]	(Paine et al., 1996)	0.44 ±0.17	1.7	(Kharasch et al., 2004a)
Nifedipine	0.78 [c]	(Holtbecker et al., 1996)	0.50 ± 0.13	1.1	(Odou et al., 2005)
Nisoldipine	0.11 [c]	(Gertz et al., 2010)	0.05	8.2	(Takanaga et al., 2000)
Sildenafil	0.78 [c]	(Gertz et al., 2010)	0.38	1.2	(Jetter et al., 2002)
Simvastatin	0.66 [e]	(Obach et al., 2006)	≤0.5	3.6	(Lilja et al., 2004)
Quinidine	0.90 [c]	(Darbar et al., 1997)	0.71 ± 0.17	1.05 [g]	(Damkier et al., 1999)
Tacrolimus	0.14 [c]	(Floren et al., 1997)	0.25 ± 0.10	6.6 [i]	(Liu et al., 2009)
Triazolam	0.75 [c]	(Masica et al., 2004)	0.55-0.60 [h]	2.0	(Sugimoto et al., 2006)

F_g, fraction of dose of victim drug that escapes intestinal first-pass extraction; F, oral bioavailability; [a]obtained from Brunton et al. (Brunton et al., 2010) unless indicated otherwise; [b]ratio of the area under the plasma concentration-time curve in the presence to absence of grapefruit juice, unless indicated otherwise; [c]estimated using intravenous administration, systemic clearance, and oral bioavailability data; [d]obtained from Kharasch et al., 2004b; [e]determined by in vitro to in vivo extrapolation using in vitro intrinsic clearance data; [f]determined from anhepatic patients; [g]ratio of maximum concentration in the presence to absence of grapefruit juice; [h]obtained from Masica et al., 2004; [i]ratio of trough concentrations in liver transplant recipients following one week of treatment and chronic grapefruit juice consumption.

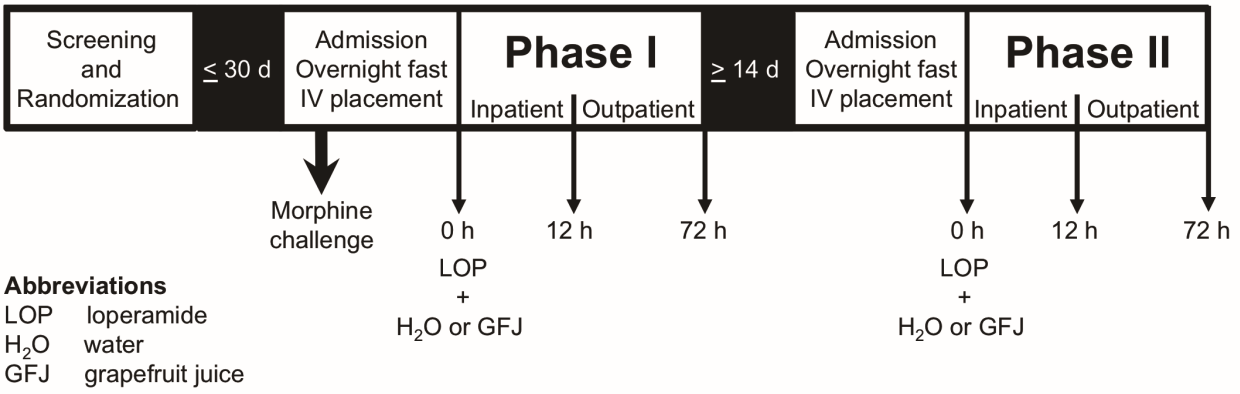

Figure 2.1. Clinical study design and procedures. As a positive control for miosis, 9 subjects were administered morphine sulfate (0.07 mg/kg; 5-min intravenous infusion); pupil diameter was measured before and at 5, 10, 20, 30, 60, 90 and 120 min after infusion. After an overnight fast, subjects (n = 16) were administered 16 mg loperamide with either 240 ml of water (control) or grapefruit juice (treatment). Blood and dark-adapted pupil diameter measurements were obtained before and 0.5, 1, 2, 3, 4, 5, 6, 8, 10, and 12 h after loperamide administration on the first day of each study phase. Subjects returned as outpatients for blood draws and pupil diameter measurements at 24, 36, 48, and 72 h after loperamide administration. The two phases were separated by at least two weeks.

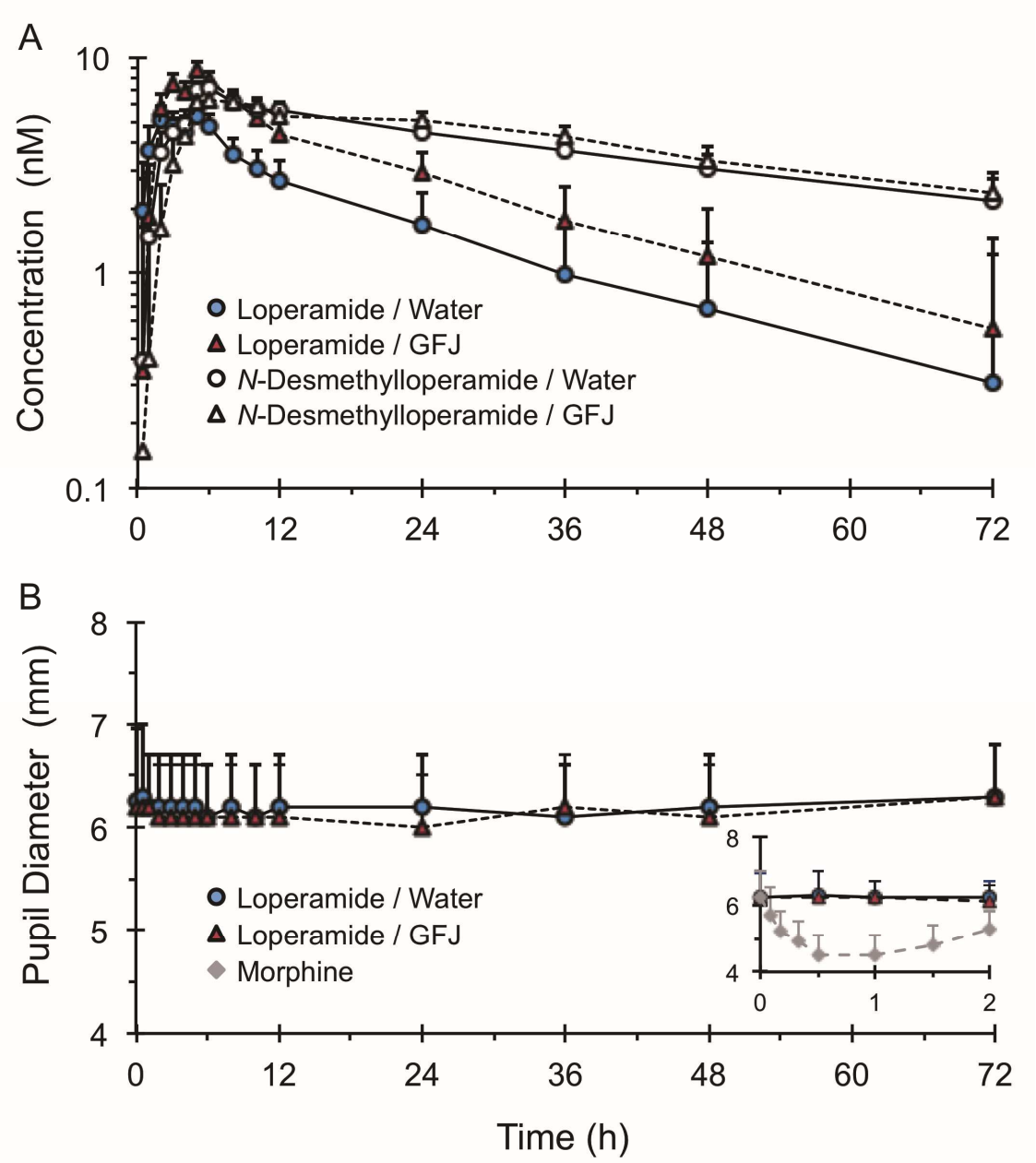

Figure 2.2. Loperamide (solid symbols) and *N*-desmethylloperamide (open symbols) plasma concentrations (A) and pupil diameter measurements (B) in 16 healthy volunteers administered loperamide (16 mg) with 240 ml of water (circles, solid lines) or grapefruit juice (triangles, dashed lines). The inset depicts the 0-2 h pupil diameter-time profile after loperamide (in the absence and presence of grapefruit juice) and morphine (diamonds) administration for the 9 volunteers administered the morphine challenge (0.07 mg/kg intravenously). Symbols and error bars denote the geometric mean and upper 90% confidence intervals, respectively.

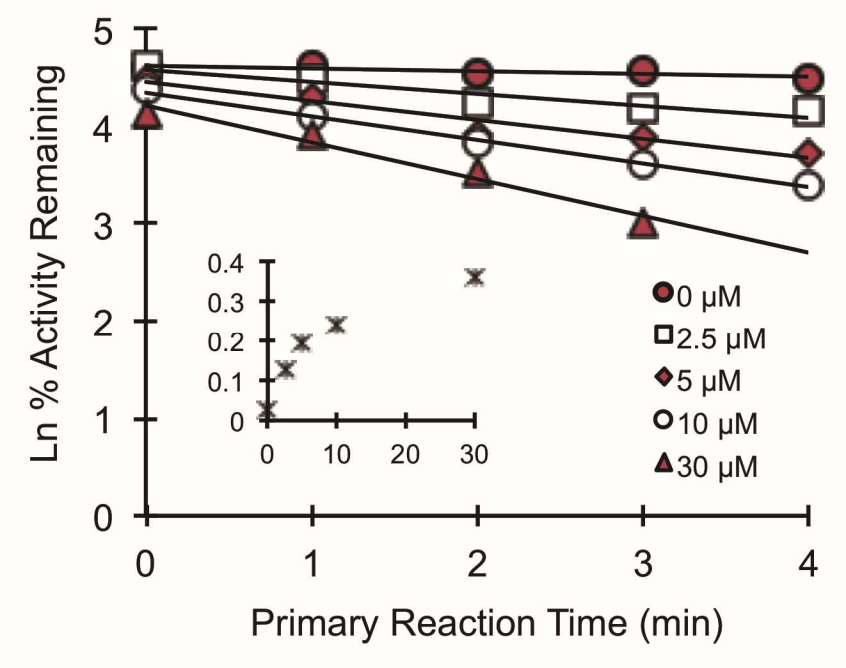

Figure 2.3. Time- and concentration-dependent inhibition of loperamide *N*-desmethylation by DHB in human intestinal microsomes. Symbols denote the mean of duplicate incubations, all of which deviated by <20%. Lines denote linear regression of the initial mono-exponential decline; solid lines denote nonlinear least-squares regression of observed values using Phoenix® WinNonlin® (v6.3). The inset depicts the apparent enzyme inactivation rate as a function of DHB concentration.

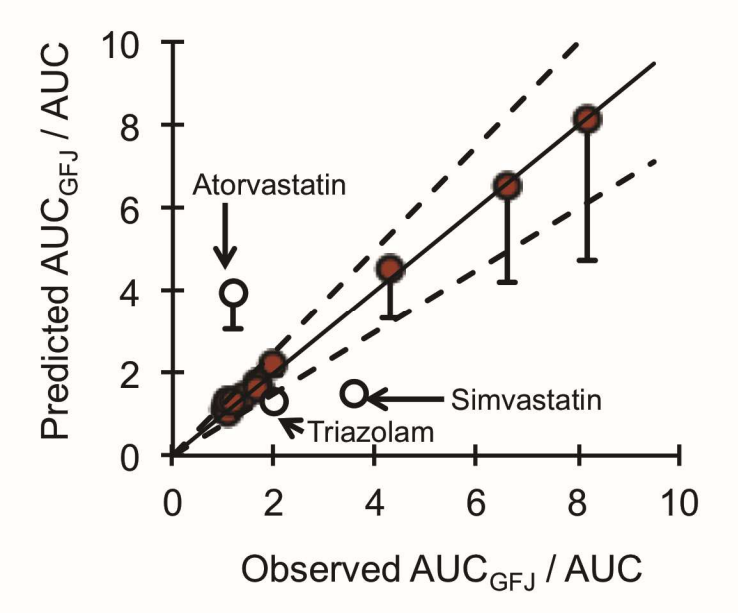

Figure 2.4. Relationship between the predicted and observed AUC_{GFJ}/AUC for 15 test drug substrates of the 'grapefruit juice effect' due to inhibition of intestinal CYP3A4. Predictions were made using a mechanistic static model. The solid line denotes unity. Dashed lines denote 25% variability around the line of unity. Error bars denote predicted values at an I_g of 0.05 μM (lower) and 50 μM (upper, which are smaller than the circles); circles denote the predicted values at an I_g of 5 μM. Closed circles denote predictions that were accurate to within 25% of observed values. Open circles denote predictions that were >25% of observed values.

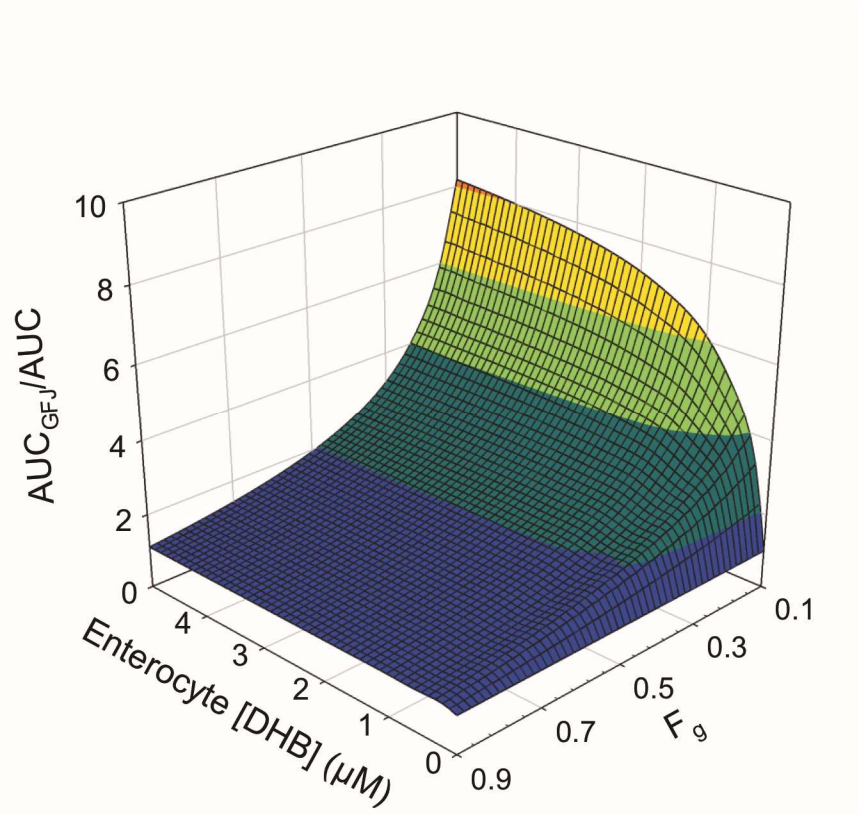

Figure 2.5. Relationship between the magnitude of a grapefruit juice-drug interaction (defined by AUC_{GFJ}/AUC) for varying enterocyte concentrations of DHB (I_g) and the fraction of victim drug escaping intestinal extraction (F_g). Simulations were conducted using Phoenix® WinNonlin® and eq. 2.

REFERENCES

Brunton LL, Chabner BA and Knollmann BC (2010) Appendix II, in *Goodman & Gilman's: The Pharmalogical Basis of Therapeutics* (Brunton L ed), McGraw Hill Medical.

Damkier P, Hansen LL and Brosen K (1999) Effect of diclofenac, disulfiram, itraconazole, grapefruit juice and erythromycin on the pharmacokinetics of quinidine. *Br J Clin Pharmacol* **48**:829-838.

Darbar D, Dell'Orto S, Morike K, Wilkinson GR and Roden DM (1997) Dietary salt increases first-pass elimination of oral quinidine. *Clin Pharmacol Ther* **61**:292-300.

Ducharme MP, Warbasse LH and Edwards DJ (1995) Disposition of intravenous and oral cyclosporine after administration with grapefruit juice. *Clin Pharmacol Ther* **57**:485-491.

Floren LC, Bekersky I, Benet LZ, Mekki Q, Dressler D, Lee JW, Roberts JP and Hebert MF (1997) Tacrolimus oral bioavailability doubles with coadministration of ketoconazole. *Clin Pharmacol Ther* **62**:41-49.

Gertz M, Harrison A, Houston JB and Galetin A (2010) Prediction of human intestinal first-pass metabolism of 25 CYP3A substrates from in vitro clearance and permeability data. *Drug Metab Dispos* **38**:1147-1158.

Hirota N, Ito K, Iwatsubo T, Green CE, Tyson CA, Shimada N, Suzuki H and Sugiyama Y (2001) In vitro/in vivo scaling of alprazolam metabolism by CYP3A4 and CYP3A5 in humans. *Biopharm Drug Dispos* **22**:53-71.

Holtbecker N, Fromm MF, Kroemer HK, Ohnhaus EE and Heidemann H (1996) The nifedipine-rifampin interaction. Evidence for induction of gut wall metabolism. *Drug Metab Dispos* **24**:1121-1123.

Jetter A, Kinzig-Schippers M, Walchner-Bonjean M, Hering U, Bulitta J, Schreiner P, Sorgel F and Fuhr U (2002) Effects of grapefruit juice on the pharmacokinetics of sildenafil. *Clin Pharmacol Ther* **71**:21-29.

Kharasch ED, Walker A, Hoffer C and Sheffels P (2004a) Intravenous and oral alfentanil as in vivo probes for hepatic and first-pass cytochrome P450 3A activity: noninvasive assessment by use of pupillary miosis. *Clin Pharmacol Ther* **76**:452-466.

Kharasch ED, Hoffer C, Whittington D and Sheffels P (2004b) Role of hepatic and intestinal cytochrome P450 3A and 2B6 in the metabolism, disposition, and miotic effects of methadone. *Clin Pharmacol Ther* **76**:250-269.

Kharasch ED, Bedynek PS, Walker A, Whittington D and Hoffer C (2008) Mechanism of ritonavir changes in methadone pharmacokinetics and pharmacodynamics: II. Ritonavir effects on CYP3A and P-glycoprotein activities. *Clin Pharmacol Ther* **84**:506-512.

Lennernas H (2003) Clinical pharmacokinetics of atorvastatin. *Clin Pharmacokinet* **42**:1141-1160.

Lilja JJ, Kivisto KT, Backman JT, Lamberg TS and Neuvonen PJ (1998) Grapefruit juice substantially increases plasma concentrations of buspirone. *Clin Pharmacol Ther* **64**:655-660.

Lilja JJ, Neuvonen M and Neuvonen PJ (2004) Effects of regular consumption of grapefruit juice on the pharmacokinetics of simvastatin. *Br J Clin Pharmacol* **58**:56-60.

Liu C, Shang YF, Zhang XF, Zhang XG, Wang B, Wu Z, Liu XM, Yu L, Ma F and Lv Y (2009) Co-administration of grapefruit juice increases bioavailability of tacrolimus in liver transplant patients: a prospective study. *Eur J Clin Pharmacol* **65**:881-885.

Lundahl J, Regardh CG, Edgar B and Johnsson G (1997) Effects of grapefruit juice ingestion--pharmacokinetics and haemodynamics of intravenously and orally administered felodipine in healthy men. *Eur J Clin Pharmacol* **52**:139-145.

Masica AL, Mayo G and Wilkinson GR (2004) In vivo comparisons of constitutive cytochrome P450 3A activity assessed by alprazolam, triazolam, and midazolam. *Clin Pharmacol Ther* **76**:341-349.

Obach RS, Walsky RL, Venkatakrishnan K, Houston JB and Tremaine LM (2005) In vitro cytochrome P450 inhibition data and the prediction of drug-drug interactions: qualitative relationships, quantitative predictions, and the rank-order approach. *Clin Pharmacol Ther* **78**:582-592.

Obach RS, Walsky RL, Venkatakrishnan K, Gaman EA, Houston JB and Tremaine LM (2006) The utility of in vitro cytochrome P450 inhibition data in the prediction of drug-drug interactions. *J Pharmacol Exp Ther* **316**:336-348.

Odou P, Ferrari N, Barthelemy C, Brique S, Lhermitte M, Vincent A, Libersa C and Robert H (2005) Grapefruit juice-nifedipine interaction: possible involvement of several mechanisms. *J Clin Pharm Ther* **30**:153-158.

Paine MF, Shen DD, Kunze KL, Perkins JD, Marsh CL, McVicar JP, Barr DM, Gillies BS and Thummel KE (1996) First-pass metabolism of midazolam by the human intestine. *Clin Pharmacol Ther* **60**:14-24.

Paine MF, Widmer WW, Hart HL, Pusek SN, Beavers KL, Criss AB, Brown SS, Thomas BF and Watkins PB (2006) A furanocoumarin-free grapefruit juice establishes furanocoumarins as the mediators of the grapefruit juice-felodipine interaction. *Am J Clin Nutr* **83**:1097-1105.

Paine MF, Widmer WW, Pusek SN, Beavers KL, Criss AB, Snyder J and Watkins PB (2008) Further characterization of a furanocoumarin-free grapefruit juice on drug disposition: studies with cyclosporine. *Am J Clin Nutr* **87**:863-871.

Reddy P, Ellington D, Zhu Y, Zdrojewski I, Parent SJ, Harmatz JS, Derendorf H, Greenblatt DJ and Browne K, Jr. (2011) Serum concentrations and clinical effects of atorvastatin in patients taking grapefruit juice daily. *Br J Clin Pharmacol* **72**:434-441.

Schwarz UI, Johnston PE, Bailey DG, Kim RB, Mayo G and Milstone A (2006) Impact of citrus soft drinks relative to grapefruit juice on ciclosporin disposition. *Br J Clin Pharmacol* **62**:485-491.

Sugimoto K, Araki N, Ohmori M, Harada K, Cui Y, Tsuruoka S, Kawaguchi A and Fujimura A (2006) Interaction between grapefruit juice and hypnotic drugs: comparison of triazolam and quazepam. *Eur J Clin Pharmacol* **62**:209-215.

Takanaga H, Ohnishi A, Murakami H, Matsuo H, Higuchi S, Urae A, Irie S, Furuie H, Matsukuma K, Kimura M, Kawano K, Orii Y, Tanaka T and Sawada Y (2000) Relationship between time after intake of grapefruit juice and the effect on pharmacokinetics and pharmacodynamics of nisoldipine in healthy subjects. *Clin Pharmacol Ther* **67**:201-214.

Yasui N, Kondo T, Furukori H, Kaneko S, Ohkubo T, Uno T, Osanai T, Sugawara K and Otani K (2000) Effects of repeated ingestion of grapefruit juice on the single and multiple oral-dose pharmacokinetics and pharmacodynamics of alprazolam. *Psychopharmacology (Berl)* **150**:185-190.

CHAPTER 3 : CHARACTERIZING THE ABUSE POTENTIAL OF OPIOIDS USING PHYSIOLOGICALLY-BASED PHARMACOKINETIC / PHARMACODYNAMIC MODELING: CASE STUDY WITH THE GRAPEFRUIT JUICE-LOPERAMIDE INTERACTION.[2]

Introduction

Opioid abuse in the US is second to alcohol abuse with respect to the proportion of individuals admitted to publically-funded treatment programs (National Institute of Drug Abuse, 2011; National Institute of Drug Abuse, 2014). Opioids are associated with chemical dependence- and overdose-related hospitalization (Meyer et al., 2014; National Institute of Drug Abuse, 2014). Prescription opioids are implicated in approximately 6% of total reported hospital admissions, exceeding all other prescription medications (National Institute of Drug Abuse, 2014). These observations have led to increased restrictions on opioid prescribing (Bohnert et al., 2011), which, combined with ready access to pharmacokinetic 'boosting' agents (e.g., grapefruit juice), may promote alternate means of abuse.

Anecdotal reports (Daniulaityte et al., 2013) and case studies (Johansen and Jensen, 2004; Sklerov et al., 2005) describe abuse of the over-the-counter anti-diarrheal agent loperamide, which acts on μ-opioid receptors in the gastrointestinal tract to slow motility. Despite having high potency toward the μ-opioid receptor (K_D, 0.5-1.5

[2] This chapter will be submitted to Clinical Pharmacokinetics as an original research paper and is presented in the style of the journal. Ainslie GR, Zamek-Gliszczynski MJ, Pollak GP, Kharasch ED and Paine MF. Characterizing the abuse potential of opioids using a physiologically-based pharmacokinetic/pharmacodynamic modeling approach: a case study with the grapefruit juice-loperamide interactions. *Clin Pharmacokinet*.

nM) (Terenius, 1975; Kalvass et al., 2007), central nervous system (CNS) effects are not apparent at usual (≤16 mg) or even supratherapeutic (24-32 mg) doses in healthy volunteers (Baker, 2007). This lack of effect is due to both a very low oral bioavailability (~0.3%) (Yu et al., 2004) and efficient efflux at the blood-brain barrier (BBB) by P-glycoprotein (P-gp), an apically-located transporter expressed in brain endothelial cells and other cell types, including enterocytes and hepatocytes (Paine et al., 2005a). The low oral bioavailability reflects both incomplete absorption in the intestine, due in part to P-gp, and extensive pre-systemic ('first-pass') metabolism in the intestine and liver, primarily by cytochrome P450 (CYP) 3A4 and CYP2C8. Opioid abusers describe using higher doses (70-200 mg) of loperamide to overcome these barriers, sometimes in combination with CYP3A4 and dual CYP3A4/P-gp inhibitors (Daniulaityte et al., 2013). Grapefruit juice (GFJ) is a readily accessible dual CYP3A4/P-gp inhibitor that has been implicated with loperamide abuse (Daniulaityte et al., 2013). This juice is an extensively studied dietary substance that can increase the systemic exposure of orally administered 'victim' drugs, including the opioids loperamide (Ainslie et al., 2014), oxycodone (Nieminen et al., 2010), and alfentanil (when administered orally) (Kharasch et al., 2004a), by inhibiting intestinal CYP3A4 in an irreversible manner (Bailey et al., 2013).

Clinical assessment of loperamide abuse claims presents challenges. For example, administering loperamide to healthy volunteers at doses reported to elicit euphoric effects (≥70 mg) would pose both safety and ethical concerns. In addition, recruiting opioid abusers may produce a highly variable cohort, requiring a large sample size. Physiologically-based pharmacokinetic/pharmacodynamic (PBPK/PD) modeling

would help allay these challenges. However, interaction predictions involving 'perpetrators' that are complex mixtures, such as GFJ, pose additional challenges. Dietary substances in general are mixtures that vary markedly in phytochemical composition, both between brands and batches of the same brand. Identification of a single marker constituent predictive of the mixture would mitigate this complexity. One such constituent in GFJ, 6',7'-dihydroxybergamottin (DHB), was demonstrated recently to predict the effect of whole juice on the systemic exposure of 13 of 16 victim CYP3A4 and CYP3A4/P-gp substrates, including loperamide, using a mechanistic static model (Ainslie et al., 2014).

The lack of a definitive loperamide concentration-CNS effect relationship in humans precludes development of a PD component of a predictive PBPK/PD model. The PD of seven μ-opioid agonists (alfentanil, fentanyl, loperamide, meperidine, methadone, morphine, sufentanil) were determined using a murine model of antinociception (Kalvass et al., 2007). Excluding loperamide (due to the lack of data for humans), unbound brain concentration required to elicit half the maximum effect ($EC_{50,brain,unbound}$) correlated with human equipotent intravenous dose (r^2 = 0.98), supporting mouse as a suitable model for opioid brain disposition and pharmacology in humans. Although mouse $EC_{50,brain,unbound}$ was correlated to human intravenous dose, a maximum attainable effect (E_{max}) measured using a hot-plate latency test flick assay, does not translate to clinical measures of opioid effect. This discordance could be addressed by recovering an E_{max} using a readily obtainable and sensitive endpoint (change in pupil diameter) in humans and an exemplar opioid.

Alfentanil is a short-acting opioid indicated for analgesia during surgical procedures. Unlike other opioids (e.g., morphine, methadone, and oxycodone), the plasma concentration-effect relationship is not associated with a time delay, i.e., counterclockwise hysteresis. These characteristics, combined with the availability of extensive preclinical and clinical data, render alfentanil an ideal exemplar opioid to recover key parameters needed to develop the PD component of a PBPK/PD model for loperamide.

The goal of the present work was to determine an alfentanil-equivalent dose of loperamide, in the absence and presence of GFJ, to assess the abuse potential of loperamide. First, a PBPK/PD model for alfentanil was developed using PD parameters recovered from clinical and in vivo mouse studies. Second, PBPK/PD model robustness was assessed further using a second, well-studied opioid, methadone. Third, a PBPK model describing the GFJ-loperamide interaction was developed using DHB as a surrogate of whole juice. Fourth, a PBPK/PD model for loperamide was developed using alfentanil PD parameters to predict a PD endpoint (change in pupil diameter). Finally, using the DHB-loperamide interaction model and the PBPK/PD model for loperamide, an alfentanil equivalent dose of loperamide was determined with and without GFJ. This work provides an initial assessment of loperamide abuse potential in healthy volunteers by comparing the simulated pupillary response with that of alfentanil. This PBPK/PD modeling approach may be more broadly applied to other populations, opioids, or perpetrator xenobiotics.

1. Methods

1.1. Materials and Chemicals

Loperamide hydrochloride and D_6-loperamide were purchased from Toronto Research Chemicals Inc. (North York, Ontario Canada). DHB was purchased from Sigma Aldrich (St. Louis, MO) (for binding experiments) or from Caymen Chemical (Ann Arbor, MI) (as analytical standard for quantification in human plasma). Psoralen was purchased from Caymen Chemical. LC-MS/MS grade acetonitrile, methanol, dimethylsulfoxide, ethyl acetate, and formic acid were purchased from Thermo Fisher (Waltham, MA).

1.2. Recovery of Binding and Partitioning Properties

1.2.1. Plasma Protein and Brain Tissue Binding

The unbound fraction for loperamide and DHB in human plasma and rat brain tissue was determined experimentally by equilibrium dialysis (Zamek-Gliszczynski et al., 2012).

1.2.2. Blood to Plasma Partition Ratio

Loperamide and DHB were added to fresh human whole blood to yield final concentrations of 0.1, 1, and 10 µM. After 2 h at 37°C, blood cells and plasma were separated by centrifugation (3000 rpm, 4°C, 10 min). Aliquots of whole blood and plasma were precipitated with methanol:acetonitrile (1:1, v:v) containing internal standard. The supernatants were quantified for loperamide or DHB by LC-MS/MS Blood to plasma (B/P) ratios were calculated as the ratio of analyte in blood to that in plasma (Zamek-Gliszczynski et al., 2013).

1.3. Determination of DHB Pharmacokinetics

1.3.1. Quantification of DHB in Human Plasma

Plasma samples from a GFJ-loperamide interaction study (Ainslie et al., 2014) were quantified for DHB concentrations. Plasma had been stored at -80°C and was thawed at room temperature under low light conditions. Calibration standards and quality controls were prepared using blank human plasma (Bioreclamation, Baltimore, MD) at concentrations ranging from 0.25-1000 and 0.8-800 nM, respectively. Ethyl acetate (500 µL) containing 400 nM internal standard (psoralen) was added to thawed plasma (100 µL) to precipitate proteins. Samples were vortexed for 3 min at room temperature then centrifuged (2000 x g, 10 min, 4℃). Supernatant (400 µl) was transferred to 0.6 mL cluster tubes and dried under heated (50℃) nitrogen gas. Residues were reconstituted in 95% water:5% acetonitrile:0.1% formic acid (v:v:v).

Samples (10 µl) were injected onto a Thermo Aquasil C18 column (3 µm, 2.1 x 50 mm). Analytes were eluted using a gradient initially held at 95% mobile phase A (water with 0.1% formic acid) and 5% mobile phase B (acetonitrile with 0.1% formic acid) for 0.4 min. Mobile phase B was increased linearly for 1.1 min to 95%, maintained for 0.2 min, then returned to initial conditions over 6 sec. The column was equilibrated for 2 min. Eluent was directed to waste for the first 0.4 min then to a Sciex API 6500 hybrid triple quadrupole mass spectrometer (Framingham, MA). The mass spectrometer was operated in multiple reaction monitoring (MRM) mode, with a source temperature of 250℃ and ion spray voltage of 2500 V. MRM transitions for DHB and psoralen were 273.2→203.1 (collision energy, 25 mV) and 187.1→131.2 (collision energy, 32 mV), respectively. DHB was quantified using peak area ratios, calibration standards, and Multiquant™ software (v3.0, AB Sciex, Framingham, MA). The lower limit of

quantification was 250 pM based on FDA guidelines (US Food and Drug Administration, 2013).

1.3.2. Pharmacokinetic Analysis

Pharmacokinetic outcomes were obtained *via* standard non-compartmental methods using Phoenix® WinNonlin® (v6.3, Certara, St. Louis, MO). The maximum concentration (C_{max}) and time to reach C_{max} (t_{max}) were obtained directly from the plasma concentration-time profiles. Area under the plasma concentration-time curve (AUC) from time zero to 4 h (AUC_{0-4h}) was determined using the trapezoidal method with linear up/log down interpolation.

1.4. Physiologically-Based Pharmacokinetic Model Development

PBPK models for loperamide, DHB, alfentanil, and methadone were developed using the 'Full PBPK model' (Fig. 1) within Simcyp® (version 13, Certara), a population-based simulator.

1.4.1. Model Parameterization: Absorption

Loperamide and DHB absorption were described using the Advanced Dissolution, Absorption, and Metabolism (ADAM) model, which considers intestinal metabolism and transport and is required to assess interactions at the level of the gut (Jamei et al., 2009). Human enteric permeability coefficients ($P_{eff,man}$) were predicted using data obtained from MDCK (loperamide) (Tran et al., 2004) or Caco-2 (DHB) (Paine et al., 2005b) cells (Table 3.1). First-order absorption rate constants (k_a) for alfentanil, *R*-methadone, and *S*-methadone were obtained from the literature (Yang et al., 2006).

1.4.2. Model Parameterization: Distribution

Molecular weight, logP, and pKa were obtained from the literature (Table 1). Plasma protein binding, brain tissue binding, and B/P ratios were obtained experimentally (section 2.2.2) or from the literature (Table 3.1). Partitioning into tissue compartments was predicted within Simcyp® using 'method 2' (Berezhkovskiy, 2011). Model-predicted volumes of distribution at steady state (V_{ss}) were compared to literature values to confirm the appropriateness of the tissue distribution model.

1.4.3. Model Parameterization: Metabolism

Loperamide is metabolized primarily to *N*-desmethylloperamide by CYP2B6, -2C8, -2D6, and -3A4 (Kim et al., 2004). Alfentanil is metabolized primarily to noralfentanil and *N*-phenylpropionamide by CYP3A4/5 (Klees et al., 2005). Methadone is metabolized to 2-ethyl-1,5-dimethyl-3,3-diphenylpyrrolinium (EDDP) by CYP2B6 and CYP3A4 in a stereospecific manner (Chang et al., 2011). V_{max} and K_m obtained from recombinant CYPs were available for the three opioids (Table 3.1). The K_m (1 μM) and V_{max} (19 pmol/min/pmol CYP3A4) for DHB were predicted using K_i (1 μM) (Ohnishi et al., 2000; Paine et al., 2004) and ADMET™ predictor (Simulations Plus, Lancaster, CA) estimates, respectively, and compared to reported DHB plasma concentrations, of which the detection limit was 2.7 nM (Goosen et al., 2004).

1.4.4. Model Parameterization: Excretion

Biliary clearance of each compound was either low (<5%) or not reported (Brown et al., 2004) and was not considered. Because ~1% of a loperamide dose is recovered in the urine (Baker, 2007), renal clearance for loperamide was not considered. Renal clearance for alfentanil (1.0 L/h) and methadone (1.8 L/h) (Yang et al., 2006) were available and were included in the respective models.

1.4.5. Brain Compartment Concentrations

The permeability-limited four-compartment brain model (Figure 3.1B) within Simcyp® was used to simulate intracranial brain blood, brain mass, cranial cerebrospinal fluid (CSF), and spinal CSF drug concentrations. The passive permeability of each compound was estimated in Simcyp® (Table 3.2), and whole organ P-gp-mediated efflux was determined by scaling in vitro P-gp mediated transport clearance parameters based on BBB surface area within Simcyp®. The intrinsic P-gp-mediated transport clearance for loperamide ($CL_{T,int}$, 1.67 µL/min) was obtained from MDCK cells (Tran et al., 2004). Methadone $CL_{T,int}$ (2 µL/min) was obtained from Caco-2 cells (Hassan et al., 2009) and was assumed to be the same for the two enantiomers. Alfentanil is not a P-gp substrate (Wandel et al., 2002).

1.5. Pharmacodynamic Model Parameterization

1.5.1. Pharmacodynamic Parameter Recovery for Alfentanil

Alfentanil plasma concentration-time and effect (miosis)-time data from a previous healthy volunteer study (Kharasch et al., 2004a) were used to recover plasma E_{max} for pupillary miosis after intravenous or oral administration. E_{max} and plasma EC_{50} ($EC_{50,plasma,total}$) were recovered using equation 1 and a fixed Hill coefficient (γ) obtained from mouse (1.8) (Kalvass et al., 2007):

$$E_{obs} = \frac{E_{\max} \bullet C_{obs}^{\gamma}}{EC_{50,plasma,total}^{\gamma} + C_{obs}^{\gamma}} \qquad \text{Equation 1}$$

where E_{obs} denotes the observed effect (miosis, mm), $EC_{50,plasma,total}$, total plasma concentration required to elicit half E_{max}; and C_{obs} denotes observed plasma concentration.

1.5.2. Pharmacodynamic Model Development

Because human CNS PD data for loperamide do not exist, parameters ($EC_{50,brain,unbound}$, γ) obtained from mouse (Kalvass et al., 2007) were used (Table 3.2). This approach was applied to alfentanil data as a 'training set' and to methadone data as a 'validation set'. Unbound brain concentration ($C_{brain,unbound}$) was assumed to drive effects. PD model simulations for alfentanil and loperamide were conducted using Simcyp® (Figure 1) and equation 2:

$$E_{sim} = \frac{E_{\max} \bullet C_{brain,unbound}^{\gamma}}{EC_{50,brain,unbound}^{\gamma} + C_{brain,unbound}^{\gamma}} \qquad \text{Equation 2}$$

where E_{sim} denotes the simulated pupillary response (mm).

Due to limitations of Simcyp®, PD simulations for *R*- and *S*-methadone were conducted using Phoenix® WinNonlin® and equation 3 to allow for unbound concentrations of both enantiomers to drive effect:

$$E_{sim} = \frac{E_{\max} \bullet C_{unbound,brain,R-Meth}^{\lambda}}{EC_{50,unbound,brain}^{\lambda} + C_{unbound,brain,R-Meth}^{\lambda}} + \frac{E_{\max} \bullet C_{unbound,brain,S-Meth}^{\gamma}}{EC_{50,unbound,brain}^{\gamma} + C_{unbound,brain,S-Meth}^{\gamma}} \qquad \text{Equation 3}$$

Alfentanil and loperamide miosis-time profiles were simulated in Phoenix WinNonlin® to ensure equivalent outcomes across software platforms.

1.6. PBPK and PBPK/PD Model Evaluation

Model-predicted loperamide AUC from time 0 to 72 h ($AUC_{0\text{-}72h}$), C_{max}, and t_{max} were compared to observed outcomes (Ainslie et al., 2014). DHB model-simulated plasma-concentration-time profiles were compared to observed profiles (section 2.3.1). The primary endpoints, maximum observed response (R_{max}) and area under the effect-time curve (AUEC), for loperamide, alfentanil, and methadone were compared to observed values (Skarke et al., 2003; Kharasch et al., 2004b; Mukwaya et al., 2005; Niemi et al., 2006). Predictions were considered successful if model-predicted

pharmacokinetic (AUC, C_{max}) and pharmacodynamic (AUEC and R_{max}) endpoints were within 30% of observe endpoints (Brantley et al., 2013).

1.7. Loperamide Dose Escalation Simulations

Loperamide PK and PD were simulated in virtual populations of healthy volunteers, with doses ranging from 2-200 mg in the absence and presence of DHB (5 mg). Simulations were conducted in a cohort (n = 100) of equal numbers of men and women and in separate cohorts of men (n = 100) and women (n = 100) to assess potential sex differences. The primary endpoint was R_{max}. Model-predicted loperamide R_{max} was compared to oral alfentanil observed and model-predicted R_{max} to determine the alfentanil-equivalent dose of loperamide.

2. RESULTS

2.1. Performance of the PBPK DHB-loperamide interaction model

The PBPK model for loperamide modestly over-predicted geometric mean $AUC_{0\text{-}72\ h}$ (by 1.3-fold). C_{max}, t_{max}, and terminal half-life were predicted to within 20% of observed outcomes (Table 3.3, Figure 3.2). DHB was detected in the plasma of 14 of 16 subjects, and PK outcomes were recoverable in 11 subjects (Figure 3.2C). The PBPK model for DHB predicted median DHB $AUC_{0\text{-}4h}$, and C_{max} to within 10% of observed values (Figure 3.2C, Table 3.3). The model-predicted ratio of loperamide AUC in the presence to absence of DHB was underpredicted by 20%.

2.2. Performance of the alfentanil PBPK/PD model

Plasma concentration- and pupil miosis-time data and a sigmoidal direct effect model were used to recover a population mean (%CV) E_{max} and $EC_{50,plasma,total}$ of 6.5 (40%) mm and 54.2 nM (12%), respectively. The recovered E_{max} was used for subsequent PD modeling.

The alfentanil PBPK model was developed using human in vitro and clinical data. The PD model used an E_{max} recovered from human pupil miosis-time data and an $EC_{50,brain,unbound}$ from mouse (Kalvass et al., 2007). Plasma concentration- and miosis-time profiles were simulated for both intravenous and oral administration of alfentanil and compared to observed data (Figure 3.3). With intravenous alfentanil, model-predicted geometric mean [90% CI] V_{ss} (0.54 [0.53-0.55] L/kg) lay within the observed range (0.30-0.65 L/kg). With oral administration, model-predicted geometric mean AUC and C_{max} were within 22% of observed outcomes. PD simulations of oral alfentanil

underpredicted R_{max}, by 30%. The overpredicted AUC, combined with the underpredicted R_{max}, resulted in an accurate prediction of AUEC.

2.3. Simulated methadone profiles to substantiate the modeling framework

The plasma concentration-time profile of both enantiomers following an oral dose (9.9 mg) of racemic methadone (4.95 mg assumed for each enantiomer) agreed with the plasma concentration-time data from two independent clinical studies (Figure 3.4A) (Kharasch et al., 2004b; Ke et al., 2014). The model-predicted methadone geometric mean R_{max}, which accounted for both enantiomers, was within 10% of the observed R_{max} (Kharasch et al., 2004b).

2.4. Simulated loperamide dose escalation studies

Escalating doses (2-200 mg) of loperamide were simulated in 100 virtual healthy subjects (50 men, 50 women) in the absence and presence of the marker GFJ constituent DHB (5 mg). In the absence of DHB, a 72 mg dose of loperamide was predicted to achieve the model-predicted oral alfentanil R_{max} (1.4 mm), whereas a 96 mg dose was predicted to achieve the observed alfentanil R_{max} (2.0 mm) (Fig. 5). The presence of DHB was predicted to lower the alfentanil-equivalent dose of loperamide dose by ~30% (Fig.3.5). Virtual trials with 100 men or women indicated a slight leftward shift in the dose-response profile for women compared to men (Fig. 3.5B).

3. Discussion

Increased restrictions on opioid prescribing may promote alternate means of abuse. Anecdotal and case reports describe abuse of the over-the-counter opioid, loperamide, in combination with the readily accessible PK boosting agent, GFJ (Daniulaityte et al., 2013). Given the ethical and safety concerns associated with clinical determination of the loperamide dose needed to elicit CNS opiate-like effects in both the absence and presence of GFJ, a PBPK/PD modeling and simulation approach was used to address these limitations.

Alfentanil was used as an exemplar opioid due to a straightforward plasma concentration-effect relationship and the availability of rich clinical plasma concentration-effect data. Alfentanil was used to recover E_{max}, as measured by a clinically relevant, sensitive, and noninvasive endpoint, change in pupil diameter. The recovered E_{max} (6.5 mm) lay within the constraints of human physiology (minimal pupil diameter, 0.5-1.5 mm; average dark-adapted pupil diameter, 7.3-8.7 mm) (Campbell and Gubisch, 1966; Bradley et al., 2010; Bradley et al., 2011). Alfentanil model-predicted AUC, C_{max}, AUC, AUEC and R_{max} were within the predefined criterion (≤30%). R_{max} was used as a primary outcome for dose escalation analysis.

Because evaluation of an alfentanil PBPK/PD model using an E_{max} recovered from alfentanil data is circular, the model was tested with a second opioid. Additionally, given that loperamide is a P-gp substrate, unlike alfentanil, the ideal test opioid would be a P-gp substrate. Methadone was selected because it is both a P-gp substrate (Hassan et al., 2009) and rich clinical plasma concentration- and pupil diameter-time data are available (Skarke et al., 2003; Kharasch et al., 2004b; Mukwaya et al., 2005;

Niemi et al., 2006). As such, methadone could be used to evaluate the scaling of in vitro (P-gp transport clearance) to that at the BBB using in human using a relative activity factor. Finally, a PBPK model was available (Yang et al., 2006) that could be adapted to Simcyp® and expanded to include brain distribution and PD parameters. Using the approach applied to alfentanil, the PBPK model-simulated AUC and C_{max} for *R*- and *S*-methadone were within 30% of observed values.

Although methadone has several positive attributes as a test opioid, the fact that the drug exists as a racemic mixture adds to the PD modeling complexity. The *R*-enantiomer is 10-fold more potent than the *S*-enantiomer at the μ-opioid receptor (Pert and Snyder, 1973). Murine effect data for methadone were recovered following administration of the racemic mixture (Kalvass et al., 2007), and clinical studies involve the racemic mixture. Accordingly, the E_{max} equation (equation 2) was modified to account for the additive effect of *R*- and *S*-methadone (equation 3). The predicted R_{max} was within 30% of observed R_{max}; however, the predicted time to reach R_{max} was delayed compared to observed data. This observation may imply a limitation in the distributional model within Simcyp® or by the tissue partitioning method (described in section 2.4.2). Despite these caveats, the accurate prediction of the primary outcome, R_{max}, substantiated the loperamide PBPK/PD model.

A loperamide PBPK model developed using a 'bottom-up' approach successfully predicted plasma C_{max} and AUC, permitting development of an interaction model with GFJ. Because GFJ is a complex mixture of phytochemical constituents, the candidate marker constituent, DHB, was selected as a surrogate of whole juice. As demonstrated recently, a mechanistic static model involving DHB predicted the magnitude of a

CYP3A-mediated GFJ interaction (AUC ratio of the victim drug in the presence to absence of GFJ) for 13 of 16 victim drugs, including the three opioids examined in the current work, to within 25% of observed ratios (Ainslie et al., 2014).

The DHB PBPK model was developed and evaluated using in-house plasma concentration-time data obtained from a GFJ-loperamide interaction study (Ainslie et al., 2014). DHB was quantified in the plasma and in the test juice, permitting evaluation of the DHB PBPK model. Prior to the current work, no human PK DHB information was available, and only one report described DHB being detected in human plasma (Goosen et al., 2004). However, the recovered DHB outcomes may be biased as subjects were excluded if DHB was unquantifiable. The DHB-loperamide interaction slightly underpredicted the fold increase in loperamide AUC in the presence of GFJ (1.5 versus 1.7). This outcome was not surprising given the presence of other CYP3A4/P-gp inhibitors in the juice, including bergamottin (Bailey et al., 2003; Paine et al., 2006) and structural analogs (Oda et al., 2007).

Loperamide PBPK/PD model simulations at clinically studied doses (16-24 mg) predicted the absence of a significant effect in healthy volunteer studies (Tayrouz et al., 2001; Skarke et al., 2003; Ainslie et al., 2014). Simulated loperamide dose escalation studies, in the absence of DHB, indicated that a loperamide dose of 72 mg was equivalent to an oral alfentanil dose of 1.7 mg. These results are consistent with anecdotal reports of loperamide abuse (70-200 mg) (Daniulaityte et al., 2013). Conversely, in a clinical study in which 60 mg of loperamide was administered to former opioid abusers, no significant effect was observed relative to codeine (96 mg of base) or placebo. However, this population may not be generalizable to healthy volunteers,

representing a limitation of the model. Nevertheless, this PBPK/PD modeling and simulation paradigm provides a novel approach to assess loperamide abuse potential in healthy subjects and opioid naïve patients.

The dose escalation studies stratifying by sex suggested that women are slightly more susceptible than men to a centrally acting opiate-like effect with loperamide. The predicted sex difference is likely the result of men weighing more on average than women, coupled with the lack of weight-normalized doses with model simulations. However, since loperamide is a substrate of P-gp and multiple CYPs, sex-related differences in these factors could contribute. This preliminary evaluation of sex differences exemplifies the broader applications of this PBPK/PD model that can build on the understanding of PK boosting agents, including GFJ, on the abuse potential of opioids.

In summary, an oral alfentanil-equivalent dose of loperamide was determined, with and without the readily accessible PK boosting agent, GFJ, using a PBPK/PD modeling and simulation approach. An E_{max} for alfentanil induced pupillary response was recovered to inform an alfentanil PBPK/PD model. The alfentanil PBPK/PD model successfully predicted clinical PK and PD outcomes, prompting further evaluation of the modeling approach by a second opioid. Methadone was selected as a second 'validation' opioid due to it being a P-gp substrate with available rich clinical plasma concentration-time and pupil miosis-time data. To begin to assess the abuse potential of loperamide, a loperamide-DHB PBPK interaction model was developed and predicted the magnitude of a loperamide-GFJ interaction to within 20%. Subsequently, a loperamide PBPK/PD was developed and a virtual dose-escalation study was simulated

in healthy subjects both in the absence and presence of DHB. These results indicated loperamide doses in excess of 70 mg (in the absence of GFJ) would be required to elicit a pupillary response equivalent to an oral alfentanil dose of 1.7 mg (0.23 μg/kg). This translational approach to predict opioid pharmacodynamics could be applied to patient populations and to assess the abuse and/or interaction potential of novel opioid agonists.

Table 3.1. PBPK model input parameters.

Parameter	Alfentanil	DHB	Loperamide	*R*-Methadone	*S*-Methadone
Physicochemical					
Molecular weight (g/mol)	416.5	372	477	309	309
LogP	2.16	2.79	5.13	3.95	3.95
Compound type	Monoprotic Acid	Diprotic Acid	Monoprotic Base	Monoprotic Base	Monoprotic Base
pK_a 1	7.5[a]	13.58[a]	8.6[a]	9.2[a]	9.2[a]
pK_a 2		12.8			
B/P	1.14[a]	0.6[b]	0.71[b]	1[c]	0.75[a]
$f_{u,plasma}$	0.1	0.06[b]	0.03[b]	0.16[a]	0.12[a]
Absorption					
Model type	First-order	ADAM	ADAM	First-order	First-order
k_a (h^{-1})	2.6[b]			0.58	0.58
$P_{eff,man}$ (10^{-4} cm/s)		6.202	0.586		
Distribution					
V_{ss} (L/kg)	0.55[c]	2.4[c]	14[c]	6.3[c]	4.7[c]
Elimination					
$V_{max,CYP3A4}$ (pmol/min/pmol)	6.05; 1.03[a]	19[d]	1.7[a]	6.7[a]	0.028[f]
$K_{m,CYP3A4}$ (μM)	14.1; 18.9[a]	1.2[e]	6.3[a]	13[a]	
$V_{max,CYP3A5}$ (pmol/min/pmol)	5.12; 0.36[a]				
$K_{m,CYP3A5}$ (μM)	10.7; 14.8[a]				
$V_{max,CYP2B6}$ (pmol/min/pmol)			81[a]	50.9[a]	0.427[f]
$K_{m,CYP2B6}$ (μM)			65.6[a]	691[a]	
$V_{max,CYP2C8}$ (pmol/min/pmol)			53[a]	0.2[a]	0.078[f]
$K_{m,CYP2C8}$ (μM)			11.3[a]	60[a]	
$V_{max,CYP2C19}$				0.2[a]	
$K_{m,CYP2C19}$ (μM)				60[a]	
$V_{max,CYP2D6}$ (pmol/min/pmol)			16[a]	0.2[a]	
$K_{m,CYP2D6}$ (μM)			2.8[a]	60[a]	

[a] Recovered from the literature; [b] determined experimentally within the present work; [c] determined using in silico predictive tools within Simcyp®; [d] determined using ADMET predictor; [e] K_m for DHB was estimated as the reversible inhibitory kinetic parameter, K_i; [f] values denotes an experimentally reported intrinsic clearance (μl/min/pmol P450) in place of a K_m and V_{max} for S-methadone.

Table 3.2. Pharmacodynamic model parameter input.

Parameter	Alfentanil	Loperamide	Methadone
PSB (L/h)	28.9	155.7	185.5
$f_{u,\ brain}$	0.33	0.007	0.123
CL_T (µL/min)		1.67	2.0
RAF		3.5	2.2
EC_{50} (nM)[7]	7.3	1.47	14
Hill coefficient[7]	1.8	2.7	3.7

PSB, passive permeability clearance at the blood-brain-barrier calculated within Simcyp®; $f_{u,\ brain}$, fraction of drug unbound in brain tissue; CL_T, transport mediated efflux intrinsic clearance at the blood-brain-barrier; RAF, relative activity factor used to scale transporter mediated clearance; EC_{50}, the concentration required to elicit half of the maximal effect.

Table 3.3.Observed and model-predicted pharmacokinetic and pharmacodynamic outcomes following oral opioid administration.

Outcome	Observed	Model-Predicted
Loperamide		
$AUC_{0\text{-}last}$t (nM-h)	105 [87-126]	134 [126-142]
C_{max} (nM)	6.5 [5.3-8.1]	7.2 [6.8-7-7]
T_{max} (h)	3.0 (0.5-12)	4.5 (0.95-7.3)
$t_{1/2}$ (h)	23.3 [20.7-26.3]	32.7 [25.2-42.4]
DHB		
$AUC_{0\text{-}6\ (nM\text{-}h)}$	44.0 [26.0-74.5]	47.4 [38.9-57.9)
$C_{max\ (nM)}$	21.5 [15.1-30.7]	22.8 [19.0-27-2]
T_{max} (h), median [range]	1 (0.5-4)	0.7 (0.5-1.5)
Alfentanil		
C_{max} (ng/mL)	21.0 [17.3-25.4]	22.0 [17.0-28.5]
$AUC_{0\text{-}last}$ (ng-h/mL	36.0 [29.4-44.0]	43.8 [27.5-70.0]
R_{max} (mm)	2.0 [1.6-2.5]	1.4 [1.2-1.5]
$AUEC_{0\text{-}last}$ (mm-h)	2.3 [1.7-3.1]	2.4 [2.0-2.8]
$t_{1/2}$ (h)	1.1 [0.98-1.25]	1.5 [1.2-2.1]
Methadone		
$C_{max,\ R\text{-}Meth}$ (ng/mL)	13 ± 3	11.9 ± 3.2
$AUC_{0\text{-}last,\ R\text{-}Meth}$ (ng-h/mL	461 ± 72	407 ± 146
$C_{max,\ S\text{-}Meth}$ (ng/mL)	23 ± 6	25.8 ± 8.4
$AUC_{0\text{-}last,\ S\text{-}Meth}$ (ng-h/mL	639 ± 165	667 ± 233
R_{max} (mm)	3.5 ± 1.5	3.2 ± 2.7
$AUEC_{0\text{-}last}$ (mm-h)	78 ± 39	77 ± 51

$AUC_{0\text{-}last}$, area under the plasma concentration-time curve from time zero to the last measured time point; C_{max}, maximal plasma concentration; T_{max}, time to reach C_{max}; $t_{1/2}$, terminal half-life; R_{max}, maximal pupillary response; $AUEC_{0\text{-}last}$, area under the effect-time curve from time zero to the last measured time point. Values are expressed as the geometric mean [90% Confidence intervals] except for T_{max}, which is reported the median (range).

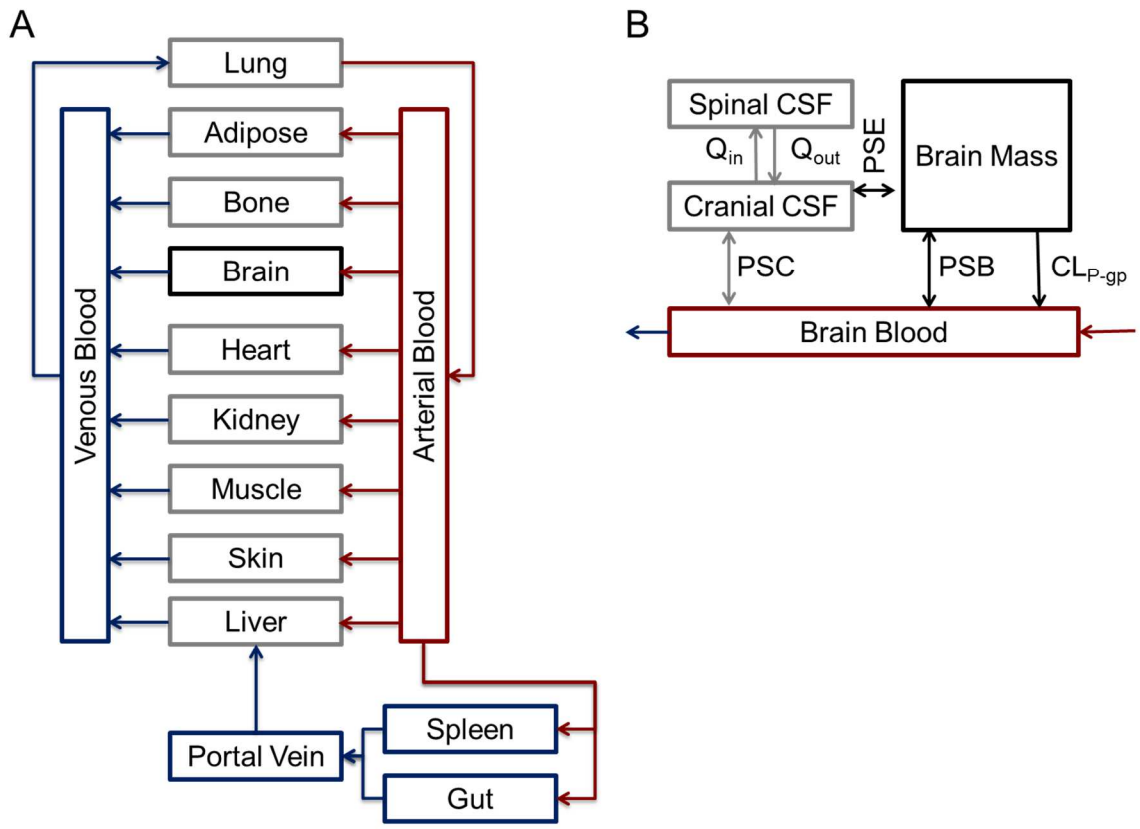

Figure 3.1. The general model structure of a physiologically-based pharmacokinetic/ pharmacodynamic model (a) the central nervous system sub compartment (b) and the pharmacodynamic effect model used for model simulations. PSB, denotes the bidirectional passive permeability clearance at the blood brain barrier; PSC, denotes the bidirectional passive permeability clearance at the cranial cerebral spinal fluid (CSF) blood barrier; PSE, denotes the bidirectional passive permeability clearance at the brain cranial CSF barrier; $CL_{p\text{-}gp}$ denotes the efflux clearance mediated by p-glycoprotein.

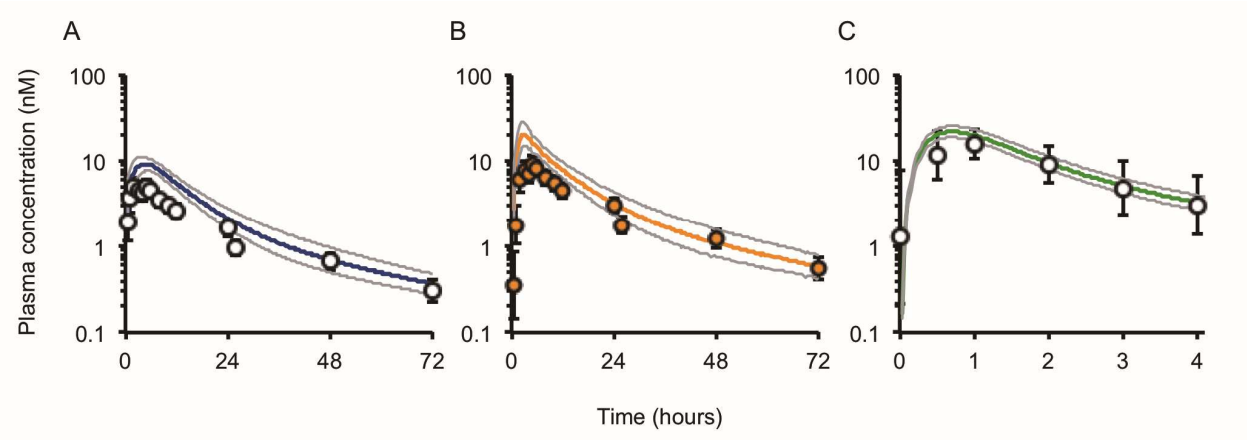

Figure 3.2. Observed geometric mean (circles) and model-predicted mean (colored lines) plasma concentration-time profiles of loperamide and the 90% confidence intervals (grey lines) when taken with water (A) or GFJ/DHB (B) and of DHB plasma concentrations (C). Model-predicted simulations were conducted using 100 virtual healthy subjects.

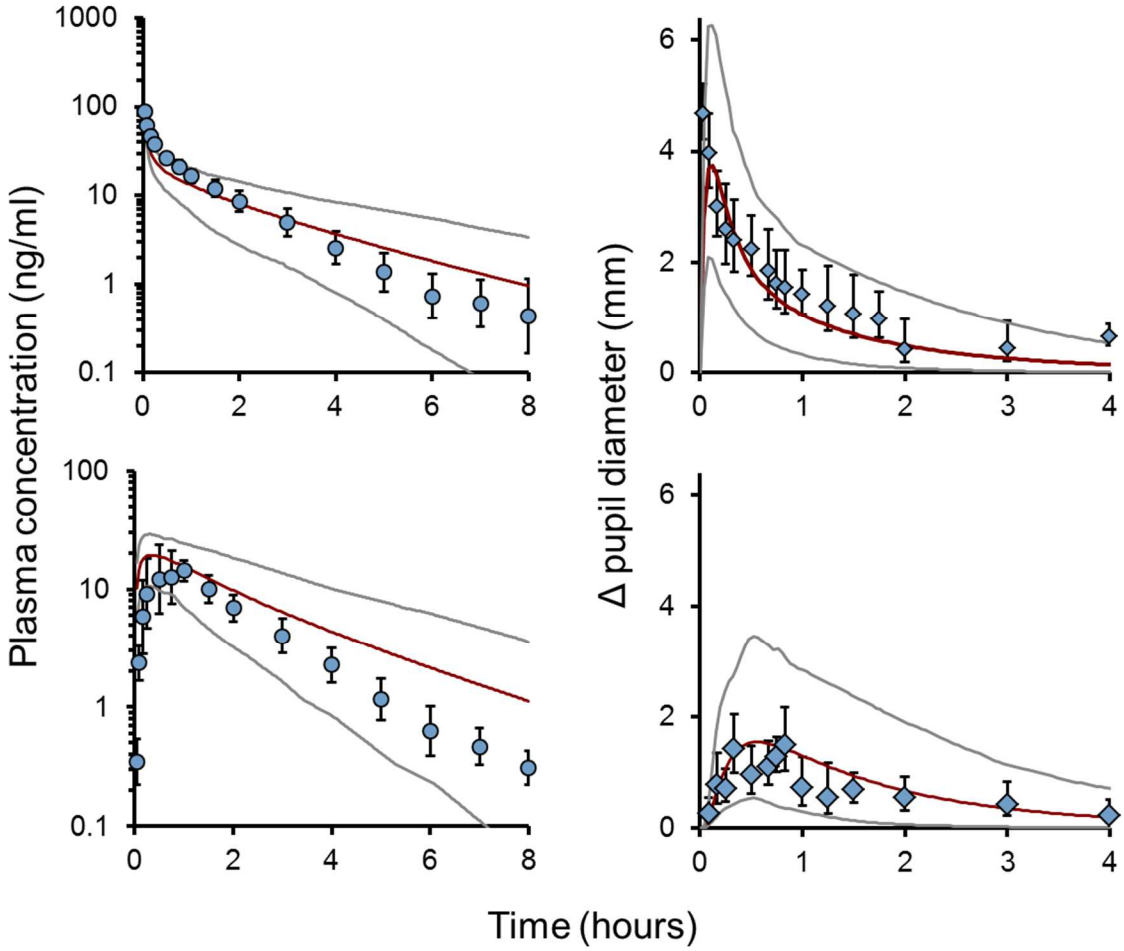

Figure 3.3. Observed geometric mean (circles, or diamonds) and model predicted (crimson lines) and the 90% confidence intervals (grey lines) of the alfentanil plasma concentration- (A,C) and effect- (B,D) time profiles after an intravenous dose (15 µg/Kg, A and B) or an oral dose (23 µg/Kg, C,D). Model-predicted simulations were conducted using 100 healthy virtual subjects.

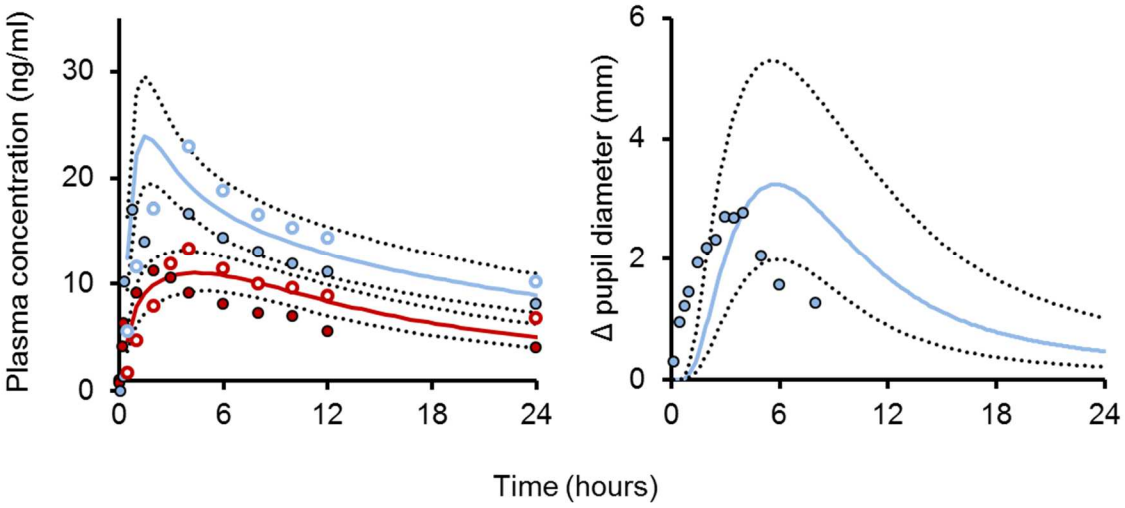

Figure 3.4. Observed geometric mean (circles) and model predicted R-methadone (red lines), S-methadone (blue lines) and the 90% confidence intervals (dashed lines) of the methadone plasma concentration- (A) and model predicted geometric mean (green line) 90% confidence intervals (solid line) and observed (circles) effect- time profiles (B) after an oral R, S-methadone (4.95 mg each). Model-predicted simulations were conducted in 100 healthy virtual subjects.

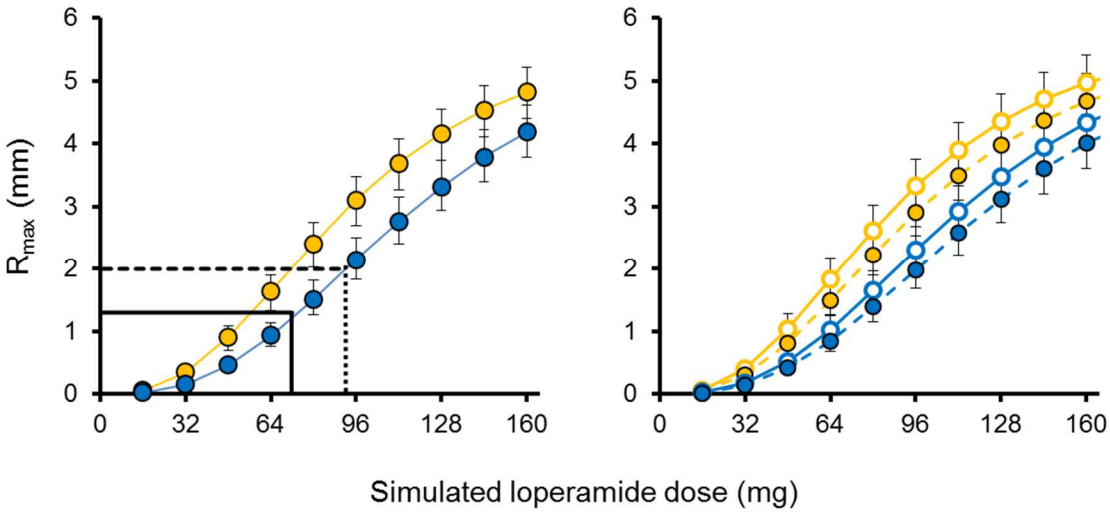

Figure 3.5. Model-predicted geometric mean maximum decrease in pupil diameter (R_{max}) with increasing loperamide dose in the absence (blue) and presence (gold) of DHB (5 mg) (A and B). Simulations represent 100 virtual healthy subjects (50 women) (A) or 200 virtual healthy subjects (100 women) (B). Grey dashed line and grey solid line (A) denote observed and predicted alfentanil (1.7 mg) maximum change in pupil diameter (R_{max}), respectively. Error bars indicate 90% confidence intervals.

REFERENCES

Ainslie GR, Wolf KK, Li Y, Connolly EA, Scarlett YV, Hull JH and Paine MF (2014) Assessment of a Candidate Marker Constituent Predictive of a Dietary Substance-Drug Interaction: Case Study with Grapefruit Juice and CYP3A4 Drug Substrates. *J Pharmacol Exp Ther*.

Bailey DG, Dresser GK and Bend JR (2003) Bergamottin, lime juice, and red wine as inhibitors of cytochrome P450 3A4 activity: comparison with grapefruit juice. *Clin Pharmacol Ther* **73**:529-537.

Bailey DG, Dresser G and Arnold JM (2013) Grapefruit-medication interactions: Forbidden fruit or avoidable consequences? *CMAJ* **185**:309-316.

Baker DE (2007) Loperamide: a pharmacological review. *Rev Gastroenterol Disord* **7 Suppl 3**:S11-18.

Berezhkovskiy LM (2011) The corrected traditional equations for calculation of hepatic clearance that account for the difference in drug ionization in extracellular and intracellular tissue water and the corresponding corrected PBPK equation. *J Pharm Sci* **100**:1167-1183.

Bohnert AS, Valenstein M, Bair MJ, Ganoczy D, McCarthy JF, Ilgen MA and Blow FC (2011) Association between opioid prescribing patterns and opioid overdose-related deaths. *JAMA* **305**:1315-1321.

Bradley JC, Bentley KC, Mughal AI, Bodhireddy H, Young RS and Brown SM (2010) The effect of gender and iris color on the dark-adapted pupil diameter. *Journal of ocular pharmacology and therapeutics : the official journal of the Association for Ocular Pharmacology and Therapeutics* **26**:335-340.

Bradley JC, Bentley KC, Mughal AI, Bodhireddy H and Brown SM (2011) Dark-adapted pupil diameter as a function of age measured with the NeurOptics pupillometer. *Journal of refractive surgery* **27**:202-207.

Brantley SJ, Gufford BT, Dua R, Fediuk DJ, Graf TN, Scarlett YV, Frederick KS, Fisher MB, Oberlies NH and Paine MF (2013) Physiologically based Pharmacokinetic Modeling Framework for Quantitative Prediction of an Herb-Drug Interaction. *CPT: Pharmacometrics & Systems Pharmacology*:doi:10.1038/psp.2013.1069.

Brown R, Kraus C, Fleming M and Reddy S (2004) Methadone: applied pharmacology and use as adjunctive treatment in chronic pain. *Postgraduate medical journal* **80**:654-659.

Campbell FW and Gubisch RW (1966) Optical quality of the human eye. *The Journal of physiology* **186**:558-578.

Chang Y, Fang WB, Lin SN and Moody DE (2011) Stereo-selective metabolism of methadone by human liver microsomes and cDNA-expressed cytochrome P450s: a reconciliation. *Basic Clin Pharmacol Toxicol* **108**:55-62.

Daniulaityte R, Carlson R, Falck R, Cameron D, Perera S, Chen L and Sheth A (2013) "I just wanted to tell you that loperamide WILL WORK": a web-based study of extra-medical use of loperamide. *Drug Alcohol Depend* **130**:241-244.

Goosen TC, Cillie D, Bailey DG, Yu C, He K, Hollenberg PF, Woster PM, Cohen L, Williams JA, Rheeders M and Dijkstra HP (2004) Bergamottin contribution to the grapefruit juice-felodipine interaction and disposition in humans. *Clin Pharmacol Ther* **76**:607-617.

Hassan HE, Myers AL, Coop A and Eddington ND (2009) Differential involvement of P-glycoprotein (ABCB1) in permeability, tissue distribution, and antinociceptive activity of methadone, buprenorphine, and diprenorphine: in vitro and in vivo evaluation. *J Pharm Sci* **98**:4928-4940.

Jamei M, Turner D, Yang J, Neuhoff S, Polak S, Rostami-Hodjegan A and Tucker G (2009) Population-based mechanistic prediction of oral drug absorption. *The AAPS journal* **11**:225-237.

Johansen SS and Jensen JL (2004) Liquid chromatography-tandem mass spectrometry determination of loperamide and its main metabolite desmethylloperamide in biological specimens and application to forensic cases. *J Chromatogr B Analyt Technol Biomed Life Sci* **811**:31-36.

Kalvass JC, Olson ER, Cassidy MP, Selley DE and Pollack GM (2007) Pharmacokinetics and pharmacodynamics of seven opioids in P-glycoprotein-competent mice: assessment of unbound brain EC50,u and correlation of in vitro, preclinical, and clinical data. *J Pharmacol Exp Ther* **323**:346-355.

Ke AB, Nallani SC, Zhao P, Rostami-Hodjegan A and Unadkat JD (2014) Expansion of a PBPK model to predict disposition in pregnant women of drugs cleared via multiple CYP enzymes, including CYP2B6, CYP2C9 and CYP2C19. *Br J Clin Pharmacol* **77**:554-570.

Kharasch ED, Walker A, Hoffer C and Sheffels P (2004a) Intravenous and oral alfentanil as in vivo probes for hepatic and first-pass cytochrome P450 3A activity: noninvasive assessment by use of pupillary miosis. *Clin Pharmacol Ther* **76**:452-466.

Kharasch ED, Hoffer C, Whittington D and Sheffels P (2004b) Role of hepatic and intestinal cytochrome P450 3A and 2B6 in the metabolism, disposition, and miotic effects of methadone. *Clin Pharmacol Ther* **76**:250-269.

Kim KA, Chung J, Jung DH and Park JY (2004) Identification of cytochrome P450 isoforms involved in the metabolism of loperamide in human liver microsomes. *Eur J Clin Pharmacol* **60**:575-581.

Klees TM, Sheffels P, Thummel KE and Kharasch ED (2005) Pharmacogenetic determinants of human liver microsomal alfentanil metabolism and the role of cytochrome P450 3A5. *Anesthesiology* **102**:550-556.

Meyer R, Patel AM, Rattana SK, Quock TP and Mody SH (2014) Prescription Opioid Abuse: A Literature Review of the Clinical and Economic Burden in the United States. *Population health management*.

Mukwaya G, MacGregor T, Hoelscher D, Heming T, Legg D, Kavanaugh K, Johnson P, Sabo JP and McCallister S (2005) Interaction of ritonavir-boosted tipranavir with loperamide does not result in loperamide-associated neurologic side effects in healthy volunteers. *Antimicrob Agents Chemother* **49**:4903-4910.

National Institute of Drug Abuse (2011) Drug-Related Hospital Emergency Room Visits, in.

National Institute of Drug Abuse (2014) Nationwide Trends.

Niemi M, Tornio A, Pasanen MK, Fredrikson H, Neuvonen PJ and Backman JT (2006) Itraconazole, gemfibrozil and their combination markedly raise the plasma concentrations of loperamide. *Eur J Clin Pharmacol* **62**:463-472.

Nieminen TH, Hagelberg NM, Saari TI, Neuvonen M, Neuvonen PJ, Laine K and Olkkola KT (2010) Grapefruit juice enhances the exposure to oral oxycodone. *Basic Clin Pharmacol Toxicol* **107**:782-788.

Oda K, Yamaguchi Y, Yoshimura T, Wada K and Nishizono N (2007) Synthetic models related to furanocoumarin-CYP 3A4 interactions. comparison of furanocoumarin, coumarin, and benzofuran dimers as potent inhibitors of CYP3A4 activity. *Chemical & pharmaceutical bulletin* **55**:1419-1421.

Ohnishi A, Matsuo H, Yamada S, Takanaga H, Morimoto S, Shoyama Y, Ohtani H and Sawada Y (2000) Effect of furanocoumarin derivatives in grapefruit juice on the uptake of vinblastine by Caco-2 cells and on the activity of cytochrome P450 3A4. *Br J Pharmacol* **130**:1369-1377.

Paine MF, Criss AB and Watkins PB (2004) Two major grapefruit juice components differ in intestinal CYP3A4 inhibition kinetic and binding properties. *Drug Metab Dispos* **32**:1146-1153.

Paine MF, Ludington SS, Chen ML, Stewart PW, Huang SM and Watkins PB (2005a) Do men and women differ in proximal small intestinal CYP3A or P-glycoprotein expression? *Drug Metab Dispos* **33**:426-433.

Paine MF, Criss AB and Watkins PB (2005b) Two major grapefruit juice components differ in time to onset of intestinal CYP3A4 inhibition. *J Pharmacol Exp Ther* **312**:1151-1160.

Paine MF, Widmer WW, Hart HL, Pusek SN, Beavers KL, Criss AB, Brown SS, Thomas BF and Watkins PB (2006) A furanocoumarin-free grapefruit juice establishes furanocoumarins as the mediators of the grapefruit juice-felodipine interaction. *Am J Clin Nutr* **83**:1097-1105.

Pert CB and Snyder SH (1973) Properties of opiate-receptor binding in rat brain. *Proceedings of the National Academy of Sciences of the United States of America* **70**:2243-2247.

Skarke C, Jarrar M, Schmidt H, Kauert G, Langer M, Geisslinger G and Lotsch J (2003) Effects of ABCB1 (multidrug resistance transporter) gene mutations on disposition and central nervous effects of loperamide in healthy volunteers. *Pharmacogenetics* **13**:651-660.

Sklerov J, Levine B, Moore KA, Allan C and Fowler D (2005) Tissue distribution of loperamide and N-desmethylloperamide following a fatal overdose. *J Anal Toxicol* **29**:750-754.

Tayrouz Y, Ganssmann B, Ding R, Klingmann A, Aderjan R, Burhenne J, Haefeli WE and Mikus G (2001) Ritonavir increases loperamide plasma concentrations without evidence for P-glycoprotein involvement. *Clin Pharmacol Ther* **70**:405-414.

Terenius L (1975) Comparison between narcotic "receptors" in the guinea-pig ileum and the rat brain. *Acta pharmacologica et toxicologica* **37**:211-221.

Tran TT, Mittal A, Gales T, Maleeff B, Aldinger T, Polli JW, Ayrton A, Ellens H and Bentz J (2004) Exact kinetic analysis of passive transport across a polarized confluent MDCK cell monolayer modeled as a single barrier. *J Pharm Sci* **93**:2108-2123.

US Food and Drug Administration (2013) Draft Guidance: Bioanalytical Method Validation. US Food and Drug Administration, Rockville, MD.

Wandel C, Kim R, Wood M and Wood A (2002) Interaction of morphine, fentanyl, sufentanil, alfentanil, and loperamide with the efflux drug transporter P-glycoprotein. *Anesthesiology* **96**:913-920.

Yang F, Tong X, McCarver DG, Hines RN and Beard DA (2006) Population-based analysis of methadone distribution and metabolism using an age-dependent physiologically based pharmacokinetic model. *Journal of pharmacokinetics and pharmacodynamics* **33**:485-518.

Yu JH, Kim HJ, Lee S, Hwang SJ, Kim W and Moon CJ (2004) LC-MS determination and bioavailability study of loperamide hydrochloride after oral administration of loperamide capsule in human volunteers. *J Pharm Biomed Anal* **36**:421-427.

Zamek-Gliszczynski MJ, Sprague KE, Espada A, Raub TJ, Morton SM, Manro JR and Molina-Martin M (2012) How well do lipophilicity parameters, MEEKC microemulsion capacity factor, and plasma protein binding predict CNS tissue binding? *J Pharm Sci* **101**:1932-1940.

Zamek-Gliszczynski MJ, Abraham TL, Alberts JJ, Kulanthaivel P, Jackson KA, Chow KH, McCann DJ, Hu H, Anderson S, Furr NA, Barbuch RJ and Cassidy KC (2013) Pharmacokinetics, metabolism, and excretion of the glycogen synthase kinase-3 inhibitor LY2090314 in rats, dogs, and humans: a case study in rapid clearance by extensive metabolism with low circulating metabolite exposure. *Drug Metab Dispos* **41**:714-726.

CHAPTER 4 : EVALUATION OF A NOVEL HUMAN MODEL TO ASSESS REVERSAL OF OPIOID EFFECTS BY NALOXONE.[3]

INTRODUCTION

Opioids are among the most frequently prescribed analgesic medications due to superior efficacy and limited alternatives to treat severe pain (Bohnert et al., 2011). In parallel, this chemical class is notorious for addiction and accidental or intentional overdose (National Institute of Drug Abuse, 2011; Meyer et al., 2014). The definitive treatment for opioid overdose is the potent μ-opioid receptor antagonist naloxone, approved for parenteral administration. Although effective, parenteral naloxone is suboptimal due to the need for medically trained personnel (at least for intravenous administration) and potentially, multiple doses, particularly for the long-acting opioids (e.g., methadone, morphine, oxycodone, heroin). One product was approved recently for intramuscular (IM) or subcutaneous administration by non-medically trained personnel (Evzio™) but is invasive and costly ($200-300/dose). Other, noninvasive, naloxone products are under development, particularly intranasal (IN) formulations (Kelly and Koutsogiannis, 2002; Merlin et al., 2010).

Development of IN naloxone formulations is not without hurdles. One is the lack of predictive pre-clinical models. Although rodent models have been shown to predict

[3] This chapter will be submitted to Clinical Pharmacology and Therapeutics as an original research paper and is presented in the style of the journal. Ainslie GR, White JR, Gufford BT, Layton ME, Padowski JM, Pollack GM and Paine MF. A novel human model to assess reversal of opioid effects by naloxone. *CPT*.

the human pharmacodynamics of opioid agonists (Kalvass et al., 2007), an analogous relationship for opioid antagonists has not been reported. Another hurdle is that, unlike for opioid agonists, the plasma concentration-effect relationship for opioid antagonists in humans cannot be readily well-characterized. In addition, the endpoints used to assess central opioid effect (*e.g.*, respiratory rate, blood oxygen saturation) are associated with low sensitivity and large inter-individual variability, necessitating large sample size to adequately power efficacy studies. Based on these observations, a cost-effective human model to characterize the reversal of opioid effects by naloxone would address an unmet need in the development of new naloxone products.

The objective of this work was to develop a noninvasive, cost-effective, and time-efficient human model to assess the opioid reversing effects by naloxone. The aims were to (1) compare the absolute bioavailability of two IN naloxone formulations with that of intramuscular (IM) naloxone, (2) evaluate the clinical effect of IN compared to IM naloxone in reversing central opioid effects, and (3) interrogate the model with a pharmacokinetic 'boosting' agent. The opioid agonist and cytochrome CYP3A probe substrate alfentanil was selected due to a straightforward plasma concentration-effect relationship and short duration of effect. Pupil miosis, the most sensitive measure of central alfentanil effect (Grunberger et al., 1990), was selected as a noninvasive, inexpensive endpoint. The CYP3A inhibitor grapefruit juice was selected as an inexpensive and readily accessible boosting agent that has been shown to augment alfentanil-induced miosis (Kharasch et al., 2004). Results provide a foundation for further testing of a novel human model to aid in optimizing dose and frequency of administration of new naloxone products in reversing opioid overdose.

RESULTS

Pharmacokinetics of naloxone. The pharmacokinetics of two IN naloxone formulations were compared to those of IM and IV naloxone. All six subjects completed all four phases. All administration routes were generally well-tolerated; five subjects reported a bitter taste and pharyngeal discomfort (tingling or burning sensation) after IN administration of at least one of the formulations, which resolved within 20-30 min.

The percent of the area under the curve (AUC) extrapolated to infinite time (AUC_{inf}) was <20% for all subjects and all administration routes (Table 4.1). The geometric mean terminal elimination half-life ($t_{1/2}$) of IM and IN naloxone was consistent with that of IV naloxone (Figure 4.2, Table 4.1). Relative to IM naloxone, geometric mean C_{max} for IN_{200} naloxone (5 mg/ml, 200 µl/nostril) was comparable, whereas that of IN_{100} naloxone (10 mg/ml, 100 µl/nostril) was doubled. Median t_{max} following IM naloxone was roughly twice that of IN_{100} naloxone, which was roughly twice that of IN_{200} naloxone. The average mean absorption time (MAT) of IN_{100} and IN_{200} naloxone was approximately 10 and two times faster, respectively, than that of IM naloxone. The geometric mean absolute bioavailability of IN_{100} and IN_{200} naloxone was 25% and 59% lower, respectively, than that of IM naloxone (Table 4.1).

***Opioid reversal effects of intramuscular and intranasal naloxone*.** Based on results from the pharmacokinetic study, IN_{100} naloxone was selected for comparison to IM naloxone in reversing the miotic effects of the test opioid, oral alfentanil, in the absence and presence of grapefruit juice. All subjects completed all six phases of the study. Naloxone, alfentanil, and grapefruit juice were generally well-tolerated; two subjects reported nausea (attributed to alfentanil and/or grapefruit juice) on all study

days that resolved within 5-20 min. One of these subjects and a different subject reported pharyngeal discomfort with IN naloxone that resolved within 30 min.

Relative to baseline, alfentanil produced miosis in all subjects during all phases (Figure 3). The mean area under the effect curve from 0-6 h ($AUEC_{0\text{-}6h}$) decreased by 40% after both IM and IN_{100} naloxone administration (Figure 4.4). Because naloxone was administered one hour after alfentanil, $AUEC_{1\text{-}6h}$ was evaluated. In the absence of grapefruit juice (days 1-3) (Figure 4.1B), IM naloxone decreased mean $AUEC_{1\text{-}6h}$ by a modestly higher extent compared to IN_{100} naloxone (68% and 54%, respectively); the maximum magnitude of miosis (R_{max}) was similar amongst the three phases (Figure 4.4). In the absence of naloxone (days 1 and 4), both the mean $AUEC_{0\text{-}6h}$ and R_{max} increased by 40% when grapefruit juice was administered 30 min prior to alfentanil. Relative to the presence of grapefruit juice but absence of naloxone (day 4), mean $AUEC_{0\text{-}6h}$ decreased by 33% and 38%, respectively, with IM and IN_{100} naloxone; mean $AUEC_{1\text{-}6h}$ showed similar trends (Figure 4.4).

DISCUSSION

Opioids are a mainstay in pain management and common drugs of choice encountered in addiction recovery programs. Although effective, these drugs are notorious for overdose, both intentional and accidental (Bohnert et al., 2011). Deaths due to opioid overdose result from illicit or licit use, either when taken alone or with concomitant medications or other xenobiotics. Parenteral naloxone is the definitive treatment for opioid overdose, yet in most cases, the first responders typically are the lay bystanders, rather than personnel trained to administer naloxone parenterally. Consequently, a market exists for novel, easy-to-use naloxone products that can be administered by non-medically trained personnel.

Evzio™, an automated device for IM or subcutaneous naloxone administration, was approved recently for in-field use by non-medically trained personnel. However, the invasive nature and high cost of this product may limit widespread use, prompting the development of noninvasive formulations. The parenteral formulation has been administered IN in the field with mixed success rates (Barton et al., 2002; Kelly and Koutsogiannis, 2002; Glaser et al., 2005; Kelly et al., 2005; Merlin et al., 2010; 2014; Sabzghabaee et al., 2014; Zuckerman et al., 2014) due in part to a limited bioavailability (~4%) (Dowling et al., 2008), requiring further development of alternate IN formulations. Given the lack of predictable efficacy relative to plasma exposure, coupled with the lack of a robust animal model, a cost-effective human model to assess reversal of opioids effects would expedite development of these new formulations. The objective of the current work was to develop a noninvasive, inexpensive, and time-efficient human model to assess the opioid reversing effects of naloxone. This model consisted of oral

alfentanil as a short-acting test opioid; pupil diameter as a sensitive, noninvasive measure of opioid central effect; grapefruit juice as a readily available pharmacokinetic booster, standardized for the marker constituent DHB, to increase the dynamic range of effect; and IN naloxone as a noninvasive and inexpensive test formulation.

Selection of a test IN naloxone formulation was based on a preliminary pharmacokinetic study in which IV, IM, and IN naloxone were administered to six healthy subjects. The pharmacokinetics of IV naloxone were consistent with the literature (Albeck et al., 1989). The absolute bioavailability of IM naloxone was higher (54% versus 35%), whereas t_{max} and terminal $t_{1/2}$ were similar, to previously reported values (Dowling et al., 2008). Absolute bioavailability of IN_{100} naloxone was superior to previously published IN formulations (40% versus 4%)(Kelly and Koutsogiannis, 2002; Dowling et al., 2008), which can be attributed to differing combinations and quantities of surfactants. The bioavailability of IN_{200} naloxone also was superior to previous IN formulations and was approximately half that of IN_{100} naloxone, which likely reflected a larger fraction of the dose lost via pharyngeal drainage. Based on these results, IN_{100} was selected for testing in the efficacy study.

Oral alfentanil elicited a pupillary response that was augmented by grapefruit juice (by 40%), consistent with a previous report (Kharasch et al., 2004). Whether or not grapefruit juice was administered prior to alfentanil, IM and IN naloxone attenuated miosis by similar extents, consistent with comparable systemic exposure to naloxone between the two routes. However, the time to maximum response appeared to be achieved more rapidly in the absence of grapefruit juice, reflective of a potential leftward shift in the time to reach C_{max}. Inclusion of a grapefruit juice, indicates that this approach

may be useful to assess the effect of additional inhibitory ‘perpetrator’ xenobiotics, including drugs and other diet-derived/natural products.

Despite encouraging results from the current work, limitations are recognized, yet addressable upon further refinement. First, given the preliminary nature of the studies, the small sample sizes precluded formal statistical comparisons between the various treatments. However, data from both studies provide fundamental information for future powered studies. For example, using $AUEC_{0\text{-}6h}$ as the primary endpoint, a post-hoc power calculation indicated a cohort of 16 subjects would be needed to detect a 25% difference in $AUEC_{0\text{-}6h}$ with 80% power, with a Type I error of 0.05. Second, although pupillometry is a noninvasive technique, intense sampling was not feasible with more than one subject present on a given study day due to the availability of one pupillometer. Increased resources would enable more intense sampling following naloxone administration, permitting thorough characterization of the rate of reversal of alfentanil-induced miosis. Third, as alfentanil is short-acting, rigorous characterization of the duration of opioid reversing effects of naloxone was not possible. As such, testing the reversing effects against long-acting opioids (e.g., methadone, oxycodone) is of interest, warranting further clinical evaluation. With modifications, including increased subject enrollment, staffing, and instrumentation, this approach is well-suited for the ‘learn and confirm’ paradigm used during early clinical development of new drug candidates.

This novel human model has applications in addition to aiding in the development of new naloxone formulations. Such applications include combinatorial naloxone medications, xenobiotic-drug interactions, and xenobiotic-combinatorial naloxone

medication interactions. Following a call by the FDA, combinatorial medications containing naloxone (e.g., Suboxone®, Targiniq™ ER) have been developed to reduce opioid abuse potential or gastrointestinal side effects. These formulations exploit the extremely low oral bioavailability of naloxone (1-2%)(Smith et al., 2012) and have been beneficial at normalizing bowel movements, although the impact on central effects has not been examined thoroughly (DePriest and Miller, 2014; Koopmans et al., 2014). Evidence that a PEGylated naloxone product (naloxegol) may be susceptible to CYP3A-mediated interactions requires further investigation to ensure that increased systemic exposure to naloxone does not lead to a central effect, leading to withdrawal symptoms in patients suffering from chronic pain.

In summary, new easy-to-use naloxone formulations and products are under development, yet no cost-effective human models to evaluate the reversal of opioid central effects have been described. A preliminary pharmacokinetic study showed that the absolute bioavailability of a test IN naloxone formulation was comparable to IM naloxone, prompting a second study to compare the opioid reversing effects of IN to IM naloxone using oral alfentanil as the model opioid. Whether or not the pharmacokinetic booster, grapefruit juice, was administered prior to alfentanil, the IN formulation appeared to be as effective as IM naloxone in reversing pupil miosis. Continued testing of this novel experimental human model is needed to substantiate these observations. In conclusion, a noninvasive, cost-effective, and time-efficient human model to assess the opioid reversing effects of naloxone was evaluated. The encouraging results warrant continued development of this promising ‘no sharps container’ approach.

METHODS

Clinical study protocols. The Washington State University Institutional Review Board reviewed and approved the study protocols and consent forms prior to subject enrollment. Potential subjects provided written informed consent and Health Insurance Portability and Accountability Act authorization before screening, which consisted of a medical history, physical examination, liver function tests, complete blood count, and urinalysis that included a 14-panel drug test (14 panel T-cup, Confirm Biosciences, San Diego, CA). All women underwent a serum pregnancy test. Subjects were eligible to participate based on screening results and inclusion/exclusion criteria (Table 4.2).

Preparation of intranasal naloxone, oral alfentanil, and grapefruit juice. Naloxone hydrochloride, polysorbate 20, and sodium lauryl sulfate were purchased from PCCA, Inc (Houston, TX). IN mucosal atomization devices (MAD Nasal™) were provided by Teleflex, Inc. (Research Triangle Park, NC). Millex® GP 0.22 µm syringe filter units (Merck Millipore, Darmstadt, Germany) and 5 micron filter needles (Becton, Dickinson and Company, Franklin Lakes, NJ) were purchased from Fisher Scientific, Inc. (Waltham, MA). Sterile saline 0.9% (Becton, Dickinson and Company, Franklin Lakes, NJ) and alfentanil 1 mg/2 ml ampules (Hospira, Inc., Lake Forest IL) were purchased from McKesson Corporation (San Francisco, CA). Grapefruit juice frozen concentrate (Great Value™) was purchased from a local store (Walmart, Post Falls, ID; lot nos. LOC4N and LOC1N).

IN naloxone was prepared by suspending naloxone hydrochloride in a vehicle containing 5% polysorbate 20 and 1% sodium lauryl sulfate dissolved in sterile saline to yield 5 or 10 mg naloxone/ml. The solutions were sterilized by filtration before transferring to syringes for administration (0.23 ml per syringe to deliver 0.1 or 0.2 ml (1

mg) per nostril, allowing for 0.13 ml dead space in MAD Nasal™). Alfentanil was prepared for oral administration by removing 2 ml from each of 4 ampules using a syringe with filter needle (total dose, 4 mg in 8 ml) and diluting into 50 ml of water. The contents from each can of grapefruit juice were thawed and pooled, and an aliquot was saved for quantitation of the marker constituent, 6',7'-dihydroxybergamottin (DHB), by LC/MS/MS (Vandermolen et al., 2013). The juice was diluted with water to achieve a final DHB concentration of ~60 μM. The diluted juice was divided into 240-ml aliquots and stored in light-protective containers at -20°C until use; the contents of each container were thawed at 4°C the evening before each study day.

Pharmacokinetic study. Healthy volunteers (5 men, 1 non-pregnant woman), aged 23-29 years, were enrolled in a three-phase, sequential, open-label study; none were taking concomitant medications. Naloxone (2 mg) was administered IV or IM (2 mg/2 ml pre-filled syringe, International Medication Systems, LTD., El Monte, CA) or IN (10 mg/ml, 100 μl/nostril or 5 mg/ml, 200 μl/nostril). Weight and blood pressure were obtained at the beginning of each study day. Plasma (15 ml) was collected serially via an indwelling IV catheter at 5, 10, 15, 30, 45, 60, 90, 120, and 240 min after naloxone administration (Figure 4.1A). Plasma was quantified for naloxone by LC/MS/MS as described previously (Fang et al., 2009).

***Opioid effect reversal study*.** Healthy volunteers (3 men, 3 non-pregnant women), aged 20-32 years, were enrolled in this six-phase, sequential, open-label study; none were taking concomitant medications or dietary/herbal supplements except for one woman who was taking bupropion chronically for >2 months prior to initiation of the study. Subjects were administered 240 ml water (study days 1-3) or grapefruit juice

(study days 4-6) 30 min prior to a single oral dose of alfentanil (4 mg) (Figure 4.1B). Naloxone (2 mg) was administered IM (study days 2 and 5) or IN (10 mg/ml, 100 µl/nostril) (study days 3 and 6) one hour after alfentanil (t_{max})(Kharasch et al., 2011) administration. Pupil diameter of the right eye was measured, at least in triplicate (coefficient of variation ≤3.3%), at 5, 10, 20, 30, 45, 60, 75, 90, 120, 150, 180, 240, 300, and 360 min after alfentanil administration using a NeurOptics VIP-200® pupillometer with a resolution of 0.1 mm (San Clemente, CA). The light intensity of the room, measured using a Sper Scientific 840021 light meter (Scottsdale, AZ), was always <1 lux. Vital signs (oxygen saturation, pulse, blood pressure) were obtained concurrent with pupil diameter. In the event of an adverse reaction to alfentanil, an extra dose of parenteral naloxone and supplemental oxygen were available. Promethazine (Actavis Inc., Parsippany, New Jersey) and epinephrine (Mylan Inc, Basking Ridge, NJ) were available as anti-nausea and anti-anaphylaxis medications, respectively.

***Pharmacokinetic and effect analysis*.** Pharmacokinetic and effect outcomes were determined via non-compartmental methods using Phoenix® WinNonlin® (v6.3, Pharsight, Mountain View, CA). Plasma concentrations outside the dynamic range of the LC/MS/MS assay were excluded from pharmacokinetic analysis. The terminal elimination rate constant (λ_z) was determined by linear regression of the terminal portion of the log-transformed concentration-time profile using at least three data points. The terminal half-life ($t_{1/2}$) was calculated as $\ln(2)/\lambda_z$. The maximum concentration (C_{max}), time to reach C_{max} (t_{max}), and last measured concentration (C_{last}) were obtained directly from the concentration-time profile. Area under the curve from time zero to the time at C_{last} (AUC_{last}) was determined using the trapezoidal rule, with linear interpolation for

intravenous administration and linear up/log down interpolation for extravascular administration. AUC_{inf} was calculated as the sum of AUC_{last} and the ratio of C_{last} to λ_z. Absolute bioavailability (F) was calculated as the ratio of the AUC_{inf} after extravascular to that after intravenous administration. Mean residence time (MRT) following intravenous (MRT_{IV}) or extravascular (MRT_{EV}) administration was calculated as the ratio of $AUMC_{inf}$ to AUC_{inf}, where $AUMC_{inf}$ denotes the area under the moment curve from time 0 to infinite time. Mean absorption time (MAT) was calculated as the difference between MRT_{EV} and MRT_{IV}.

Pupil diameter measurements were converted to miosis as a function of the percent change from a baseline (pre-dose) measurement. The maximum miotic response (R_{max}) was obtained directly from the miosis-time profile. The area under the effect-time curve from 0-6 h ($AUEC_{0\text{-}6h}$) and from 1-6 h ($AUEC_{1\text{-}6h}$) was determined using the trapezoidal rule with linear-up/log-down interpolation.

Statistical Analysis

Statistical analyses were conducted using SAS (v9.1.3; SAS Institute, Cary, NC). Differences in $AUEC_{all}$, $AUEC_{1\text{-}6\ h}$, and R_{max} between treatment groups were analyzed by standard two way ANOVA and a Bonferroni adjustment ($\alpha = 0.05$).

Table 4.1. Pharmacokinetics of naloxone after intravenous, intramuscular, and intranasal naloxone

Outcome	Administration Route			
	IV	IM	IN (100 µl/nostril)	IN (200 µl/nostril)
AUC_{last} (min*ng/mL)	650 [535-789]	347 [310-390]	266 [190-373]	147 [112-194]
AUC_{inf} (min*ng/mL)	748 [586-954]	434 [386-487]	282 [200-399]	168 [117-240]
$t_{1/2}$ (min)	91 [64-130]	100 [89-111]	61 [53-72]	80 [56-113]
C_{max} (ng/mL)	-	3.1 [2.3-4.2]	5.7 [3.3-10.0]	3.0 [1.7-5.3]
t_{max} (min), median (range)	-	22.5 (10-60)	12.5 (5-15)	5 (5-15)
MAT (min), mean ± SE	-	74 ± 8.8	6.7 ± 4.9	31 ± 22
Absolute bioavailability (%)	-	55 [43-70]	41 [27-62]	24 [15-33]

AUC_{last}, area under the plasma concentration-time curve from 0 to 240 minutes; AUC_{inf}, AUC from 0 to infinite time; $t_{1/2}$, terminal half-life; C_{max}, maximum plasma concentration; t_{max}, time to reach C_{max}; MAT, mean absorption time. Values are geometric means [90% confidence intervals] unless indicated otherwise.

Table 4.2. Clinical study inclusion and exclusion criteria.

	Pharmacokinetic Study	Opioid effect reversal study
Inclusion		
	• Men and women aged from 18 to 40 years • Ability to understand the informed consent form • Ability to participate in the study (time, transportation, *etc.*)	• Willing to abstain from grapefruit products for one week prior to and during the study • Willing to abstain from alcohol and caffeinated beverages the evening prior to each study day
Exclusion		
	• Any current major illness or chronic illness such as (but not limited to) kidney disease, hepatic disease, diabetes mellitus, hypertension, coronary artery disease, chronic obstructive pulmonary disease, cancer, or HIV • History of anemia or any other significant hematologic disorder • History of drug or alcohol addiction or major psychiatric illness • A need for chronic opioid analgesics • Use of opioid analgesics 3 weeks prior to initiation of the study • An imminent likely need for opioid analgesics (*e.g.*, planned dental or surgical procedure) • History of allergy to naloxone or other opioid antagonists, alfentanil or other opiate-like agents, promethazine or other phenothiazines	• History of intolerance to grapefruit-containing products
	• History of significant nasal allergy or other nasal pathology (*e.g.*, polyps, nasal septal deviation) • Women who are pregnant or nursing • Taking concomitant medications, both prescription and non-prescription (including herbal products) known to alter the pharmacokinetics or pharmacodynamics of naloxone or alfentanil	

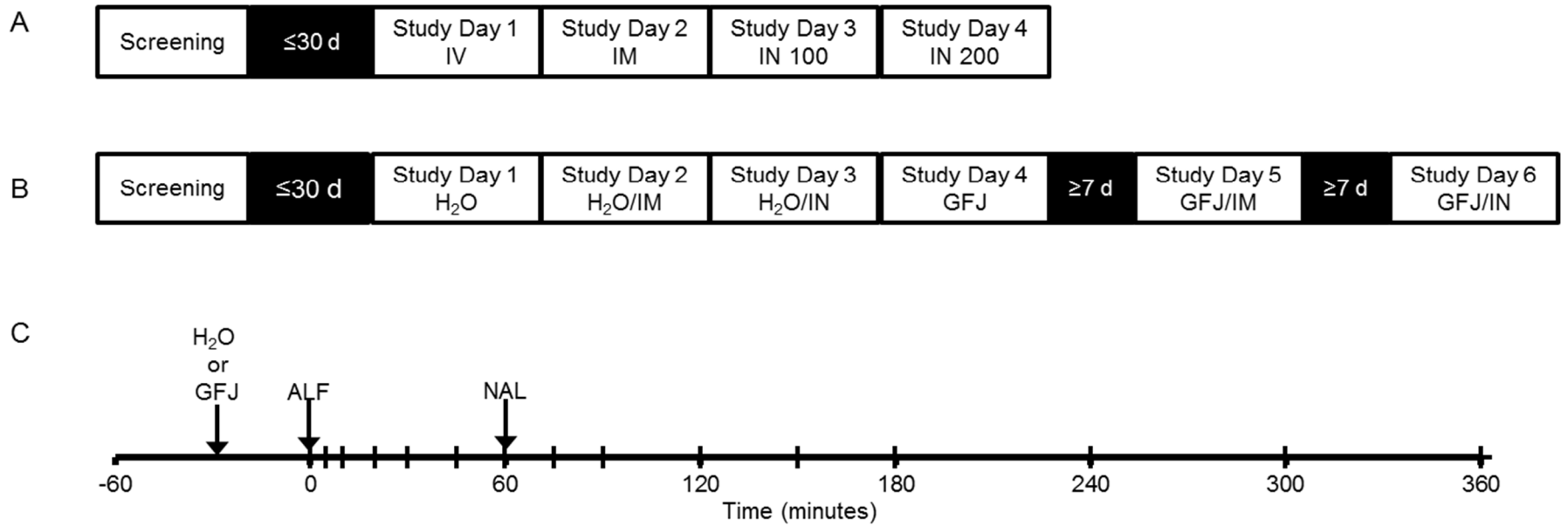

Abbreviations:

IV	intravenous	H_2O	water
IM	intramuscular	GFJ	grapefruit juice
IN 100	intranasal (100 µl/nostril)	ALF	alfentanil
IN 200	intranasal (200 µl/nostril)	NAL	naloxone

Figure 4.1. Study design and procedures**.** (A) Healthy volunteers (n = 6) were screened and underwent four study days, consisting of intravenous (IV), intramuscular (IM), or intranasal (IN, 100 or 200 µl/nostril) naloxone (2 mg) administration. Blood (15 ml) was collected at 5, 10, 15, 30, 45, 60, 90, 120, and 240 minutes after naloxone administration. (B and C) Healthy volunteers (n = 6) were screened and underwent six study days, each consisting of oral alfentanil (4 mg). Water (days 1-3) or grapefruit juice (days 4-6) was administered 30 min before alfentanil. Naloxone (2 mg) was administered IM (days 2, 5) or IN (days 3, 6) one hour after alfentanil. Pupil diameter and vital signs were measured at 0, 5, 10, 20, 30, 45, 60, 75, 90, 120, 150, 180, 240, 300, and 360 min after alfentanil.

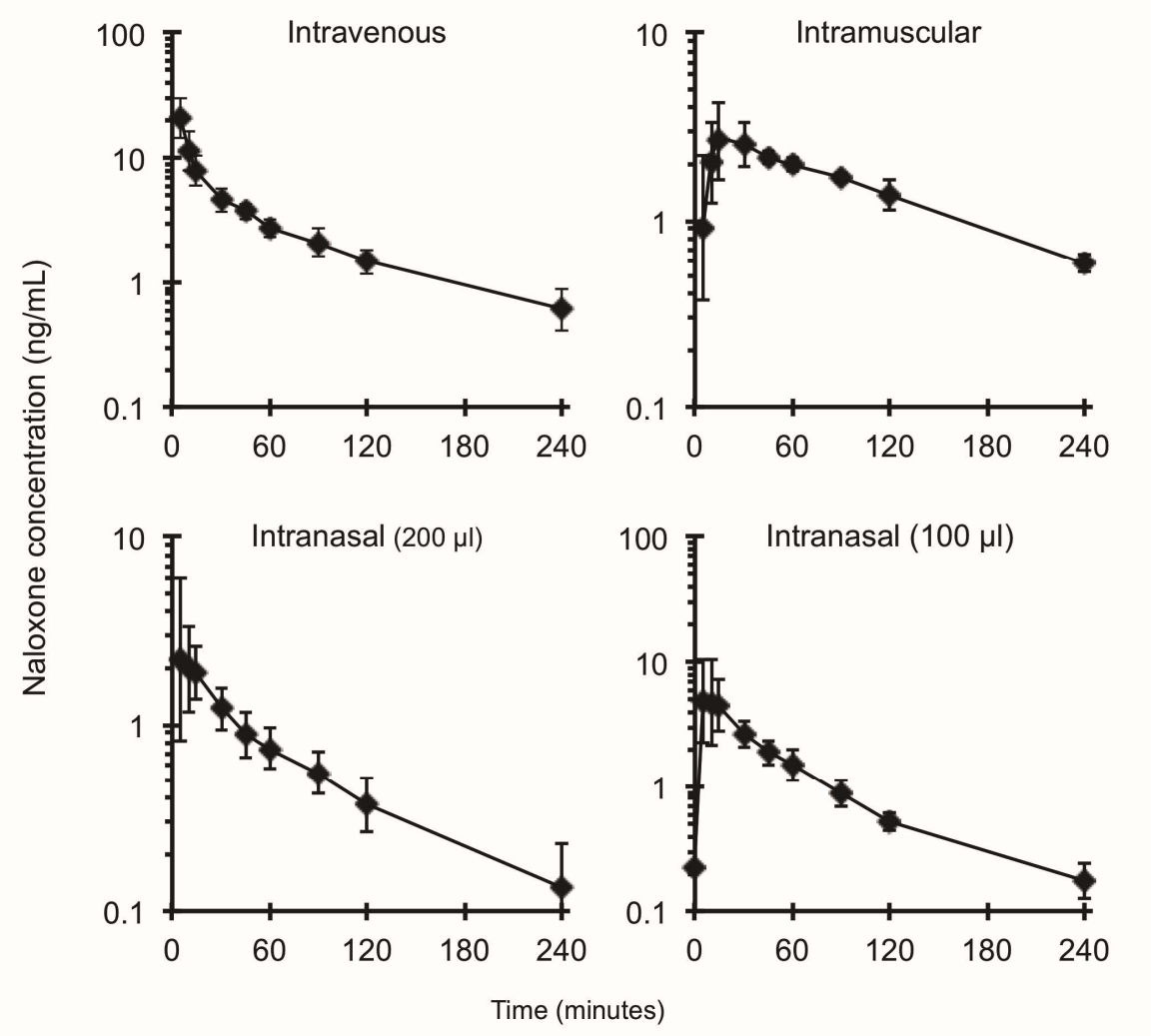

Figure 4.2. Concentration-time profiles for naloxone (2 mg) following intravenous, intramuscular, or intranasal (100/nostril or 200 µl/nostril) administration to six healthy volunteers. Diamonds denote individual concentrations, and closed circles denote geometric mean concentrations. Error bars denote 90% confidence intervals.

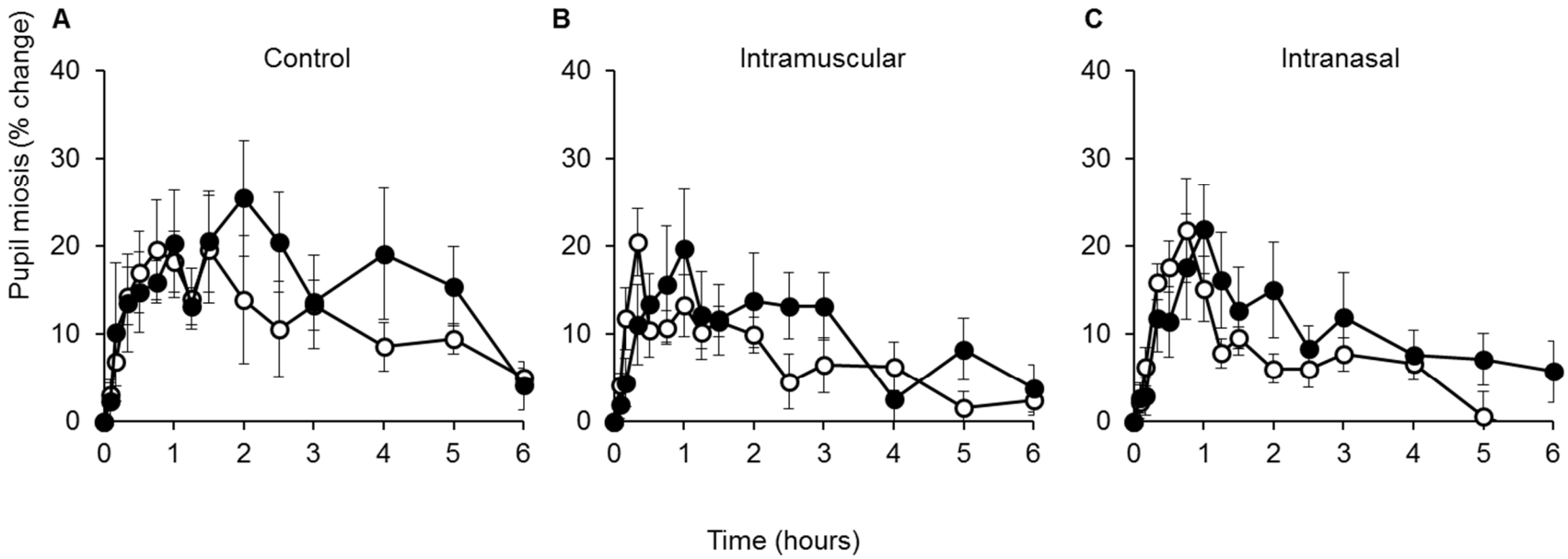

Figure 4.3. (A-C) Mean pupil miosis-time profiles after administration of oral alfentanil (4 mg) to six healthy volunteers pre-treated with water (open symbols) or grapefruit juice (closed symbols). Naloxone (2 mg) was administered intramuscularly (B) or intranasally (C) one hour after alfentanil. Error bars denote standard errors.

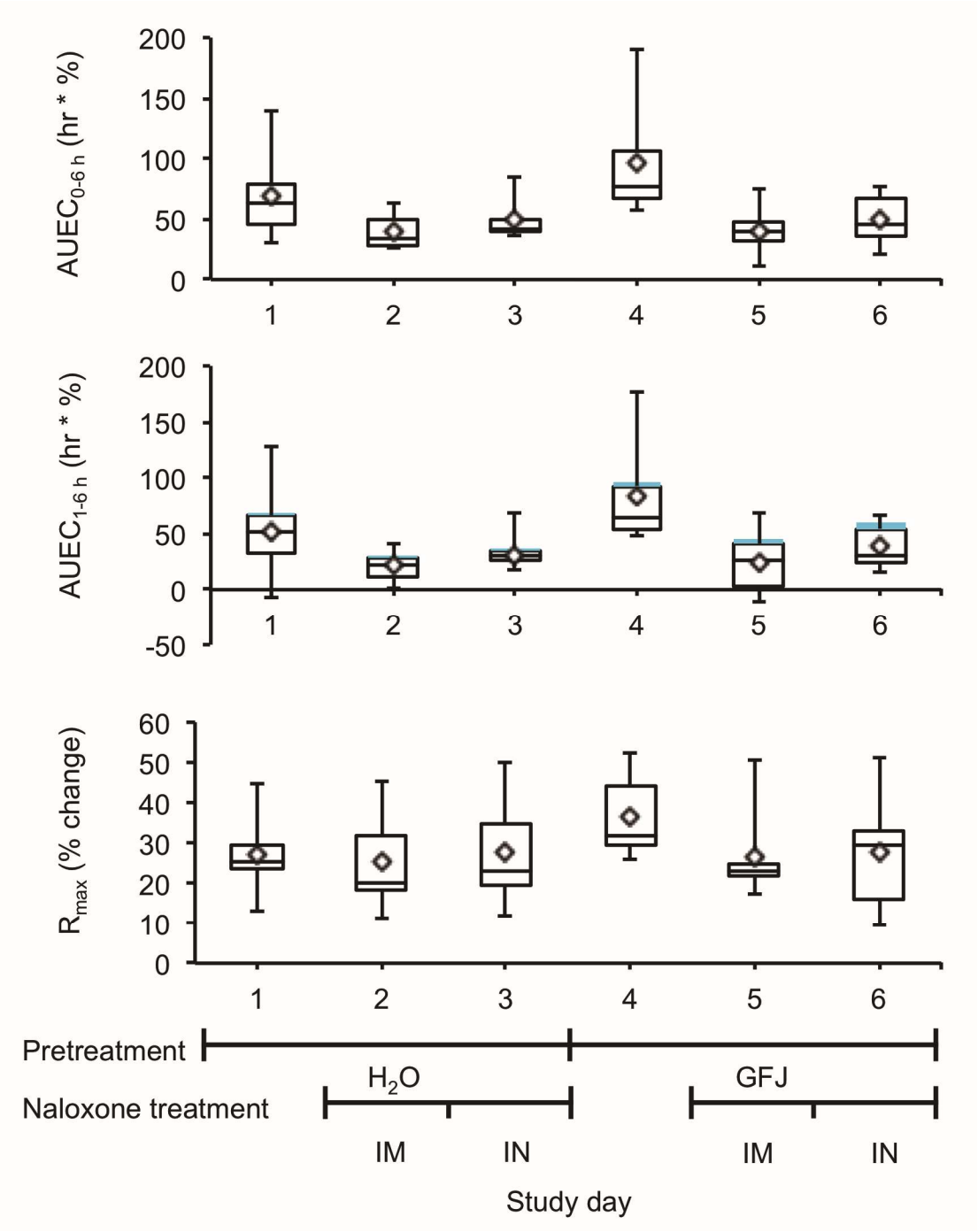

Figure 4.4. Area under the effect-time curve from 0-6 h (A) and from 1-6 h (B) and maximal pupillary response (C) following oral administration of alfentanil (4 mg) to six healthy volunteers pre-treated with water or grapefruit juice. Lines inside the boxes denote medians, the ends of the boxes denote one quartile from the median, and diamonds denote means. Error bars denote minimum and maximum values.

REFERENCES

(2014) Intranasal naloxone for treatment of opioid overdose. *The Medical letter on drugs and therapeutics* **56**:21-22.

Albeck H, Woodfield S and Kreek MJ (1989) Quantitative and pharmacokinetic analysis of naloxone in plasma using high-performance liquid chromatography with electrochemical detection and solid-phase extraction. *Journal of chromatography* **488**:435-445.

Barton ED, Ramos J, Colwell C, Benson J, Baily J and Dunn W (2002) Intranasal administration of naloxone by paramedics. *Prehospital emergency care : official journal of the National Association of EMS Physicians and the National Association of State EMS Directors* **6**:54-58.

Bohnert AS, Valenstein M, Bair MJ, Ganoczy D, McCarthy JF, Ilgen MA and Blow FC (2011) Association between opioid prescribing patterns and opioid overdose-related deaths. *JAMA* **305**:1315-1321.

DePriest AZ and Miller K (2014) Oxycodone/Naloxone: role in chronic pain management, opioid-induced constipation, and abuse deterrence. *Pain and therapy* **3**:1-15.

Dowling J, Isbister GK, Kirkpatrick CM, Naidoo D and Graudins A (2008) Population pharmacokinetics of intravenous, intramuscular, and intranasal naloxone in human volunteers. *Therapeutic drug monitoring* **30**:490-496.

Fang WB, Chang Y, McCance-Katz EF and Moody DE (2009) Determination of naloxone and nornaloxone (noroxymorphone) by high-performance liquid chromatography-electrospray ionization- tandem mass spectrometry. *J Anal Toxicol* **33**:409-417.

Glaser A, Arakaki D, Chan GM and Hoffman RS (2005) Randomised trial of intranasal versus intramuscular naloxone in prehospital treatment for suspected opioid overdose. *The Medical journal of Australia* **182**:427; author reply 427, 429.

Grunberger J, Linzmayer L, Fodor G, Presslich O, Praitner M and Loimer N (1990) Static and dynamic pupillometry for determination of the course of gradual detoxification of opiate-addicted patients. *Eur Arch Psychiatry Clin Neurosci* **240**:109-112.

Kalvass JC, Olson ER, Cassidy MP, Selley DE and Pollack GM (2007) Pharmacokinetics and pharmacodynamics of seven opioids in P-glycoprotein-competent mice: assessment of unbound brain EC50,u and correlation of in vitro, preclinical, and clinical data. *J Pharmacol Exp Ther* **323**:346-355.

Kelly AM, Kerr D, Dietze P, Patrick I, Walker T and Koutsogiannis Z (2005) Randomised trial of intranasal versus intramuscular naloxone in prehospital treatment for suspected opioid overdose. *The Medical journal of Australia* **182**:24-27.

Kelly AM and Koutsogiannis Z (2002) Intranasal naloxone for life threatening opioid toxicity. *Emergency medicine journal : EMJ* **19**:375.

Kharasch ED, Vangveravong S, Buck N, London A, Kim T, Blood J and Mach RH (2011) Concurrent assessment of hepatic and intestinal cytochrome P450 3A activities using deuterated alfentanil. *Clin Pharmacol Ther* **89**:562-570.

Kharasch ED, Walker A, Hoffer C and Sheffels P (2004) Intravenous and oral alfentanil as in vivo probes for hepatic and first-pass cytochrome P450 3A activity: noninvasive assessment by use of pupillary miosis. *Clin Pharmacol Ther* **76**:452-466.

Koopmans G, Simpson K, De Andres J, Lux EA, Wagemans M and Van Megen Y (2014) Fixed ratio (2:1) prolonged-release oxycodone/naloxone combination improves bowel function in patients with moderate-to-severe pain and opioid-induced constipation refractory to at least two classes of laxatives. *Current medical research and opinion*:1-23.

Merlin MA, Saybolt M, Kapitanyan R, Alter SM, Jeges J, Liu J, Calabrese S, Rynn KO, Perritt R and Pryor PW, 2nd (2010) Intranasal naloxone delivery is an alternative to intravenous naloxone for opioid overdoses. *The American journal of emergency medicine* **28**:296-303.

Meyer R, Patel AM, Rattana SK, Quock TP and Mody SH (2014) Prescription Opioid Abuse: A Literature Review of the Clinical and Economic Burden in the United States. *Population health management*.

National Institute of Drug Abuse (2011) Drug-Related Hospital Emergency Room Visits, *http://wwwdrugabusegov/publications/drugfacts/drug-related-hospital-emergency-room-visits%3E*, (2011).

Sabzghabaee AM, Eizadi-Mood N, Yaraghi A and Zandifar S (2014) Naloxone therapy in opioid overdose patients: intranasal or intravenous? A randomized clinical trial. *Archives of medical science : AMS* **10**:309-314.

Smith K, Hopp M, Mundin G, Bond S, Bailey P, Woodward J and Bell D (2012) Low absolute bioavailability of oral naloxone in healthy subjects. *International journal of clinical pharmacology and therapeutics* **50**:360-367.

Vandermolen KM, Cech NB, Paine MF and Oberlies NH (2013) Rapid Quantitation of Furanocoumarins and Flavonoids in Grapefruit Juice using Ultra-Performance Liquid Chromatography. *Phytochem Anal* **24**:654-660.

Zuckerman M, Weisberg SN and Boyer EW (2014) Pitfalls of Intranasal Naloxone. *Prehospital emergency care : official journal of the National Association of EMS Physicians and the National Association of State EMS Directors*.

CHAPTER 5 : CONCLUSIONS AND SIGNIFICANCE

Consuming certain foods, supplements, or exotic beverages concurrently with prescribed or over-the-counter medications is seemingly benign. However, some of these diet-derived substances are capable of modulating the exposure to conventional drugs. While a common misconception exists that ‘natural’ equates to ‘safe’, regulatory agencies are acknowledging the necessity to understand the potential for dietary substances to perpetrate drug interactions (Health Canada, 2011; European Medicines Agency: Committee for Human Medical Products, 2012; National Center for Complementary and Alternative Medicine, 2013). However, no guidelines to assess dietary substance-drug interaction liability have been formalized, and current proposed methods require improvement to keep pace with beverage, nutraceutical and pharmaceutical development. One considerable challenge in dietary substance-drug interaction risk assessment is that dietary substances typically are mixtures of varying biochemical composition. This characteristic has been exemplified with respect to the fermentation of wine, of which the characteristics of a wine are influenced by varieties of grapes, fermentation processes and seasonal changes (Paine and Oberlies, 2007). Complete characterization of all constituents in a mixture would be time consuming and costly. As such, it has been proposed that a single or few ‘marker constituents’ predictive of the whole mixture can be identified, measured and isolated for in vitro and in vivo testing. Furthermore, a marker constituent could be measured in the mixture as a means to assess its interaction liability using IVIVE methods. To test this approach, the

exemplar dietary substance GFJ was selected. GFJ perpetrates myriad drug interactions *via* irreversible inhibition of CYP3A. Consumed at normal volumes, the GFJ interaction is limited to inhibition of enteric and not hepatic CYP3A. Victim drugs include anti-cancer drugs, statins, immunosuppressants and analgesics (Won et al., 2012; Bailey et al., 2013). The interactions with analgesics are concerning given that the recent restrictions on prescription opioids may lead to alternate mean of abuse (Bohnert et al., 2011). Anecdotal accounts imply that GFJ is being used as a pharmacokinetic 'boosting agent' to increase the euphoric effects of opioids (Daniulaityte et al., 2013; Bluelight, 2014). One of these opioids, loperamide, is a peripherally acting opioid subject to a high CYP3A4/P-gp mediated first pass effect (Shen et al., 2012). Loperamide permeates the BBB, but a CNS effect at clinically tested doses (2-60 mg) is precluded by rapid P-gp mediated efflux at the BBB (Jaffe et al., 1980; Tayrouz et al., 2001; Skarke et al., 2003; Yu et al., 2004; Mukwaya et al., 2005; Streel et al., 2005; Niemi et al., 2006). The supratherapeutic doses of loperamide, reported anecdotally (70-200 mg), are sizeable compared to those tested in healthy volunteers (≤24 mg). Clinical evaluation of these claims would be unethical; therefore, alternative approaches must be sought to evaluate the abuse potential of loperamide, and other opioids, in the absence and presence of pharmacokinetic boosting agents, including GFJ.

The overall goal of this dissertation project was to develop and refine a structured approach to conduct dietary substance-drug interaction risk assessment. The global hypothesis was that the risk of a grapefruit juice-loperamide interaction can be assessed *via* an integrated translational approach. The short-term goal of this project was to assess the abuse potential of the μ-opioid receptor agonist, loperamide, when

taken concurrently with GFJ, using a marker constituent as a representative of the whole juice. The long-term objective was to develop a methodology to (1) identify marker constituents present in dietary substances reflective of the effect of a mixture on xenobiotic metabolizing enzyme-mediated interactions, (2) predict pharmacokinetic and pharmacodynamic outcomes of dietary substance-drug interactions, and (3) increase the knowledge of clinical pharmacokinetic behavior of constituents found in dietary substances. Key findings, limitations, innovations and future steps are discussed.

Aim 1. Develop robust in vitro methods to recover key kinetic parameters associated with DHB-mediated inhibition of loperamide metabolism.

Despite other candidate inhibitors present in GFJ, DHB was postulated to be a major mediator of the CYP3A-mediated GFJ effect and was tested as a marker constituent in this dissertation. Considerable work identifying DHB as a potent MBI of CYP3A has preceded that described in this dissertation; however, DHB pharmacokinetics remain understudied. To begin to address the lack of DHB clinical pharmacokinetic knowledge, a highly sensitive LC-MS/MS assay was developed (LLOQ, 250 pM), validated (Appendix A) and applied to analyze plasma samples from a GFJ-loperamide clinical interaction study where 16 subjects were administered GFJ (240 mL) containing 60 μM DHB (6.2 mg, Chapter 3, Appendix B). Additionally, quantification methods were developed and partially validated, to quantify further GFJ constituents (BG, naringin and naringenin, Appendix B) in human plasma. The pharmacokinetic analysis of DHB in human plasma was complicated by the suboptimal sampling times chosen which were selected based on loperamide pharmacokinetics. The sparse plasma sampling from time 0 to 4 h precluded recovery of robust

pharmacokinetic outcomes, but was sufficient to described $AUC_{0\text{-last}}$ and C_{max} in 11 out of 16 subjects. Plasma concentration-time profiles build on the limited qualitative DHB and BG exposure data presented by Goosen et al. (2004). With an improved understanding of DHB plasma exposure, a well-informed DHB pharmacokinetic study design can be devised or DHB predictive models (*e.g.,* PBPK) can be authenticated.

To advance a DHB-loperamide PBPK model, the recovery of additional in vitro kinetic parameters was essential. Kim et al. (2004) characterized metabolic kinetic parameters describing loperamide *N*-desmethylation in HLMs and recombinant CYPs, yet the role of intestinal metabolism of loperamide had not been determined. To estimate the contribution of the intestine to loperamide first-pass extraction, saturable metabolism parameters (K_m and V_{max}) were obtained using single donor HIMs (Appendix C,) or pooled HIMs (n=12, Appendix D). The K_m for individual donors of high, medium and low CYP3A4 expression varied from that obtained from a 12-donor pool (Appendix D). The observed difference in affinity may be due to the age or preparation method of the individual donor HIMs. The V_{max} recovered from the pooled donor lot (191 $\pm$ 11.7 pmol min^{-1} mg $protein^{-1}$) was consistent with the average of the low (60 pmol min^{-1} mg $protein^{-1}$), medium (250 pmol min^{-1} mg $protein^{-1}$) and high (290 pmol min^{-1} mg $protein^{-1}$) CYP3A4 expressing donors. Since *N*-desmethylloperamide metabolic kinetic parameters were unknown, a substrate disappearance assay was conducted in HIMs and HLMs to recover the intrinsic clearance (Appendix C).

To confirm the purported DHB-loperamide interaction in vitro, MBI kinetic parameters (K_I, k_{inact}) for DHB were recovered using HIMs (Chapter 2) and the index reaction, loperamide *N*-desmethylation. The recovered parameters (Chapter 2) were in

accordance with those recovered from midazolam and testosterone hydroxylation in single HIM donors (Paine et al., 2004).

Succeeding this in vitro assessment of the DHB-loperamide interaction in human cell fractions, a similar effort was made to assess the interaction potential in rat. The subsequent findings using rat liver microsomes (RLMs) and rat intestinal microsomes (RIMs) identified DHB as a potent reversible inhibitor of rat Cyp3a (Appendix D). However, the organ/tissue distribution in human versus that of rat cytochrome P450s varies (Cao et al., 2006). While CYP3A4 is the driver of intestinal oxidative drug metabolism in human, the rat expresses the CYP2c and Cyp2d subfamily of enzymes in addition to Cyp3a isoforms to a substantial extent (Paine et al., 2005; Cao et al., 2006; Paine et al., 2006). The measurement of MBI kinetic parameters in RLMs and RIMs using loperamide as the substrate indicated that DHB is a slower-acting MBI in rat (Appendix D). In vitro data reflect a species difference that precludes the use of rat models for human GFJ-drug interaction assessment.

A mechanistic static model was applied (Chapter 2) and successfully predicted a loperamide-GFJ interaction. To ensure that this successful IVIVE was not serendipitous, 15 previously reported GFJ-drug interaction studies were selected in accordance to a predefined criterion (within 25% of the observed AUC_{GFJ}/AUC). Twelve of these interactions were successfully predicted using DHB as a marker constituent. A sensitivity analysis indicated that the maximum predicted AUC_{GFJ}/AUC is achieved at relatively low DHB concentrations (<1.2 μM). The DHB concentrations used for interaction predictions incorporated an estimated enterocyte concentration, determined from the PBPK model described in Chapter 3.

The most noteworthy misprediction coming from this work was with atorvastatin. The atorvastatin AUC in the presence of GFJ was over predicted (300% versus 20%), which is likely due to atorvastatin being a substrate for the apically located uptake transporter, OATP2B1 (K_m, 0.2 μM). An accurate prediction of atorvastatin would require thorough characterization to identify a marker constituent and dynamic modeling to incorporate inhibition of OATP-mediated uptake transport.

These findings identified that DHB and a mechanistic static model could be used to prioritize new and existing drugs for more advanced GFJ-drug interaction modeling or for clinical evaluation. Importantly, DHB was justified for predicting the GFJ-loperamide interaction, permitting its application in dynamic, PBPK and PBPK/PD models. The following future experiments are recommended based on findings in this specific aim:

DETERMINE DHB KINETIC PARAMETERS (K_M, V_{MAX}) IN HUMAN ENZYME SOURCES USING METABOLITES IDENTIFIED IN URINE. The DHB PBPK model described in Chapter 3, accounts for only CYP3A4-mediated metabolism, as the recovery of DHB clearance is not straightforward by means of parent disappearance methods. Determination of saturable kinetic parameters for individual pathways of DHB metabolism is limited by the lack of authentic standards of DHB metabolites. Recently, several DHB metabolites have been identified in human urine samples (Regueiro et al., 2014). These metabolites could be synthetically or chemo-enzymatically synthesized for use as analytical standards and recovery of key kinetic parameters of DHB metabolism. Relevant parameters could be obtained in human microsomes (HIMs and HLMs) supplemented with NADPH, UDGPA, human S9 fractions and 3'-phosphoadenosine-5'-phosphosulfate or in human cell lines (*e.g.,* primary hepatocytes, human primary proximal tubule cells).

Data from these studies will improve DHB PBPK models and more accurately predict high (saturable) DHB doses or chronic exposure.

IDENTIFY URIDINE 5'-DIPHOSPHO-GLUCURONOSYLTRANSFERASE (UGT) ENZYMES RESPONSIBLE FOR DHB CONJUGATION. Following the recovery of metabolic kinetic parameters, recombinant, purified or overexpressed UGT enzyme sources could be used to identify the pathways relevant to DHB metabolism. In the absence of authentic standards, qualitative analysis could be conducted following incubations of DHB with UGTs and substrate disappearance methods. Increased knowledge of DHB metabolism will aid in refining the PBPK model (Chapter 3) and explain the lack of quantifiable DHB in 2 of the 16 subjects examined in Appendix B.

CONDUCT A CLINICAL STUDY TO MEASURE DHB ENTEROCYTE CONCENTRATIONS IN PATIENTS UNDERGOING GUT BIOPSIES. Although a sensitivity analysis of a mechanistic static model indicated that predicted enteric DHB concentration is only relevant at very low concentrations (<1 μM; Chapter 2), predictive models would benefit from accurate estimates of enteric DHB concentrations following a known dose of DHB in GFJ. Conducting a clinical study in patients undergoing routine intestinal biopsies would add little additional risk to patients but valuable information pertaining to DHB enteric exposure. Subjects would consume a GFJ product quantified for key constituents (*e.g.*, DHB, bergamottin, naringin, naringenin) prior to the procedure. Biopsy samples will be quantified using the highly sensitive HPLC-MS/MS assay (described in Chapter 3, Appendix A and Appendix B). Assay optimization and validation for the intestinal samples/matrices will be required. The quantification of GFJ constituents, and their metabolites, in human intestinal biopsies, following the administration of a characterized

juice, will provide clinical observations for model comparisons (PBPK or mechanistic static). Furthermore, development of a constituent juice concentration-to- constituent enterocyte concentration relationship may allow for a more direct assessment of the relative dietary substance-drug interaction risk of a given GFJ product.

TEST ADDITIONAL FURANOCOUMARINS AS A MARKER CONSTITUENT USING A MECHANISTIC STATIC MODEL. Despite the promising results supporting the use of DHB as a marker constituent of GFJ, BG and furanocoumarin conjugates should be evaluated in a likewise manner as the content varies from batch to batch. Also, certain juices (e.g., other citrus juices and soft drinks) may differ considerably from the normal rage of concentrations of constituents measured in GFJ. This simple mechanistic static modeling technique (described in Chapter 2) could be applied to determine the contribution of test furanocoumarins to the GFJ effect or with other substances containing furanocoumarins. This technique would require an accurate estimate of enteric furanocoumarin concentrations; therefore, knowledge obtained from gut biopsies would be particularly informative.

IDENTIFY MARKER CONSTITUENTS IN GFJ PREDICTIVE OF OATP-MEDIATED INTERACTIONS. For victims of the GFJ effect that are not mediated by CYP3A, but are substrates for OATPs, key marker constituents need further identification. Some work has been reported to determine that the furanocoumarins do not mediate this interaction, with naringin, naringenin and hesperidin as probable candidates (Won, 2012). PBPK models for these perpetrator constituents should be developed, along with the recovery of the appropriate metabolic (Cl_{int} and/or K_m and V_{max}) and inhibitory kinetic parameters (K_i). Identification of candidate marker constituents predictive of OATP-

mediated GFJ interactions and the recovery of their respective enzyme kinetic parameters will allow for PBPK models to be developed. The combination of a DHB PBPK interaction model with that of other marker constituents may result in a 'virtual grapefruit juice' for GFJ-drug interaction risk assessment.

CONDUCT IN VITRO-TO-IN VIVO EXTRAPOLATIONS IN RAT. The use of rats as a preclinical model to predict drug-drug interactions has been met with minimal success, due to frequent species differences in metabolism and distribution of xenobiotic metabolizing enzymes. The residue of human CYP3A4 modified by BG and DHB has been identified as Gln273 (Lin et al., 2012), but the modification in rat Cyp3a1 is unknown and may differ from that of human. In vitro data assessing DHB as an MBI and loperamide as a substrate toward rat enzyme sources (Appendix D) revealed that DHB inactivates rat Cyp3a1 less rapidly than human CYP3A4 using loperamide *N*-desmethylation as the index reaction. The species disconnect is not yet elucidated, and developing an understanding may improve the use of rat as a screening tool. A more complete understanding of DHB-mediated inactivation in rat is needed. The DHB-mediated MBI kinetic parameters should be recovered with a rat Cyp3a1 specific probe (e.g., 3-[(3,4-difluorobenzyl)oxy]-5,5-dimethyl-4-[4-methylsulfonyl)phenyl] furan-2(5H)-one, or DFB) (Michaud et al., 2007). DFB is a promising candidate as it is a fluorophore and is amendable to a plate reader assay.

EMPLOY HIGH THROUGHPUT SCREENING METHODS TO RECOVER KINETIC PARAMETERS FOR PERPETRATOR CONSTITUENTS. Parallel to the ToxCast initiative and to drug discovery, more high throughput methods of screening CYP3A inhibitors should be implemented. In light of the costs of HPLC-MS/MS based assays, plate reader-based assays would

be exceedingly more cost- and time- efficient for prioritizing marker constituents in various dietary substances. Libraries of isolated dietary substance constituents or extracts can be tested in human enzyme systems using validated CYP3A4 probes (*e.g.*, DFB). High throughput screening tools would accelerate the identification and prediction of dietary substance-drug interactions.

Aim 2. Predict the interaction risk of a GFJ with loperamide, using a single marker constituent.

A PBPK modeling and simulation approach was applied to predict the magnitude of a GFJ-loperamide interaction. As discussed in Chapter 3, the loperamide PBPK model described loperamide AUC and C_{max} to within 30% of observed outcomes. DHB plasma concentration-time profiles appeared to be predicted by a DHB PBPK model, although the sparse plasma data precluded statistical comparisons of DHB pharmacokinetic outcomes. The magnitude (AUC_{GFJ}/AUC) of the GFJ-loperamide interaction was predicted to within 20% of that observed. Following this success, DHB-loperamide interaction simulations were conducted with DHB doses reflective of the range labeled on certain dietary supplements (50-300 mg) (Appendix G). The outcomes under these conditions showed that hepatic CYP3A4 would be inhibited. Concurrent work showed that the quantities of DHB and BG in six dietary supplements tested to be far lower than labeled (<70 µg/capsule) (VanderMolen et al., 2014) (Appendix E). BG was also measured and unexpectedly detected in one product, albeit at low levels. Regardless of the unexpectedly low amount of DHB in the supplements, the in vitro reversible inhibitory potency (assessed by midazolam 1'-hydroxylation) of the mixture was greater than that of the individual DHB and BG contribution (Appendix E).

Additional evaluation of these products will be required to identify marker constituents in the products.

Proceeding with the assessment of the loperamide abuse potential, a PBPK/PD model was developed to simulate a clinically relevant pharmacodynamic endpoint (pupil miosis) in the presence and absence of DHB. A simulated loperamide dose escalation study was conducted to determine the loperamide dose required to elicit an equal pupillary response to oral alfentanil (1.7 mg). The estimated dose of ~72 mg was in line with anecdotal reports and provides some evidence to support these claims (Daniulaityte et al., 2013).

The risk of a GFJ-loperamide interaction resulting in centrally-acting effects remains low at therapeutic loperamide doses (2-16 mg), even in the presence of GFJ (Chapter 2 and Chapter 3). The proposed PBPK/PD modeling and simulation approach in Chapter 3 should be used to assess other GFJ-opioid interactions or to design clinical studies where pupillary response is an outcome. The following future experiments are recommended based on findings in this chapter:

APPLY A LOPERAMIDE PBPK/PD MODEL TO SPECIAL POPULATIONS. The loperamide PBPK/PD model developed and applied in Chapter 3 involved simulations conducted in virtual healthy volunteers. Construction of this model in the population based simulator, Simcyp®, levies the straightforward application of the model to special populations available in the software. These populations include special age groups (*e.g.,* pediatric, geriatric), patients with various conditions (*e.g.,* diabetes, obesity, hepatitis) and genetic polymorphisms. The model will be applied to these or 'customizable' populations (*e.g.*, a population enriched for poor metabolizers of CYP2D6) to identify susceptible

populations. Modeling and simulation of dietary substance-drug interaction in special populations will identify the most susceptible individuals without the added risk of clinical evaluation in these subjects.

ASSESS THE ABUSE POTENTIAL OF A GFJ-OPIOID (*I.E.* OXYCODONE) INTERACTION USING A DHB PBPK MODEL AND THE PROPOSED PBPK/PD MODELING APPROACH. A significant increase in oxycodone AUC has been reported in the presence of GFJ (Nieminen et al., 2010). Furthermore, a PBPK model of oxycodone has been published; however, converting this existing PBPK model within Simcyp® and incorporating a DHB interaction at the level of the intestine requires recombinant CYP enzyme kinetic data (K_m, V_{max}). These essential parameters should be obtained using the methods described in Appendix D. An oxycodone PBPK/PD model, developed using the methodology described in Chapter 3 will be applied similarly to that of loperamide.

ASSESS IRREVERSIBLE INHIBITION OF EXTRACTS OF DIETARY SUBSTANCES LABELED TO CONTAIN DHB. The labeled DHB and BG content did not agree with the reversible CYP3A4 inhibition of several supplement extractions (Appendix E). Accordingly, the irreversible potency should be determined using HIMs, midazolam 1'-hydroxylation and an IC_{50} shift approach. This approach will determine if unknown constituents promote MBI in HIMs. If the MBI by supplements is potent, further investigation is necessitated to identify these constituents. Since these supplements are being mislabeled for their content and sold, this information is pertinent to evaluating the safety of such products.

APPLY A DHB INTERACTION MODEL TO SUSPECTED VICTIM DRUGS. To support the long term goals of developing a model framework to assess dietary substance-drug interactions, additional perpetrator substances should be examined. Simulations could

be conducted with DHB measured in dietary supplements as described in Appendix E, or other known CYP3A inhibitors, such as the black pepper constituent piperine (K_i, 36-77 μM), that too are added to dietary supplements (Bhardwaj et al., 2002). Continued application of this approach will promote our understanding of dietary substance-drug interaction risk and help mitigate this public health concern.

Aim 3: Evaluate the performance of a human model to assess the reversal of opioid effect.

Two independent proof-of-concept clinical studies conducted in six healthy volunteers each demonstrated that (1) a novel intranasal naloxone formulation could achieve similar plasma exposures (F, 41%; $AUC_{0\text{-}6\ h}$, 266 ng/ml*min) to intramuscular naloxone (F, 55%; $AUC_{0\text{-}6\ h}$, 347 ng/ml*min) and (2) attenuation of alfentanil-induced miosis by intranasal naloxone was comparable to that of intramuscular naloxone. These studies can be used to inform robust human models to assess opioid reversal.

In the preliminary human model used to assess orally administered opioid reversal agents (Chapter 4), pupillary response was measured in six different subjects following alfentanil (4 mg) in the absence and presence of GFJ. The GFJ was quantified for DHB (60 μM) and the resulting fold AUC_{GFJ}/AUC was equal to previously published findings (Kharasch et al., 2004b). Both intramuscular and intranasal naloxone rapidly attenuated the pupillary effects induced by alfentanil; however, pupil miosis data were not rich enough to determine a difference in opioid reversal by intramuscular and intranasal naloxone formulations. This study was designed to administer naloxone at the t_{max} of alfentanil (~1 h); however, subjects reached t_{max} earlier than expected in this

cohort. Inter- and intra- individual variability in t_{max} may have complicated the interpretation of study outcomes. An alfentanil PBPK model prediction using an aged and gender matched virtual population predicted an alfentanil t_{max} (0.48 h) and time to R_{max} (0.6 h), accurately predicted the study outcomes (within 30%) (Appendix H). This same alfentanil model-prediction in the presence of DHB underpredicted the observed increase in $AUEC_{0\text{-}6\ h}$ in the presence of GFJ by >30%. The under prediction in the presence of DHB was due to a limitation of the construction of the alfentanil PBPK model. To predict an interaction at the level of the gut using in Simcyp®, the Absorption, Dissolution and Metabolism (ADAM) gut transit model must be used. The alfentanil model PBPK model was not developed using the ADAM model, because the PK was best described using a fixed first-order rate constant obtained from human clinical data. Therefore this under prediction was expected given the inappropriateness of the gut transit model for alfentanil. As such the alfentanil model should not be used for interaction predictions at the level of the gut.

Completion of this study resulted in several recommended improvements for subsequent studies using this human model for assessing opioid reversal. Due to the preliminary nature of this study, it was not powered with a sufficient number of subjects to properly evaluate intramuscular and intranasal naloxone formulations. However, findings from this work indicated 16 subjects are required to detect a 25% difference with 80% power and a Type I error of 0.05. Despite the limited number of subjects, the ability to observe the rapid return to baseline following alfentanil induce miosis was striking. The rate of which subjects return to baseline may have been better

characterized with more intense pupil diameter measurement sampling following naloxone administration.

Despite these caveats, alfentanil and pupil diameter measurements have an application beyond that of assessing opioid reversal. Alfentanil has been used as a probe for CYP3A phenotyping (Kharasch et al., 2004a) and may also be useful in evaluating dietary substances as CYP3A inhibitors, because the endpoint of pupil miosis is noninvasive and cost effective compared to pharmacokinetic analysis of FDA recommended probes (US Food and Drug Administration, 2012). Despite the greater variability and lessened sensitivity of alfentanil-induced pupil miosis compared to that of pharmacokinetic outcomes this approach would offer a means to increase study throughput at a lower monetary cost to sponsoring agencies (Kharasch et al., 2004a; Kharasch et al., 2007). The following future experiments are recommended based on findings in this chapter:

CONDUCT A POWERED CLINICAL STUDY USING AN IMPROVED HUMAN MODEL TO ASSESS THE REVERSAL OF OPIOIDS. Following two independent clinical studies evaluating naloxone pharmacokinetics and opioid reversal (Chapter 4), a powered clinical evaluation should take place. A randomized, three-phase clinical study in 16 healthy subjects will evaluate three naloxone formulations (intravenous, intramuscular, intranasal). Oral alfentanil (4 or 6 mg) will be administered, followed by naloxone (2 mg, 45 minutes after alfentanil). Blood will be collected at 5, 10, 15, 30, 45, 60, 90, 120, 240, 300 and 360 minutes after alfentanil administration and quantified for both alfentanil and naloxone. Pupil diameter and vital signs (blood pressure, O_2 saturation, respiratory rate and pulse rate) will be measured at 0, 5, 10, 20, 30, 35, 40, 45, 50, 60, 75, 90, 120, 150,

180, 240, 300, and 360 min after alfentanil. Effect outcomes of this study (pupil miosis-time, AUEC) are expected to allow for statistical comparisons between the reversal rates of alfentanil-induced miosis by naloxone. The intense sampling of both blood and pupil diameter (and other vital signs) will provide a richer data set for more advanced PK/PD modeling (discussed below). An alternative approach would involve the use of a longer acting opioid (*e.g.,* methadone, oxycodone) and an amended sampling scheme. The use of a longer acting opioid ($t_{1/2}$ > 1h, naloxone $t_{1/2}$) (Albeck et al., 1989) could provide a better measure of naloxone antagonism versus agonist depletion.

RECOVER PARAMETERS OF NALOXONE EFFECT USING DECONVOLUTION METHODS. Experimental designs to measure the in vivo potency of naloxone are not simple. Using alfentanil and naloxone plasma concentration-time data and pupil diameter-time measurements, deconvolution methods and Phoenix® WinNonlin® (Mountain View, CA) software, may aid in comparing outcomes of naloxone clinical effect through the recovery of relative parameters constructed in the model.

ASSESS COMPLEX DDI OR DIETARY SUBSTANCE-OPIOID INTERACTIONS. Orally administered combinatorial medications containing naloxone require that naloxone is extracted sufficiently *via* first-pass metabolism (DePriest and Miller, 2014; Koopmans et al., 2014). Naloxone is primarily metabolized by UGT2B7 enzymes that are expressed in the liver, kidney and intestine (Gill et al., 2012). A complex pharmacokinetic interaction perpetrated by an inhibitor of naloxone glucuronidation may elevate systemic naloxone concentrations such that the intended effects of the active opioid are attenuated. Recently, dietary substances (e.g., kaempherol, silibinin) have been identified as potent UGT inhibitors (Gufford et al., 2014). Clinical evaluation of these

perpetrator constituents should be conducted in a healthy volunteer study. Naloxone plasma concentrations and pupil diameter should be measured following administration of a combinatorial product (*e.g.*, Suboxone®, *Targiniq™ ER*) in the absence and presence of a test perpetrator substance.

Summary and Significance

Pharmaceuticals undergo rigorous evaluation prior to market appearance in accordance to U.S. FDA regulations and well-defined guidelines to assess the DDI potential of a new chemical entity. However the FDA has limited jurisdiction in regards to the regulation of dietary substances. Although regulatory agencies are acknowledging the importance of dietary substance-drug interaction risk, the burden of proof is not on the manufacturer of the product; instead, interaction studies are frequently conducted by public sector, academic and pharmaceutical laboratories. A framework to alleviate the cost and increase the throughput of dietary substance-drug interaction risk assessment is essential.

This dissertation project expanded on translational methods to quantitatively predict a dietary substance-drug interaction. Using In vitro systems, IVIVE, PBPK/PD modeling and simulation, and clinical evaluations a GFJ-loperamide interaction was rigorously evaluated. These tools were employed to test a revised framework to study dietary substance-drug interactions mediated by CYP enzymes. The application of a loperamide PBPK/PD model concluded the likelihood of loperamide-induced central opiate-like effects is low at therapeutic doses (2-16 mg) even with GFJ. However, this model supported some of the anecdotal claims, which suggest an abuse potential at

extreme loperamide doses (70-200 mg). These findings may prove useful for agencies to make informed regulatory decisions.

The emphasis of this dissertation was to improve on currently proposed methodologies to predict dietary substance-drug interaction risk, by predicting pharmacodynamic endpoints and increasing the throughput of clinical evaluation of dietary substance-opioid interactions. The overall outcomes of this dissertation will provide investigators and regulatory agencies with a framework to evaluate dietary substance-drug interaction risk in a less invasive, time- and cost-efficient manner than presently achieved. Ideally, the in vitro and PBPK modeling and simulation approach will allow for prospective dietary substance-drug interaction risk assessment. These translational approaches will facilitate safer cohesion between conventional pharmacotherapy and alternative medicine practices.

REFERENCES

Albeck H, Woodfield S and Kreek MJ (1989) Quantitative and pharmacokinetic analysis of naloxone in plasma using high-performance liquid chromatography with electrochemical detection and solid-phase extraction. *Journal of chromatography* **488**:435-445.

Bailey DG, Dresser G and Arnold JM (2013) Grapefruit-medication interactions: Forbidden fruit or avoidable consequences? *CMAJ* **185**:309-316.

Bhardwaj RK, Glaeser H, Becquemont L, Klotz U, Gupta SK and Fromm MF (2002) Piperine, a major constituent of black pepper, inhibits human P-glycoprotein and CYP3A4. *J Pharmacol Exp Ther* **302**:645-650.

Bluelight (2014) What is it in grapfruit juice tht potentiates opioids?, in, vBulletin.

Bohnert AS, Valenstein M, Bair MJ, Ganoczy D, McCarthy JF, Ilgen MA and Blow FC (2011) Association between opioid prescribing patterns and opioid overdose-related deaths. *JAMA* **305**:1315-1321.

Cao X, Gibbs ST, Fang L, Miller HA, Landowski CP, Shin HC, Lennernas H, Zhong Y, Amidon GL, Yu LX and Sun D (2006) Why is it challenging to predict intestinal drug absorption and oral bioavailability in human using rat model. *Pharm Res* **23**:1675-1686.

Daniulaityte R, Carlson R, Falck R, Cameron D, Perera S, Chen L and Sheth A (2013) "I just wanted to tell you that loperamide WILL WORK": a web-based study of extra-medical use of loperamide. *Drug Alcohol Depend* **130**:241-244.

DePriest AZ and Miller K (2014) Oxycodone/Naloxone: role in chronic pain management, opioid-induced constipation, and abuse deterrence. *Pain and therapy* **3**:1-15.

European Medicines Agency: Committee for Human Medical Products (2012) Guidline on the Investigation of Drug Interactions.

Gill KL, Houston JB and Galetin A (2012) Characterization of in vitro glucuronidation clearance of a range of drugs in human kidney microsomes: comparison with liver and intestinal glucuronidation and impact of albumin. *Drug Metab Dispos* **40**:825-835.

Goosen TC, Cillie D, Bailey DG, Yu C, He K, Hollenberg PF, Woster PM, Cohen L, Williams JA, Rheeders M and Dijkstra HP (2004) Bergamottin contribution to the grapefruit juice-felodipine interaction and disposition in humans. *Clin Pharmacol Ther* **76**:607-617.

Health Canada (2011) Guidance Document for Industry- Reporting Adverse Reactions to Marketed Health Products. Health Canada, Ottawa, Ontario., in.

Jaffe JH, Kanzler M and Green J (1980) Abuse potential of loperamide. *Clin Pharmacol Ther* **28**:812-819.

Kharasch ED, Walker A, Hoffer C and Sheffels P (2004a) Intravenous and oral alfentanil as in vivo probes for hepatic and first-pass cytochrome P450 3A activity: noninvasive assessment by use of pupillary miosis. *Clin Pharmacol Ther* **76**:452-466.

Kharasch ED, Hoffer C, Whittington D and Sheffels P (2004b) Role of hepatic and intestinal cytochrome P450 3A and 2B6 in the metabolism, disposition, and miotic effects of methadone. *Clin Pharmacol Ther* **76**:250-269.

Kharasch ED, Walker A, Isoherranen N, Hoffer C, Sheffels P, Thummel K, Whittington D and Ensign D (2007) Influence of CYP3A5 genotype on the pharmacokinetics and pharmacodynamics of the cytochrome P4503A probes alfentanil and midazolam. *Clin Pharmacol Ther* **82**:410-426.

Kim KA, Chung J, Jung DH and Park JY (2004) Identification of cytochrome P450 isoforms involved in the metabolism of loperamide in human liver microsomes. *Eur J Clin Pharmacol* **60**:575-581.

Koopmans G, Simpson K, De Andres J, Lux EA, Wagemans M and Van Megen Y (2014) Fixed ratio (2:1) prolonged-release oxycodone/naloxone combination improves bowel function in patients with moderate-to-severe pain and opioid-induced constipation refractory to at least two classes of laxatives. *Current medical research and opinion*:1-23.

Lin HL, Kenaan C and Hollenberg PF (2012) Identification of the residue in human CYP3A4 that is covalently modified by bergamottin and the reactive intermediate that contributes to the grapefruit juice effect. *Drug Metab Dispos* **40**:998-1006.

Michaud J, Leblond FA, Naud J, Boisvert C, Desbiens K, Nicoll-Griffith DA and Pichette V (2007) Use of a fluorescent substrate for the selective quantification of rat CYP3A in the liver and the intestine. *Journal of pharmacological and toxicological methods* **55**:209-213.

Mukwaya G, MacGregor T, Hoelscher D, Heming T, Legg D, Kavanaugh K, Johnson P, Sabo JP and McCallister S (2005) Interaction of ritonavir-boosted tipranavir with loperamide does not result in loperamide-associated neurologic side effects in healthy volunteers. *Antimicrob Agents Chemother* **49**:4903-4910.

National Center for Complementary and Alternative Medicine (2013) Dietary Supplement-Drug Interaction Expert Panel Meeting. *9000 Rockville Pike, Bethesda, Maryland 20892*.

Niemi M, Tornio A, Pasanen MK, Fredrikson H, Neuvonen PJ and Backman JT (2006) Itraconazole, gemfibrozil and their combination markedly raise the plasma concentrations of loperamide. *Eur J Clin Pharmacol* **62**:463-472.

Nieminen TH, Hagelberg NM, Saari TI, Neuvonen M, Neuvonen PJ, Laine K and Olkkola KT (2010) Grapefruit juice enhances the exposure to oral oxycodone. *Basic Clin Pharmacol Toxicol* **107**:782-788.

Paine MF, Criss AB and Watkins PB (2004) Two major grapefruit juice components differ in intestinal CYP3A4 inhibition kinetic and binding properties. *Drug Metab Dispos* **32**:1146-1153.

Paine MF, Ludington SS, Chen ML, Stewart PW, Huang SM and Watkins PB (2005) Do men and women differ in proximal small intestinal CYP3A or P-glycoprotein expression? *Drug Metab Dispos* **33**:426-433.

Paine MF, Hart HL, Ludington SS, Haining RL, Rettie AE and Zeldin DC (2006) The human intestinal cytochrome P450 "pie". *Drug Metab Dispos* **34**:880-886.

Paine MF and Oberlies NH (2007) Clinical relevance of the small intestine as an organ of drug elimination: drug-fruit juice interactions. *Expert Opin Drug Metab Toxicol* **3**:67-80.

Regueiro J, Vallverdu-Queralt A, Negreira N, Simal-Gandara J and Lamuela-Raventos RM (2014) Identification and quantification of grapefruit juice furanocoumarin metabolites in urine: an approach based on ultraperformance liquid chromatography coupled to linear ion trap-Orbitrap mass spectrometry and solid-phase extraction coupled to ultraperformance liquid chromatography coupled to triple quadrupole-tandem mass spectrometry. *Journal of agricultural and food chemistry* **62**:2134-2140.

Shen GL, Zhuang XM, Yuan M, Sun HX and Li H (2012) Evaluation of P-glycoprotein mediated in vitro loperamide biliary excretion with sandwich-cultured rat hepatocytes model. *Yao Xue Xue Bao* **47**:459-465.

Skarke C, Jarrar M, Schmidt H, Kauert G, Langer M, Geisslinger G and Lotsch J (2003) Effects of ABCB1 (multidrug resistance transporter) gene mutations on disposition and central nervous effects of loperamide in healthy volunteers. *Pharmacogenetics* **13**:651-660.

Streel B, Ceccato A, Klinkenberg R and Hubert P (2005) Validation of a liquid chromatographic-tandem mass spectrometric method for the determination of loperamide in human plasma. *J Chromatogr B Analyt Technol Biomed Life Sci* **814**:263-273.

Tayrouz Y, Ganssmann B, Ding R, Klingmann A, Aderjan R, Burhenne J, Haefeli WE and Mikus G (2001) Ritonavir increases loperamide plasma concentrations without evidence for P-glycoprotein involvement. *Clin Pharmacol Ther* **70**:405-414.

US Food and Drug Administration (2012) Draft Guidance: Drug Interaction studies-study design, data analysis, implications for dosing, labeling recommendations. US Food and Drug Administration, Rockville, MD.

VanderMolen KM, Ainslie GR, Paine MF and Oberlies NH (2014) Labeled content of two furanocoumarins in dietary supplements correlates with neither actual content nor CYP3A inhibitory activity. *J Pharm Biomed Anal* **98**:260-265.

Won CS (2012) Intergrated apoaches to identify and predict pharmacokinetic-based dietary substance-drug interactions., in *Division of Pharmacotherapy and Experimental Therapeutics* p 260, University of North Carolina at Chapel Hill, Chapel Hill.

Won CS, Oberlies NH and Paine MF (2012) Mechanisms underlying food-drug interactions: inhibition of intestinal metabolism and transport. *Pharmacol Ther* **136**:186-201.

Yu JH, Kim HJ, Lee S, Hwang SJ, Kim W and Moon CJ (2004) LC-MS determination and bioavailability study of loperamide hydrochloride after oral administration of loperamide capsule in human volunteers. *J Pharm Biomed Anal* **36**:421-427.

APPENDICES

APPENDIX A: METHOD DEVELOPMENT AND VALIDATION OF AN HPLC-MS/MS METHOD TO QUANTIFY 6',7'-DIHYDROXYBERGAMOTTIN AND OTHER GRAPEFRUIT JUICE CONSTITUENTS IN HUMAN PLASMA.

METHODS

Materials and chemicals. DHB and psoralen were purchased Caymen Chemical (Ann Arbor, MI). LC/MS/MS grade acetonitrile, methanol, dimethyllsulfoxide, ethyl acetate, and formic acid were purchased from Thermo Fisher (Waltham, MA). Pooled human plasma was purchased from Bioreclamation (Baltimore, MD).

Calibration standard preparation and sample extraction. Calibration standards and quality controls were prepared using blank human plasma at concentrations ranging from 0.25-1000 and 0.8-1000 nM for DHB and BG, respectively; and from 1-2000 and 10-1500 nM for naringin and naringenin, respectively. Thawed plasma samples (100 µL) were added to microcentrifuge tubes and extracted by adding ethyl acetate (500 µL) containing 400 nM internal standard (psoralen). Samples were vortexed for 3 minutes at room temperature then centrifuged (2000 x g, 10 minutes, 4℃) to separate the aqueous and organic phases. Supernatant (400 µl) was transferred to 0.6 mL cluster tubes and dried under heated nitrogen gas (50℃). Samples were reconstituted with 100 µL of 95% water:5% acetonitrile:0.1% formic acid (v/v/v) to replicate initial chromatographic conditions.

Chromatographic conditions for the quantification of grapefruit juice constituents in human plasma *via* HPLC-MS/MS. Plasma samples, standards and QCs (10 µl) were separated on a Thermo Aquasil C18 column (3 µm, 2.1 x 50 mm). Analytes were eluted using a gradient initially held at 95% mobile phase A (Nanopure water with 0.1% formic acid) water and 5% mobile phase B (LC/MS/MS grade acetonitrile with 0.1% formic acid) for 0.4 minutes. Mobile phase B was increased linearly for 1.1 minutes to 95%, maintained for 0.2 minutes, then returned to initial conditions over 0.1 minutes. The column was equilibrated for 2 minutes. Eluent was directed to waste for the first 0.4 minutes then to a mass detector.

Detection of DHB using a Sciex API 5600 TripleTOF mass spectrometer. The API TripleTOF mass spectrometer (Framingham, MA) was operated in positive ion mode, with a source temperature of 350℃, an ion spray voltage of 3500 V, a decoupling potential (DP) of 25 V and a collision energy (CE) of 20 mV. The mass range of 203.15-203.18 m/z was selected for quantification.

Optimized detection of DHB using Sciex API 6500 hybrid triple quadrupole mass spectrometer. The Sciex API 6500 hybrid triple quadrupole mass spectrometer (Framingham, MA) was operated in multiple reaction monitoring (MRM) mode, with a source temperature of 250℃, an ion spray voltage of 2500 V, a DP of 25 V and MRM transitions for DHB and psoralen of 273.2→203.1 (CE, 25 mV) and 187.1→131.2 (CE, 32 mV), respectively.

Optimized detection of BG on a Sciex API 6500 hybrid triple quadrupole mass spectrometer. The Sciex API 6500 hybrid triple quadrupole mass spectrometer (Framingham, MA) was operated in multiple reaction monitoring (MRM) mode, with a

source temperature of 550℃, an ion spray voltage of 5500 V, DP of 25 V and MRM transitions for BG of 339.6→147.1 (CE, 47 mV).

Detection of naringin and naringenin on a Sciex API 6500 hybrid triple quadrupole mass spectrometer. The mass spectrometer was operated in MRM mode, with a source temperature of 350℃, an ion spray voltage of 5500 V, DP of 25 V, and MRM transitions for naringin and naringenin of 579→271 (CE, -32 mV) and 273→153 (CE, 47 mV), respectively.

Stability of DHB in human plasma stored at -80˚C. Plasma (10 mL) was spiked with DHB (10 mM in DMSO) to a final concentration of 100 nM DHB. Aliquots (20 x 500 µl) were then stored at -80°C on February 2, 2013 (first aliquot was never frozen, but was extracted for DHB quantification). On selected dates, an aliquot was removed from storage and extracted along with freshly prepared calibration standards as described above. Extracted samples (n=3) were injected for HPLC-MS/MS analysis in triplicate.

Freeze-thaw stability of DHB in human plasma. Spiked human plasma was prepared as described above (100 nM DHB). Unlike before, aliquots underwent refreeze (>24 h) and thaw (<2 h) cycles over the course of two weeks total. Each extraction was quantified using calibration standards as described earlier and analyzed by HPLC-MS/MS in triplicate. The lower limit of quantification was 250 pM based on FDA guidelines (US Food and Drug Administration, 2013).

Data analysis. All quantification was conducted using peak area ratios (psoralen as the internal standard) and calibration standards. Data is presented as the mean and standard deviation. Accuracy is determined by the calculated concentration relative to the nominal concentration and precision is reported as CV% and relative error (RE).

RESULTS

DHB was readily quantifiable at the lowest tested calibration standard (250 pM) with a covariate of variance (%CV) <15% and a signal to noise ratio >10 (Table A.1; Figure A.1). BG, naringin and naringenin were quantifiable at their lowest prepared standard concentrations (0.5, 1 and 1 nM, respectively) with acceptable accuracy and precision. The signal to noise ratio for BG varied from 5-7 at 250 pM, but was consistent >10 at 500 pM, confirming its LLOQ to be 500 pM based on the predefined criteria. The internal standard, psoralen, was chromatographically resolved from DHB (Figure A.1) and from BG (RT, 2.8 min), naringin (RT, 1.32) and naringenin (RT, 1.44).

The stability of DHB spiked into plasma and stored at -80°C was assessed to determine the validity of quantifying archived clinical plasma samples for DHB. The calculated DHB concentration decreased by less than 10% over an 18-month span of storage (Figure A.2). Assessment of freeze thaw cycles indicated a 20% decrease in DHB after 3 freeze-thaw cycles and only ~65% remained after a 5^{th} freeze-thaw cycle.

DISCUSSION

Following thorough optimization a highly sensitive assay to detect DHB was developed. Methods were also devised to quantify BG, naringin and naringenin, although the latter were not fully validated methods, and include mass spectrometer conditions incompatible with DHB precluding optimal simultaneous quantification of all four analytes. Sub nanomolar concentrations could be reliably measured for DHB (250 pM) and BG (500 pM), achieving the sensitivity necessary to obtain plasma pharmacokinetics of these analytes in human due to their low plasma exposures (Goosen et al., 2004). The high micromolar to millimolar concentrations of naringin and naringenin measured in GFJ (Vandermolen et al., 2013) taken together with preliminary analysis of human plasma samples indicated these analytes could be more readily detected in human plasma following GFJ consumption than DHB and BG. Therefore lower calibration standards were not tested.

All optimized methods were achieved using a Sciex 6500 hybrid triple quadrupole mass spectrometer and the reported conditions, however early development began using a high-resolution time-of-flight mass detector. This instrument was used early on in the DHB plasma stability experiments presented (Figure A.2) on the dates of February 2, 2013 and April 2nd 2013. This difference in platform may explain the apparent higher concentrations measured on those dates compared to the later dates. Despite this instrumentation difference, DHB appeared to be stable in human plasma stored at -80°C for at least 18-months. However, repeated freeze thawing was detrimental to DHB stability after 2-3 cycles.

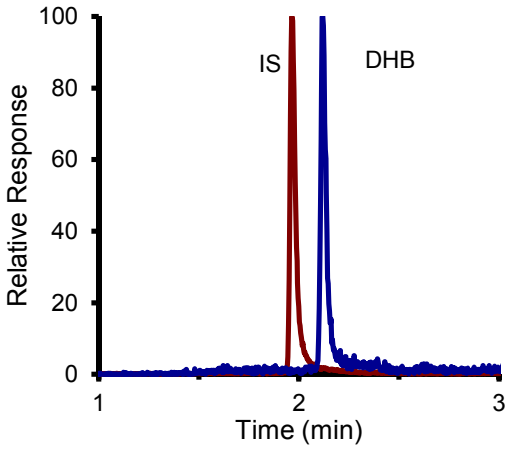

Figure A.1. HPLC-MS/MS separation and detection of 6',7'-Dihydroxybergamottin (DHB) and the internal standard (IS) psoralen at the lower limit of DHB quantification (250 pM). Signals are normalized to the maximal measured response per MRM trace.

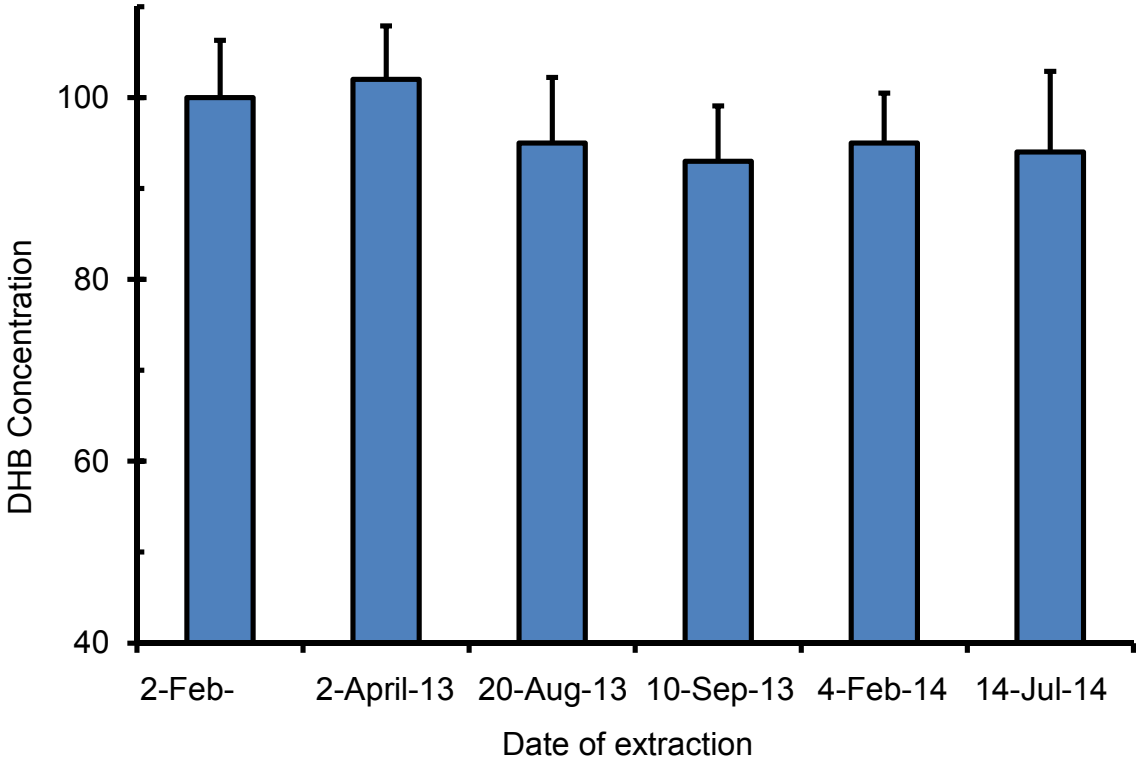

Figure A.2. DHB stability following storage at -80°C. The date shown corresponds to the date of extraction and analysis and the measured DHB concentration was determined from interpolation of 8 calibration standards (10-1000 nM). Extractions performed on 2/2/2013 and 4/2/2013 were quantified on an AB Sciex TripleTOF and the remained on an AB Sciex 6500 mass spectrometer. Bars denote the mean ± SD of triplicate extractions.

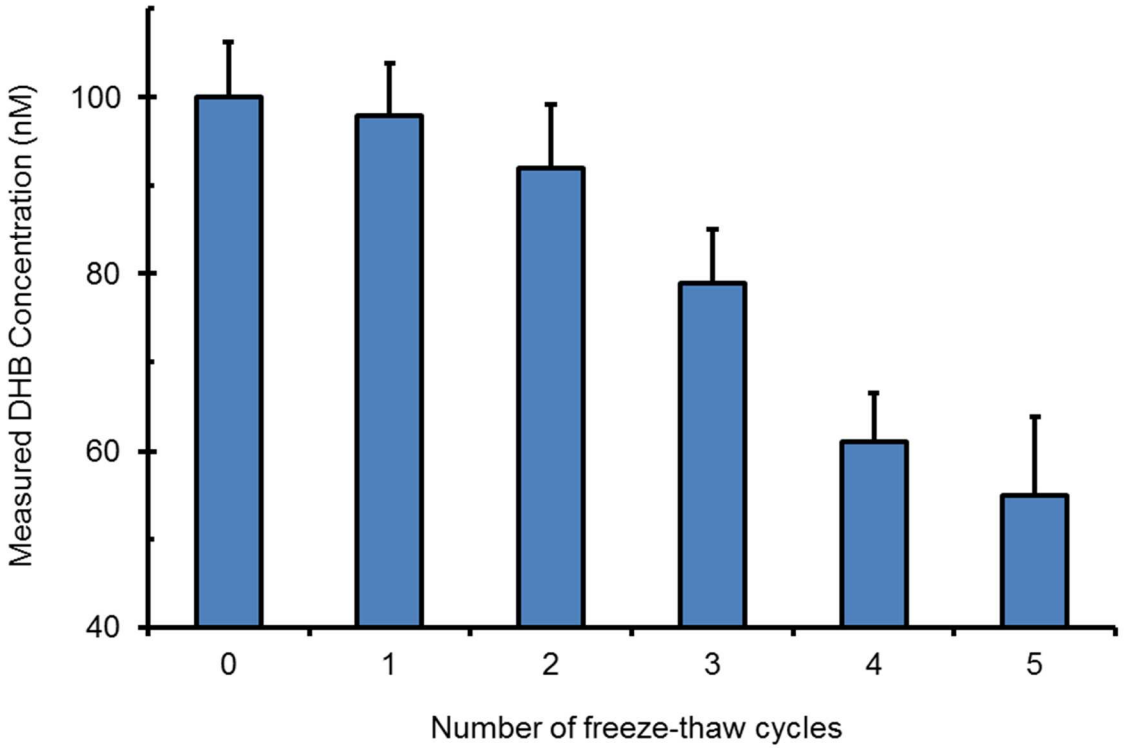

Figure A. 3. DHB quantification of human plasma samples spiked with 100 nM DHB and having undergone freeze-thaw cycles (as denoted). Bars denote the mean ± SD of triplicate extractions.

Table A.1. Precision (%CV) and accuracy (RE) Inter- and intra-day variability of DHB in human plasma (n=3).

	Intraday		Interday	
	%CV	RE	%CV	RE
6',7'-Dihydroxybergamottin				
1.6 nM	0.72	2.3	2.12	10
16 nM	1.2	-1.9	13.52	-13
80 nM	0.91	-2.0	3.95	-10
800 nM	0.99	2.7	2.92	12
Bergamottin				
1.6 nM	1.2	-3.1	5.12	-12
16 nM	1.1	3.0	3.61	10
80 nM	0.82	4.5	3.92	8.7
800 nM	0.99	2.9	2.94	13
Naringen				
1.6 nM	4.2	7	11.2	14
16 nM	2.2	-4.8	6.5	-11
80 nM	1.9	-5.2	5.6	-13
800 nM	1.1	3.2	7.2	8.2
Naringenin				
1.6 nM	2.1	-4.4	12.3	-14
16 nM	1.21	5.7	2.25	12
80 nM	0.99	3.1	3.45	9.1
800 nM	1.02	7.3	5.61	10

APPENDIX B: CHARACTERIZATION OF FURANOCOUMARIN METABOLITES IN HUMAN PLASMA FOLLOWING GRAPEFRUIT JUICE CONSUMPTION.

METHODS

Materials and chemicals. See chapter 3.

Human Sample procurement. See chapter 3.

Human plasma. Plasma samples from a grapefruit juice-loperamide interaction study (Ainslie et al., 2014) were quantified for DHB and BG. Subjects (n=16) consumed 240 mL of grapefruit juice quantified for DHB (70 μM). Blood was collected prior to and 0.5, 1, 2, 3, 4, and 6 h after GFJ consumption. Plasma was stored at -80°C and thawed at room temperature under low light conditions.

Quantification of furanocoumarins and their metabolites by HPLC-MS/MS. Plasma samples were quantified for DHB and BG as described in appendix A.

Data analysis. Pharmacokinetic outcomes were obtained *via* standard non-compartmental methods using Phoenix WinNonlin (v6.3). The maximum concentration (C_{max}), time to reach C_{max} (t_{max}), and last measurable concentration (C_{last}) were obtained directly from the plasma concentration-time profiles. The terminal elimination rate constant (λ_z) was determined by linear regression of the terminal portion of the log-transformed concentration-time profile using at least three data points. Area under the plasma concentration-time curve (AUC) from time zero to 4 h ($AUC_{0\text{-}4h}$) was determined using the trapezoidal method with linear up/log down interpolation. The AUC from time zero to infinity ($AUC_{0\text{-}inf}$) was calculated as the sum of $AUC_{0\text{-}4h}$ and C_{4h}/λ_z.

RESULTS

In human plasma samples, BG was below the limit of quantification in all tested samples although DHB was detected in 14 out of 16 subjects and 11 subjects had a sufficient quantifiable data to determine pharmacokinetic outcomes (Table B.1). A secondary observation during the quantification of DHB in human plasma was an unexpected peak using the MRM transitions corresponding to DHB, in certain subjects (n=5, Figure B.1). This extraneous peak is hypothesized to correspond to a DHB conjugate, undergoing in source fragmentation. Recently, DHB glucuronide conjugates had been identified and measured in human urine (Regueiro et al., 2014).

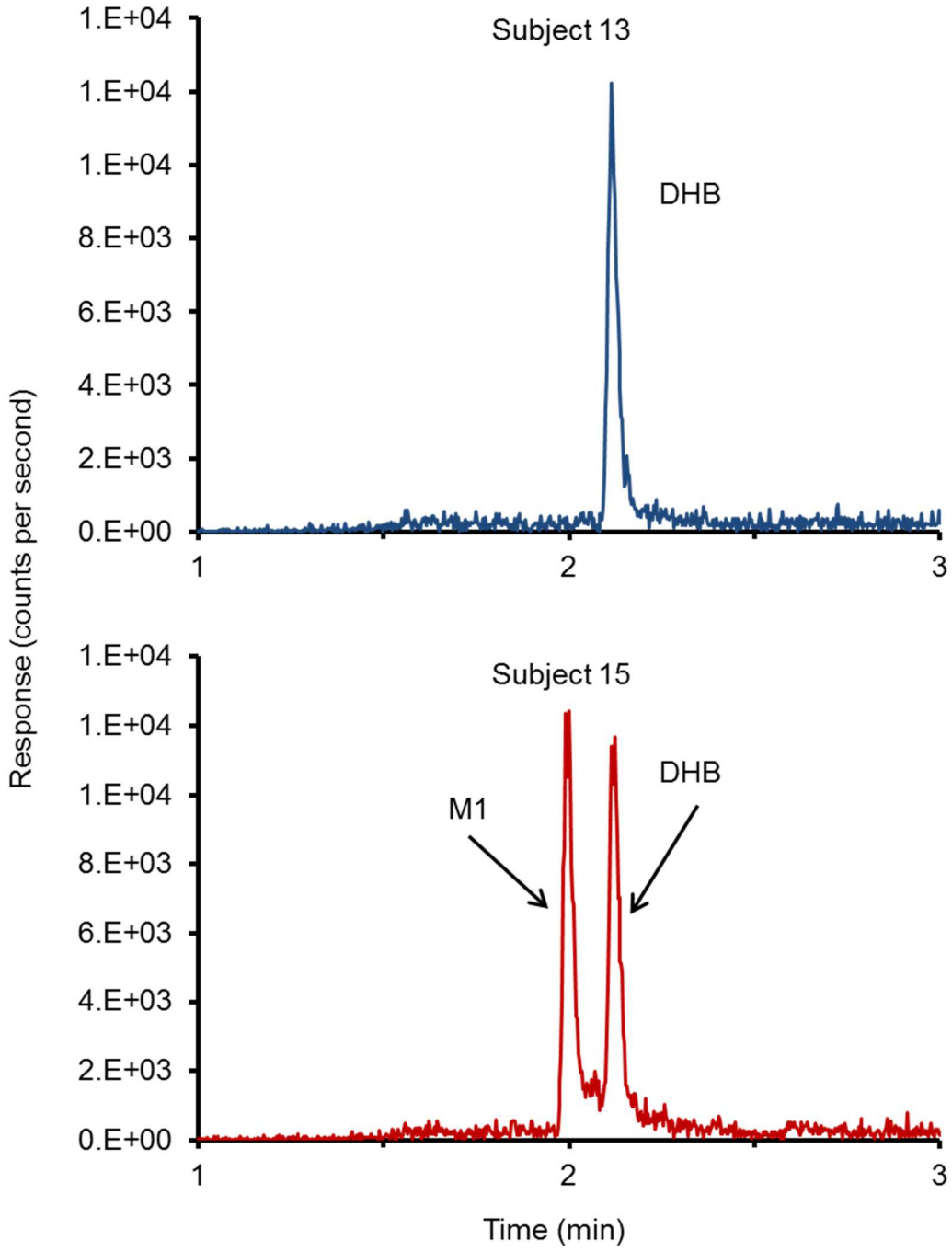

Figure B.1. Representative chromatograms following HPLC-MS/MS analysis of plasma from two subjects 4 h after consuming grapefruit juice. Subject 13 (top) with only DHB detected and subject 15 (bottom) with DHB and a suspected metabolite.

Table B.1. Individual DHB pharmacokinetic outcomes.

Subject	λ_Z (h^{-1})	T_{max} (h)	C_{max} (nM)	$AUC_{0\text{-}4h}$ (h*nM)	$AUC_{0\text{-}inf}$ (h*nM)
1	0.337	1	12.9	18.8	23.7
2	0.744	0.5	18.3	33.6	36.2
3	0.578	0.5	36.1	69.3	79.3
4					
6	1.699	0.5	3.7	6.6	6.6
7	0.855	1	13.4	24.0	25.3
8	0.530	0.5	54.7	115.5	141.1
9					
10	1.064	1	11.2	15.1	15.5
11		1	15.8	10.0	
12	0.447	1	31.1	63.3	77.7
13		3	62.6	98.9	
14	0.246	0.5	32.5	88.5	
15	0.554	0.5	45.6	48.7	54.6
16		4	17.2	25.7	
18	0.401	1	22.8	51.3	

λ_Z, terminal elimination slope; T_{max}, time to maximal concentration (C_{max}); $AUC_{0\text{-}4\ h}$, area under the plasma concentration-time curve from 0-4 h; AUC_{inf}, AUC from 0 h extrapolated to infinite time. [a]The percent of area extrapolated from 4 h to infinite time.

APPENDIX C: RECOVERY OF IN VITRO KINETIC PARAMETERS OF LOPERAMIDE AND N-DESMETHYLLOPERAMIDE METABOLISM IN HUMAN INTESTINAL MICROSOMES FROM INDIVIDUAL DONORS.

METHODS

Materials. See chapter 2.

Microsomes. Human intestinal microsomes were obtained from individual donors selected as high (HI5-J7), medium (HI7-J7) and low (HI8-J7/J8) CYP3A4 protein content (Paine et al., 2006).

Recovery of saturable kinetic parameters for loperamide *N*-desmethylation. Loperamide *N*-desmethylation was assessed under linear conditions for microsomal protein concentration and time (0.1 mg/mL; 20 min) at 37°C and a total incubation volume of 200 µL. The substrate, loperamide, was incubated from 0.2-50 µM and initiated by the addition of NADPH (1 mM). Incubations were terminated and the primary loperamide metabolite, *N*-desmethylloperamide was quantified using methods described in chapter 2.

Recovery of *N*-desmethylloperamide intrinsic clearance in human liver and intestinal microsomes. *N*-Desmethylloperamide (1 µM) was incubated in HIMs (0.1 mg/ml) collected from a single donor (HI7J7) or HLMs (0.1 mg/ml) from pooled donors (n=50) for 30 minutes at 37˚C. Time points (0.25-30 minutes) were collected with the removal of 25 µL of incubation mixture, precipitated with 400 µL of acetonitrile containing 0.1% formic acid (v/v) and internal standard (D_3- *N*-desmethylloperamide,

500 nM) in 96-well plates. Plates were centrifuged at 2000 x g for 5 minutes, and 300 µL of supernatant were transferred to the final analysis plate. The final plate was dried down under heated nitrogen gas (50˚C) then reconstituted in 300 µL of 95% water:5% Methanol : 0.1% formic acid (v/v/v) and analyzed by HPLC-MS/MS. The intrinsic clearance (CL_{int}) was determined by equation C.1 (Di et al., 2012).

HPLC-MS/MS quantification of *N*-desmethylloperamide. Samples (7 µL) were separated on an Atlantis C18 column (2.1 X 50 cm, 3µm). The mobile phase gradient was carried out on a Shimazdu LC-20AD solvent delivery system and analytes were detected with a Sciex TripleTOF 5600 mass spectrometer. The HPLC method is described in detail in chapter 2. Analyte detection was achieved with a decoupling potential of 25 V and a collision energy of 35 mV, with a mass range for quantification of 252.1000-252.8000 for N-desmethyl loperamide and 255.1000-255.8000 m/z. Analyte peak integration and sample quantitation was conducted using Analyst software (v1.6; Applied Biosystems, Framingham, MA). The lower limit of quantification (LLOQ) was 0.9 nM and the upper limit of quantification (ULOQ) was 1000 nM.

Data analysis. A linear regression model was fit to the data in Pheonix® WinNonlin®. The intrinsic clearance was determined using equation C.1 assuming a free fraction of 1.

$$Cl_{\text{int},inc} = \frac{-k\left(\frac{V}{M}\right)}{f_{u,inc}} \qquad \text{Equation C.1}$$

Where *k* is the slope, *V* is the volume of the incubation, *M* is the amount of microsomal protein in the incubation and $f_{ub,\ inc}$ is the unbound fraction in the incubation.

RESULTS

Saturable kinetic parameters for loperamide were recovered by HIMs of three individual donors. The recovered K_m in high, medium and low CYP3A4 expressing individual donors was 12.4, 15.2, and 21.8 μM, respectively, and V_{max} was 61, 250, 290 pmol/min/ mg protein, respectively (Figure C.1).

The intrinsic clearance of loperamide (taken as the ratio of V_{max} to K_m) for high, medium and low donors was 23.1, 16.4 and 2.8 μL/min/mg protein, respectively.

The intrinsic clearance for *N*-desmethylloperamide determined by the parent disappearance method was 18.41 and 39.08 μL/min/mg protein by HIMs and HLMs, respectively (Figure C.2).

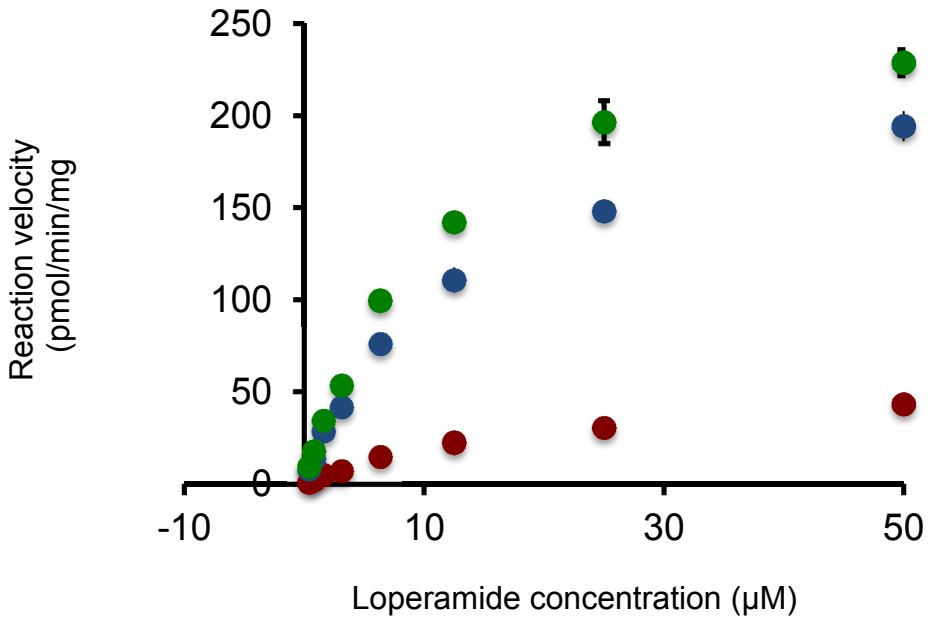

Figure C.1. Michaelis-Menten plot for *N*-desmethylation of loperamide by HIMs in a high (green), medium (blue) and low (red) CYP3A4 expressing donor. Symbols and error bars denote means and S.D.'s, respectively.

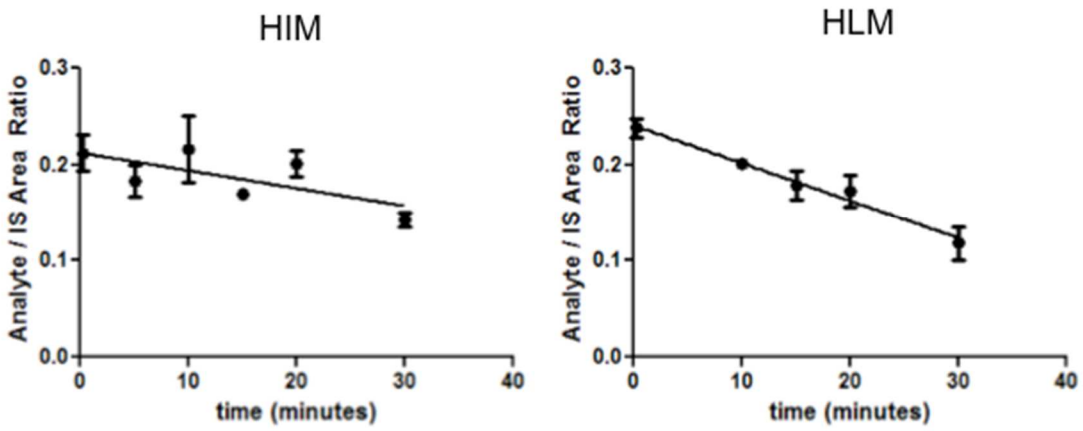

Figure C.2. Parent disappearance of *N*-desmethylloperamide by HIMs (left) and HLMs (right).Symbols denote the mean and S.D.'s of triplicate incubations and the solid line denotes the model fit.

APPENDIX D: RECOVERY OF IN VITRO KINETIC PARAMETERS OF LOPERAMIDE METABOLISM AND INHIBITORY KINETIC PARAMETERS OF DHB IN RAT.

METHODS

Materials and Chemicals. See chapter 2.

Rat enzyme sources. Recombinant rat enzymes were a purchased from BD Biosciences (San Jose, CA). Pooled (n=400) rat liver microsomes (RLMs) and pooled (n=200) rat intestinal microsomes (RIMs) were purchased from XenoTech (Lenexa, KS).

***N*-Desmethylloperamide formation in recombinant rat P450 enzymes**. Loperamide (1 µM) was incubated (37°C) for 20 minutes in recombinant rat P450 enzymes (Cyp1a1, Cyp2a1, Cyp2a2, Cyp2b1, Cyp2c11, Cyp2c13, Cyp2c13, Cyp2c6, Cyp2d1, Cyp2d2, Cyp2e1 and Cyp3a1) at an enzyme concentration of 50 pmol P450/mL and a total incubation volume of 200 µL. Incubations were initiated with NADPH (2 mM) and terminated at the end of each incubation by the transfer of 100 µl of incubation mixture to a 96-well plate containing 300 µl of acetonitrile/0.1% (v/v) formic acid and internal standard (500 nM D_3-*N*-desmethylloperamide). Plates were centrifuged at 2000 x g for 10 min, and 200 µl of supernatant were transferred to clean plates. The contents were dried under heated nitrogen (50°C), reconstituted in 200 µl of 95% water:5% acetonitrile:0.1% formic acid (v/v/v) (initial chromatographic conditions), and analyzed for *N*-desmethylloperamide by LC/MS/MS (see below).

Determination of loperamide kinetic parameters (K_m and V_{max}) in human and rat microsomes. Loperamide *N*-desmethylation was assessed under linear

conditions for microsomal protein concentration and time in HLMs (0.1 mg/mL; 10 min), HIMs (0.1 mg/mL; 20 min), RLMs (0.075 mg/mL; 10 min) and RIMs (0.075 mg/mL; 20 min) at 37°C and a total incubation volume of 200 µL. The substrate, loperamide, was incubated from 0.2-50 µM.

Reversible inhibition of loperamide metabolism by DHB in human and rat microsomes. Loperamide was incubated at its K_m as determined above for each enzyme source in the presence of DHB (ranging from 0-50 µM). Incubations were initiated with NADPH and terminated as described above. IC_{50} values were recovered using equation D.1. after evaluating alternative models. Goodness-of-fit was assessed by visual comparison of observed with predicted concentration-time profiles, residual analysis, Akaike's Information Criteria, and precision of parameter estimates (CV%).

$$v = \frac{v_0}{1 + \frac{[DHB]}{IC_{50}}} \qquad \text{Equation D.1}$$

v denotes the observed reaction velocity; v_o is the control velocity, in the absence of DHB; [DHB] denotes the concentration of DHB in units of µM; IC_{50} is the concentration of DHB required inhibit loperamide *N*-desmethylation by 50%.

Determination of mechanism-based inhibition parameters (K_I and k_{inact}) in human and rat microsomes. Time- and concentration-dependent inhibition of CYP3A4 activity by DHB in HLMs, HIMs, RLMs and RIMs was assessed as described in chapter 2. Briefly, primary incubation mixtures consisted of HLMs, HIMs (5 mg/mL) RLMs or RIMs (4 mg/mL), DHB (0, 2.5, 5, 10, 30 or 60 µM), and potassium phosphate buffer (0.1 M, pH 7.4). The mixtures were equilibrated at 37°C for 5 min before initiating reactions with NADPH (1 mM final concentration), yielding a final volume of 80 µl; the final

concentration of DMSO was ~1% (v/v). At designated times from 0-5 min, an aliquot (10 µl) was removed and diluted 20-fold into secondary incubation mixtures containing loperamide and NADPH (1 mM), yielding a final loperamide concentration of 60 µM. Secondary reactions were terminated after 20 min (HIMs, RIMs) or 10 min (HLMs, RLMs) as described above. *N*-desmethylloperamide formation was measured by HPLC-MS/MS. Parameters were recovered as described in chapter 2.

HPLC-MS/MS determination of *N*-desmethylloperamide and didesmethylloperamide in rCYP P450 and microsomes. *N*-Desmethylloperamide was quantified as described in chapter 2. Didesmethlloperamide was qualified simultaneous to *N*-desmethylloperamide with the MRM transitions of 449.1→238.0 and a CE of 33 mV.

Data analysis. *N*-Desmethllyopmide formation in recombinant enzyme systems is presented as the mean of duplicate incubations. Reversible inhibition assays were conducted in triplicate and kinetic parameter estimates are presented as the estimate ± S.E.'s. MBI kinetic data are presented as the mean of duplicate incubations and their kinetic parameters are presented as estimates ± S.E.'s.

RESULTS

The primary human metabolite of loperamide, *N*-desmethylloperamide, was formed by 5 of the 11 tested rat Cyp P450 enzymes, namely, Cyp2c13, Cyp2d1, Cyp2d2, Cyp2e1, Cyp3a1 (Figure D.1). The formation velocity by Cyp3a1 was the greatest yet comparable to that of Cyp2c11 and Cyp2d1. Cyp2d1 catalyzed *N*-desmethylloperamide formation approximately two fold faster than Cyp2d2. Didesmethylloperamide was below the limit of quantification in all incubations, but was detectable (above 0.1 nM) in those conducted in Cyp3a1.

Saturable loperamide concentrations were achieved in all tested microsomal systems (Figure D.2). The apparent K_m of loperamide *N*-desmethylation was approximately half that in human by both liver and intestinal microsomes compared to rat. V_{max} determined by RIMs was 18% greater than that by HIMs. V_{max} in RLMs was twofold greater than in HLMs. Didesmethylloperamide was below the limit of quantification in all incubations (1 nM).

DHB showed potent reversible inhibition (IC_{50}) in all tested microsomal systems. Mechanism-based inhibition of loperamide *N*-desmethlyation by DHB was measured in four microsomal systems (HLMs, HIMs, RLMs, RIMs). DHB showed MBI activity in HLMs, HIMs and RLMs with similar K_I's. The maximal inactivation rate (k_{inact}) measured in these enzyme sources varied. DHB was a most effective MBI in HIMs followed by HLMs then RLMs. DHB showed weak MBI in RIMs precluding accurate parameters estimate recovery.

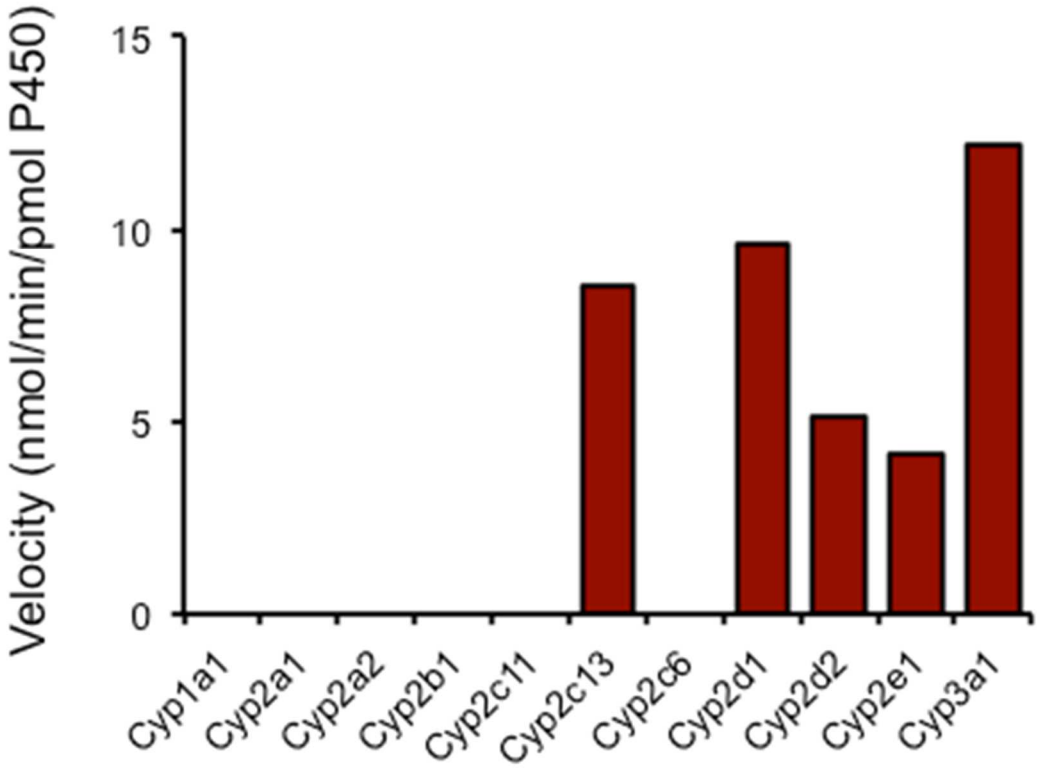

Figure D. 1. Rat P450 enzymes catalyzing the formation of *N*-desmethylloperamide from loperamide (1 μM). Reactions were initiated with NADPH (2 mM). Bars denote means of duplicate incubations. *N*-Desmethylloperamide was below the limit of quantification (0.9 nM) in incubations conducted in Cyp1a1, Cyp2a1, Cyp2a2, Cyp2b1, Cyp2c11 and Cyp2c6.

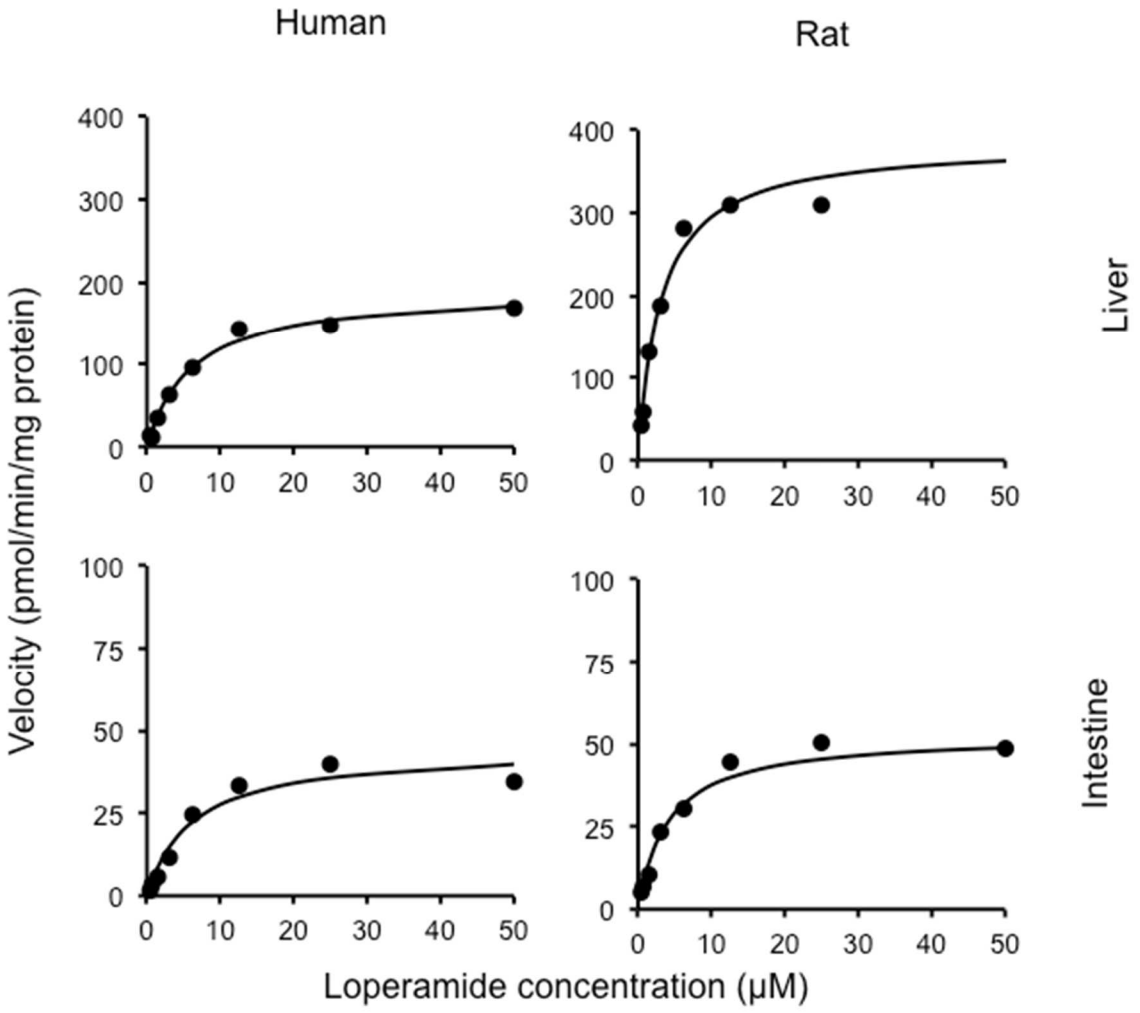

Figure D.2. *N*-Desmethylloperamide formation at increasing loperamide concentrations in HLMs (top left), RLMs (top right), HIMs (bottom left) and RIMs (bottom right). Observed data (circles) are presented as the mean of triplicate incubations. Covariate of variation was <10% for all points. Lines denote the model fit. The velocity of formation with 50 μM loperamide by RLMs exceeded the upper limit of quantification.

Table D.1. In vitro kinetic parameters for loperamide (K_m and V_{max}) and DHB (IC_{50}, k_{inact} and K_I) in human and rat microsomes. Table 1.1

Parameter	HLMs	RLMs	HIMs	RIMs
V_{max} (pmol/min/mg protein)	191.4 ± 11.7	384.9 ± 20.2	44.4 ± 2.7	52.8 ± 2.2
K_m (μM)	6.14 ± 1.2	3.1 ± 0.4	6.13 ± 1.1	4.1 ± 0.6
IC_{50} (μM)	N.D.	2.2 ± 0.2	2.1 ± 0.2	3.2 ± 0.3
k_{inact} (min^{-1})	0.24 ± 0.02	0.19 ± 0.02	0.38 ± 0.02	N.R.
K_I (μM)	3.4 ± 1.0	5.0 ± 2.7	5.1 ± 0.9	N.R.

DHB, 6',7'-Dihydroxybergamottin; HLMs, human liver microsomes; HIMs, human intestinal microsomes; RLMs, rat liver microsomes; RIMs, rat intestinal microsomes; V_{max}, maximal *N*-desmethylloperamide formation rate; K_m, loperamide concentration required to reach half V_{max}; IC_{50}, the DHB concentration required to inhibited *N*-desmethylloperamide formation by 50% with loperamide incubated at its K_m; k_{inact}, the maximal enzyme inactivation rate; K_I, the DHB concentration required to reach half k_{inact}; N.D., experimental value was not determined or conducted; N.R., parameter estimate could not be recovered.

APPENDIX E: INHIBITORY POTENCY OF SUPPLEMENTS LABELED TO CONTAIN DHB AND/OR BG TOWARD CYP3A ACTIVITY.[4]

METHODS

Materials and chemicals. 6′,7′-Dihydroxybegamottin was purchased from Cayman Chemical (Ann Arbor, MI; purity ≥ 98.0%); bergamottin was purchased from Sigma-Aldrich (purity ≥ 98.0). Midazolam (purity ≥ 99.9%), 1'-hydroxymidazolam (purity ≥ 98.0%), ketoconazole (purity ≥ 98.0%), alprazolam (purity ≥ 99.0%), and NADPH were purchased from Sigma-Aldrich. Simply Grapefruit brand GFJ was purchased from SimplyOrange Juice Co. (Apopka FL; lot AMC3 E 01:13). Methanol (MeOH) was purchased from Fischer Scientific (Waltham, MA). UPLC-grade water and acetonitrile were purchased from Fisher Scientific. Pooled HIMs (n = 18 donors) were purchased from Xenotech (Lenexa, KS). Six supplements labeled to contain DHB and/or bergamottin were purchased from the following sources: SciFit DHB 300 (SciFit, Oakmont, PA; lot 57454), Trisorbagen (Anabolic Xtreme, Tempe AZ; lot 202609), Xceler8 DHB (VitaSport, Chino Hills, CA; lot US 37700), AttentionLink (Hi-Tech Pharmaceuticals, Inc., Norcross, GA; lot 08132039), Finaflex 1-Alpha (Redefine Nutrition, Alpharetta, GA; lot 824912013), and Finaflex 1-Andro (Redefine Nutrition, Alpharetta, GA; lot 0500313).

[4] This appendix previously appeared as an article in the Journal of Pharmaceutical and Biomedical Analysis and is printed with permission from Elsevier. The original citation is as follows: VanderMolen KW, Ainslie GR, Paine MF and Oberlies NH. Labeled content of two furanocoumarins in dietary supplements correlates with neither actual content nor CYP3A inhibitory activity. *J Pharm Biomed Anal*. 2014 Sep;98:260-5.

Extraction of supplements labeled to contain DHB. See previously described methods (Vandermolen et al., 2013).

CYP3A inhibition assay. A dilution scheme was devised using the product with the highest measured amount of DHB (SciFit DHB 300). The corresponding extract was reconstituted with methanol (130 µL), which was diluted 1:10 in methanol. Each of these methanolic solutions was dilu

ted further into incubation mixtures (see below) to yield final DHB concentrations of 1 and 0.1 µM; the higher concentration approximates the K_i of DHB towards CYP3A using HIMs as an enzyme source and midazolam as the probe substrate. (Paine et al., 2004) All other supplements were reconstituted and diluted in the same manner as SciFit DHB 300. A grapefruit juice extract was reconstituted with methanol (50 µL), an aliquot was further diluted 1:10 in methanol. These methanolic solutions were diluted further into incubation mixtures to yield final DHB concentrations of 1 and 0.1 µM.

Incubation mixtures, prepared in 96-well plates, consisted of midazolam (4 µM), HIMs (0.05 mg/mL protein), inhibitor (diluted extract, DHB, bergamottin, ketoconazole) or vehicle control, and potassium phosphate buffer (100 mM, pH 7.4). The final concentrations of DHB, bergamottin, and ketoconazole were 1 and 0.1 µM; the final concentration of methanol (v/v) was 1.0%. After equilibrating the mixtures for 5 min at 37°C, reactions were initiated with NADPH (1 mM final concentration), yielding a final volume of 200 µL. Reactions were terminated after 4 min by removing a 100-µL aliquot and adding to 300 µL of ice-cold CH_3CN containing internal standard (300 µg/mL alprazolam). Samples were vortexed (~30 s) and centrifuged (3000 *g* × 10 min at 4 °C), after which 100 µL of supernatant were removed and analyzed for 1′-hydroxymidazolam

by LC-MS-MS on an API 6500 QTrap operated in MRM mode and equipped with an electrospray ionization source. Calibration standards were matrix-matched and were linear from 3.9 to 2000 nM. The QTrap was coupled to a Shimadzu Nextera UHPLC system (Kyoto, Japan). Chromatographic separation of midazolam, 1′-hydroxymidazolam, and alprazolam was achieved with a Thermo Scientific Aquasil C_{18} (2.1 × 50 mm, 3 μm) HPLC column (Waltham, MA) using a gradient method following a 7-μL injection of each supernatant. The gradient system consisted of A, 0.1% formic acid in water and B, 0.1% formic acid in acetonitrile, at a flow rate of 0.75 mL/min: 0-0.4 min, 5% B; 0.4-1.5 min, 5-95% B; 1.5-2.1 min, 95% B; 2.1-2.11, 95-5% B; 2.11-3.0, 5% B. Sample and column temperatures were 4°C and 40°C, respectively. Quality controls (QCs) of 10, 100, and 1500 nM were used to assess accuracy. All standards and QCs were accurate to within 20% of the nominal value; QC precision was <15% relative error.

RESULTS

The mean ± SD vehicle control reaction velocities of 1-hydroxymidazolam formation was 416 ± 29 pmol/min/mg protein. The CYP3A inhibitor, ketoconazole, abolished 1'-hydroxymidazolam formation at 1 μM and inhibited activity by ~75% at 0.1 μM (Figure D.1). Bergamottin showed no inhibition at the concentrations tested. DHB at 0.1 and 1 μM inhibited activity by 5 and 42%, respectively. Except for bergamottin, concentration dependency was observed for each treatment ($p<0.05$; 2-way ANOVA with Bonferroni adjustment). The CYP3A inhibitory activity of SciFit was similar to that of the grapefruit juice extract, which, like SciFit, was diluted such that the final concentrations of DHB were 0.1 and 1 μM. If the grapefruit juice extract were normalized to SciFit based on the initial volume of methanol added to the extract (50 μL and 130 μL for grapefruit juice and SciFit, respectively), SciFit would be approximately 2.5x more potent than a glass of grapefruit juice. In addition to SciFit, two supplements (Trisorbagen and AttentionLink) demonstrated potent inhibition of CYP3A activity despite very low measured amounts of DHB and bergamottin. Finaflex 1-Alpha appeared to stimulate CYP3A activity at the lower concentration, which has been observed with low concentrations of bergamottin (< 2.5 μM) in incubations with HIMS and midazolam. (Paine et al., 2005)

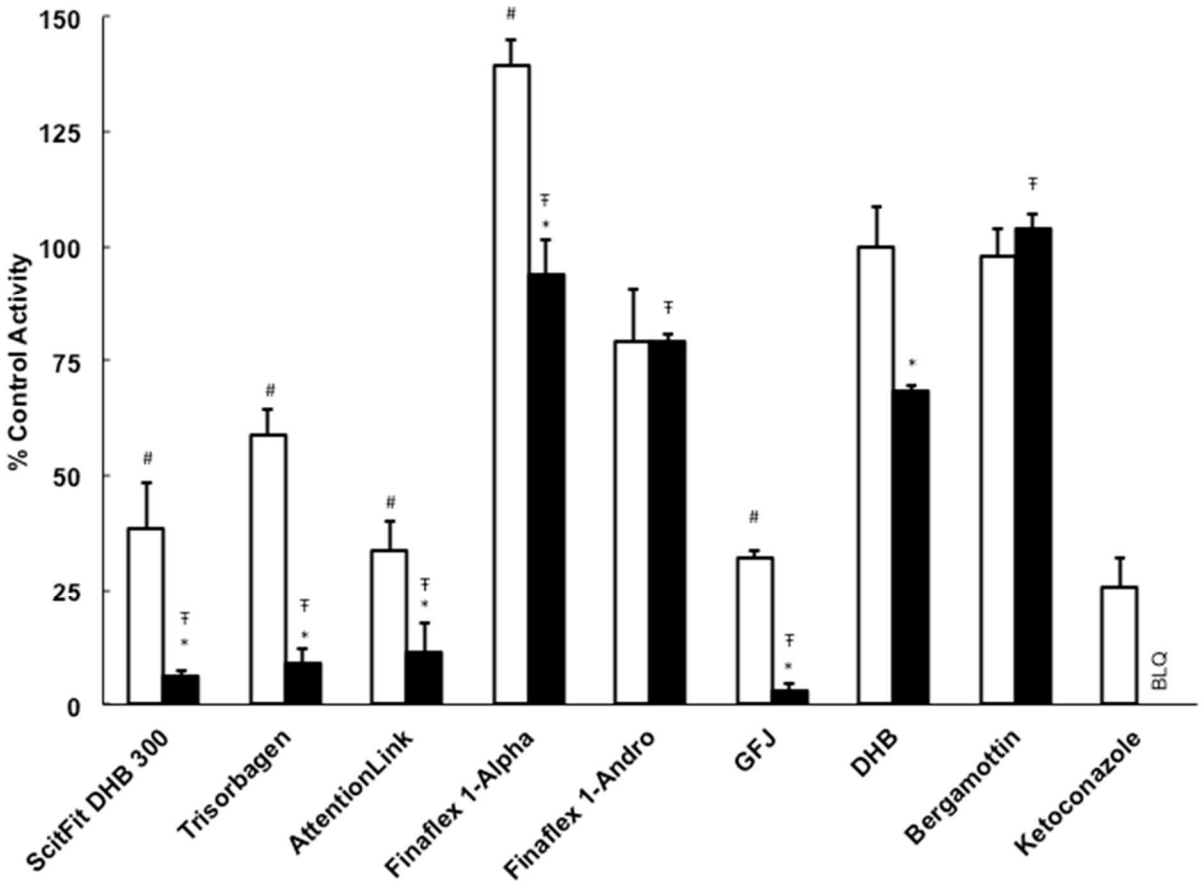

Figure E.1. Comparison of the effects of supplements labeled to contain 6',7'-dihydroxybergamottin (DHB) with known CYP3A inhibitors on CYP3A activity in human intestinal microsomes. Pure DHB and bergamottin, as well as the known CYP3A inhibitor ketoconazole, were tested at 0.1 μM (open bars) or 1 μM (solid bars). The methanolic extract of SciFit was tested such that the final concentration of DHB was 0.1 or 1 μM. All other supplement extracts were tested at the same dilutions as SciFit (10x and 1x; open bars and closed bars, respectively). The grapefruit juice extract (GFJ) was tested such that the final concentration of DHB was 0.1 or 1 μM. The concentrations of DHB in the incubations containing SciFit, GFJ, and purified DHB were the same (0.1 and 1 μM; open and filled blue bars, respectively). Bars and error bars denote the means and SDs, respectively, of triplicate incubations. Inhibition by ketoconazole at 1 μM was below the limit of quantification. $^{*}p < 0.05$ versus the 10x dilution; $^{\#}p < 0.05$ versus pure DHB at 0.1 μM; $^{\mp}p < 0.05$ versus pure DHB at 1 μM. Statistical comparisons were made via two-way ANOVA with a Bonferroni adjustment.

APPENDIX F: A PHYSIOLOGICALLY-BASED PHARMACOKINETIC MODEL OF LOPERAMIDE.

METHODS

Physiologically-based pharmacokinetic model development. A model structure was devised to incorporate intestinal and hepatic metabolism of loperamide (Figure F.1). Partition coefficients (kp's) were calculated using GasroPlus (v8.0; Simulation Plus Inc., Lancaster, CA). Physiological parameters for blood flow (Q) and tissue weights were obtained from the International Commission on Radiological Protection. Loperamide k_a was recovered from the clinical data (Ainslie et al., 2014). Metabolism kinetic parameters for loperamide (K_m and V_{max}) and *N*-desmethylloperamide (CL_{int}) were obtained in appendix C. PBPK models for loperamide and *N*-desmethylloperamide using Berkley Madonna (v8.3.18; University of California at Berkeley, Berkeley, CA) using the code provided below.

Data analysis. Model-predicted pharmacokinetic outcomes were compared to the clinical study described in chapter 2. Non-compartmental methods were used as described in appendix B.

RESULTS

The model predicted loperamide $AUC_{0\text{-}72\ h}$ (94 nM*h) and C_{max} (4.5 nM) was within 15 and 30 % of the observed geometric mean [90% CI] values (110 [90-130] and 6.5 [5.3-8.1], respectively.

The model under predicted *N*-desmethylloperamide $AUC_{0\text{-}72}$ (225 nM*h) and C_{max} (4.8 nM) by 20 and 40 %, respectively, compared to observed geometric mean {90% CI] $AUC_{0\text{-}72\ h}$ (280 [260-300] nM*h) and C_{max} (7.9 [6.7-9.2] nM).

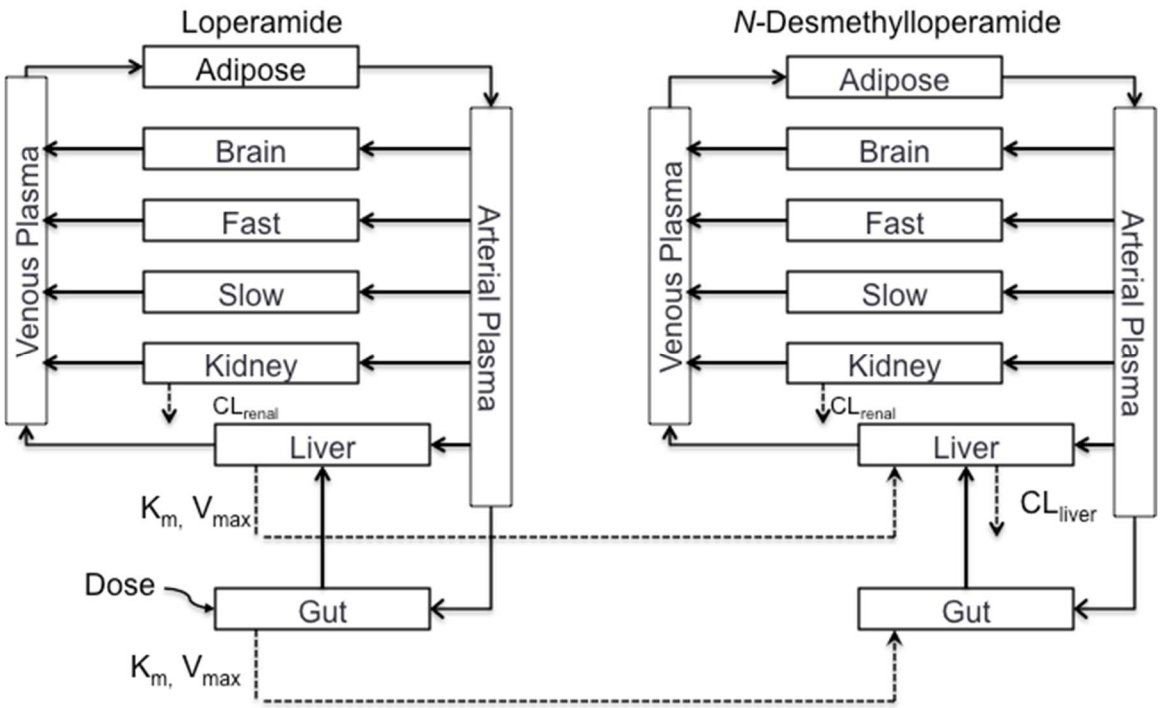

Figure F.1. Loperamide PBPK model structure.

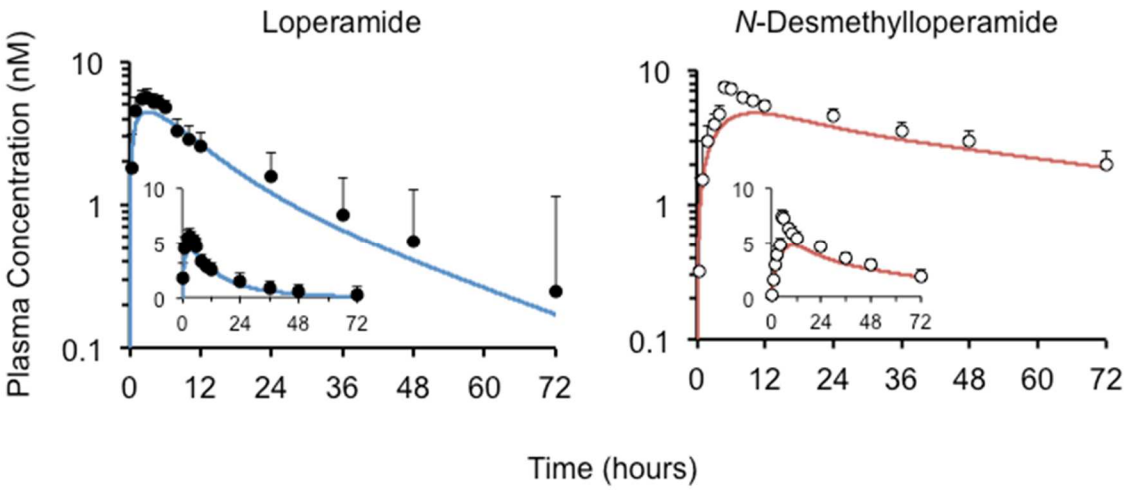

Figure F.2. Model simulated plasma concentration-time profiles of loperamide (left, blue line) and *N*-desmethylloperamide (right, red line) on log-axis and with linear axis (inset). Observed clinical data for loperamide (closed circles) and *N*-desmethylloperamide (open circles). Observed values are presented as geometric mean and the upped 90% confidence interval.

Berkeley Madonna code for Loperamide:

```
; Berkeley Madonna script
; *** Loperamide ***
;
; Garrett Ainslie (University of North Carolinia)
; Compiled on: 2012-10-05
;
; =========
;
CV = ( (CVfa * Qfa) + (CVbr * Qbr) + (CVgu * Qgu) + (CVki * Qki) + (CVrpd * Qrpd) +
(CVspd * Qspd) + (CVli * Qli)) / QC    ; venous concentration (nmol/L)
CA = (QC * CV) / (QC + (1))    ; arterial concentration (nmol/L)
dCV = ( (dCVfa * Qfa) + (dCVbr * Qbr) + (dCVgu * Qgu) + (dCVki * Qki) + (dCVrpd *
Qrpd) + (dCVspd * Qspd) + (dCVli * Qli)) / QC    ; venous concentration (nmol/L)
dCA = (QC * dCV) / (QC + (1))    ; arterial concentration (nmol/L)

;CONCENTRATIONS
Cfa = Afa / Vfa    ; cellular concentration (nmol/L)
Cbr = Abr / Vbr    ; cellular concentration (nmol/L)
Cgu = Agu / Vgu    ; cellular concentration (nmol/L)
Cki = Aki / Vki    ; cellular concentration (nmol/L)
Cspd = Aspd / Vspd    ; cellular concentration (nmol/L)
Cli = Ali / Vli    ; cellular concentration (nmol/L)
CVfa = Cfa / Pfab    ; venous organ concentration (nmol/L)
CVbr = Cbr / Pbrb    ; venous organ concentration (nmol/L)
CVgu = Cgu / Pgub    ; venous organ concentration (nmol/L)
CVki = Cki / Pkib    ; venous organ concentration (nmol/L)
CVspd = Cspd / Pspdb    ; venous organ concentration (nmol/L)
CVli = Cli / Plib    ; venous organ concentration (nmol/L)
Crpd = Arpd / Vrpd    ; cellular concentration (nmol/L)
CVrpd = Crpd / Prpdb    ; venous organ concentration (nmol/L)
CX = CA / 1    ; exhaled concentration (nmol/L)

dCfa = dAfa / Vfa    ; cellular concentration (nmol/L)
dCbr = dAbr / Vbr    ; cellular concentration (nmol/L)
dCgu = dAgu / Vgu    ; cellular concentration (nmol/L)
dCki = dAki / Vki    ; cellular concentration (nmol/L)
dCspd = dAspd / Vspd    ; cellular concentration (nmol/L)
dCli = dAli / Vli    ; cellular concentration (nmol/L)
dCVfa =dCfa / dPfab    ; venous organ concentration (nmol/L)
dCVbr = dCbr / dPbrb    ; venous organ concentration (nmol/L)
dCVgu = dCgu / dPgub    ; venous organ concentration (nmol/L)
dCVki = dCki / dPkib    ; venous organ concentration (nmol/L)
dCVspd = dCspd / dPspdb    ; venous organ concentration (nmol/L)
dCVli = dCli / dPlib    ; venous organ concentration (nmol/L)
```

```
dCrpd = dArpd / Vrpd    ; cellular concentration (nmol/L)
dCVrpd = dCrpd / dPrpdb    ; venous organ concentration (nmol/L)
dCX = dCA / 1    ; exhaled concentration (nmol/L)
; Parameters
; ==========
;
;FLOWS
QC = QCC * BWc    ; cardiac output (L/h)
QbrC = 0.12    ; fractional blood flow
QCC = 11.22    ; cardiac allometric constant (L/h/kg^CAE)
QfaC = 0.05    ; fractional blood flow
QkiC = 0.171922    ; fractional blood flow
QliC = 0.25    ; fractional blood flow
QPC = 15    ; respiratory allometric constant (L/h/kg^RAE)
QguC = 0.141127
QspdAC = 0.27    ; overall fractional blood flow
QspdC = QspdAC - QfaC    ; fractional blood flow

Qfa = QfaC * QC    ; scaled fractional blood flow
Qbr = QbrC * QC    ; scaled fractional blood flow
Qgu = QguC * QC    ; scaled fractional blood flow
Qki = QkiC * QC    ; scaled fractional blood flow
QrpdAC = 1 - QspdAC    ; overall fractional blood flow
QrpdC = QrpdAC - (QbrC + QguC + QkiC + QliC)    ; fractional blood flow
Qrpd = QrpdC * QC    ; scaled fractional blood flow
Qli = QliC * QC    ; scaled fractional blood flow
Qspd = QspdC * QC    ; scaled fractional blood flow

;VOLUMES
BW = 70    ; body mass (kg)
VT = 0.857    ; proportion of vascularised tissue
VfaC = 0.214    ; fractional volume
VbrC = 0.02    ; fractional volume
VspdAC = 0.43    ; overall fractional volume
VliC = 0.0257    ; fractional volume
VguC = 0.02    ; fractional volume, estimated
Vgu = VguC * BW    ; scaled fractional volume
VkiC = 0.03405    ; fractional volume
VspdC = VspdAC - VfaC    ; fractional volume
Vki = VkiC * BW    ; scaled fractional volume
Vspd = VspdC * BW    ; scaled fractional volume
Vfa = VfaC * BW    ; scaled fractional volume
Vbr = VbrC * BW ; scaled fractional volume
Vli = VliC * BW    ; scaled fractional volume
VrpdAC = VT - VspdAC    ; overall fractional volume
VrpdC = VrpdAC - (VbrC + VguC + VkiC + VliC)    ; fractional volume
```

```
Vrpd = VrpdC * BW    ; scaled fractional volume

;PARTITIONING

;===LOP====
Pfab = 2.46    ; tissue:blood partition coefficient
Pbrb = 1.93    ; tissue:blood partition coefficient
Pkib = 2.99    ; tissue:blood partition coefficient
Prpdb = 1    ; tissue:blood partition coefficient
Pspdb = 0.8    ; tissue:blood partition coefficient
Plib = 3.2    ; tissue:blood partition coefficient
Pgub = 1    ; tissue:blood partition coefficient

;====dLOP====

dPfab = 16.88    ; tissue:blood partition coefficient
dPbrb = 9.19    ; tissue:blood partition coefficient
dPkib = 3.46    ; tissue:blood partition coefficient
dPrpdb = 1    ; tissue:blood partition coefficient
dPspdb = 3.53    ; tissue:blood partition coefficient
dPlib = 5.74    ; tissue:blood partition coefficient
dPgub = 1    ; tissue:blood partition coefficient

;DOSING
Ka = .437012    ; oral uptake rate (/h)
PDOSE = 16    ; oral dose (mg)

MW = 447 ;LOP molecular weight
PPDOSE = PDOSE * 1000 *1000/ MW    ; scaled oral dose (nmol)

;METABOLISM
VmaxCivMME01li = 3718    ; maximum rate of metabolism (molar; in vitro; microsomal)
(mol/h/kg)
KmME01li = Kmli   ; Michaelis constant (nmol/L)
Kmli = 16.9 * 1000 ;Michaelis constant (umol / L converted to nmol / L)

VmaxCivMME01gu = 1423    ; maximum rate of metabolism (molar; in vitro;
microsomal) (mol/h/kg)
KmME01gu = Kmgu
Kmgu = 12.42 *1000 ; Michaelis constant (umol/L converted to nmol/L)
VmaxME01li = VmaxCivMME01li * BWc     ; maximum rate of metabolism (entire
organism) (umol/h)
VmaxME01gu = VmaxCivMME01gu * BWc    ; maximum rate of metabolism (entire
organism) (umol/h)

;ALLOMETRY
```

```
CAE = 0.75    ; cardiac allometric exponent
DS = 0.33    ; proportion of dead space (not involved in gas exchange)
RAE = 0.75    ; respiratory allometric exponent
P = 1 - DS    ; proportion of inhaled gas involved in gas exchange
BWc = BW ^ CAE    ; cardiac scaling output factor (kg)

; Run settings
; ============
;
METHOD STIFF
DTMIN = 1e-11
DTMAX = 0.010
DTOUT = 0
TOLERANCE = 1e-11
STARTTIME = 0
STOPTIME =72

; Dynamics
; ========
;

MRS = PPDOSE * exp((-Ka * TIME))    ; amount remaining in stomach (kg)
TIS = Ka * MRS    ; total input from stomach (kg)

;MRgu = (VmaxME01gu * CVgu) / (KmME01gu + CVgu)    ; rate of change of
metabolism (mg/h/kg)
MRgu = (VmaxME01gu * Cgu) / (KmME01gu + Cgu)    ; rate of change of metabolism
(mg/h/kg)

FA = 0.02
d/dt (uptake) =  (TIS )    ; uptake derivative (kg)
INIT uptake = 0

d/dt (AMgu) =  MRgu    ; amount metabolised derivative (kg)
INIT AMgu = 0

MRli = (VmaxME01li * CVli) / (KmME01li + CVli)    ; rate of change of metabolism
(nmol/h/kg)
;MRli = (VmaxME01li * Cli) / (KmME01li + Cli)    ; rate of change of metabolism
(nmol/h/kg)

;====LOP====
d/dt (AMli) = MRli    ; amount metabolised derivative (kg)
INIT AMli = 0

d/dt (Ali) = (Qli * (CA - CVli) ) - MRli
```

```
INIT Ali = 0

d/dt (Afa) = Qfa * (CA - CVfa)
INIT Afa = 0

d/dt (Abr) = Qbr * (CA - CVbr)
INIT Abr = 0

d/dt (Agu) = (Qgu * (CA - CVgu) + TIS*FA) - MRgu
INIT Agu = 0

d/dt (Aki) = Qki * (CA - CVki)
INIT Aki = 0

d/dt (Arpd) = Qrpd * (CA - CVrpd)
INIT Arpd = 0

d/dt (Aspd) = Qspd * (CA - CVspd)
INIT Aspd = 0

;===dLOP====
Fm=0.9

d/dt (dAMli) = MRli*Fm     ; amount metabolised derivative (kg)
INIT dAMli = 0

d/dt (dAli) = (Qli * (dCA - dCVli) ) + MRli - dMRli
INIT dAli = 0

dMRli = (dVmaxME01li * dCVli) / (dKmME01li + dCVli)    ; rate of change of metabolism
(nmol/h/kg)
dVmaxME01li = 10000
dKmME01li = 8000

d/dt (dAfa) = Qfa * (dCA - dCVfa)
INIT dAfa = 0

d/dt (dAbr) = Qbr * (dCA - dCVbr)
INIT dAbr = 0

d/dt (dAgu) = (Qgu * (dCA - dCVgu) )+ MRgu
INIT dAgu = 0

d/dt (dAki) = Qki * (dCA - dCVki)
INIT dAki = 0
```

```
d/dt (dArpd) = Qrpd * (dCA - dCVrpd)
INIT dArpd = 0

d/dt (dAspd) = Qspd * (dCA - dCVspd)
INIT dAspd = 0


DISPLAY KA, VmaxCivMME01gu, VmaxCivMME01li, Kmli, Kmgu,
dVmaxME01li,dKmME01li, dPfab,Pfab, Pgub, Fa

DISPLAY CV, dCV
```

APPENDIX G: PHYSIOLOGICALLY-BASED PHARMACOKINETIC DHB-LOPERAMIDE INTERACTION MODEL SIMULATIONS.

METHODS

Model simulations. Simulations were conducted using the PBPK models described for loperamide and DHB in chapter 3 using Simcyp®. Loperamide (16 mg) was simulated and the absence and presence of DHB (50 & 300 mg) to represent the labeled DHB content in certain dietary substances. Virtual trials were conducted in 100 virtual healthy subjects.

RESULTS

Pharmacokinetic outcomes of loperamide and DHB. The PBPK interaction model predicted an increase in loperamide exposure by DHB in a dose-dependent manner. A 50 mg dose of DHB was predicted to increase loperamide C_{max} and $AUC_{0\text{-}72\ h}$ by 260% and 140 %, respectively, with no change to $t_{1/2}$. A 300 mg dose of DHB was predicted to increase loperamide C_{max} and $AUC_{0\text{-}72\ h}$ by 320 and 190 %, respectively (Table G.1). The increase in loperamide plasma exposure was accompanied by an increase in $t_{1/2}$, indicating DHB-mediated inhibition of hepatic CYP3A4. To further interrogate the model, the simulated loperamide fraction metabolized by individual CYP isoforms was examined. At this dose of DHB (300 mg) the fraction metabolized (f_m) by CYP3A4 was decreased by three fold, prompting compensation (increased f_m) by CYP2C8 and CYP2D6 in the liver (Figure G.1). The fraction excreted in the urine remained constant.

DHB $AUC_{0\text{-}72\ h}$ and C_{max} was not dose linear from 50 -300 mg. The terminal half-life of the 300 mg dose was 20-fold greater than at 50 mg, reflective of the model only accounting of CYP3A4-mediated metabolism and of extensive suicide inhibition by DHB.

.

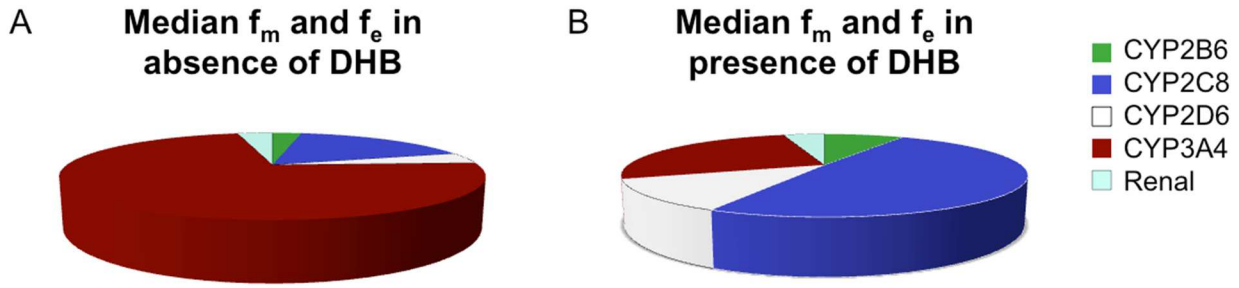

Figure G.1. Simulated loperamide hepatic fraction metabolized (f_m) by hepatic CYP2B6 (green), CYP2C8 (blue), CYP2D6 (white) and CYP3A4 (red) and the fraction excreted (f_e, cyan) in urine of loperamide (16 mg) in the absence (A) and presence (B) of a 300-mg dose of DHB. Results represent a trial conducted in 100 virtual healthy subjects.

Table G.1. Pharmacokinetic outcomes following oral loperamide and DHB

	DHB dose (mg)		
	0	50	300
Loperamide			
C_{max} (nM)	9.6 [8.9-10.4]	35.1 [33.3-36.9]	40 [38-42]
$AUC_{0\text{-}72\ h}$ (nM*h)	164 [152-178]	388 [363-415]	473 [440-507]
$t_{1/2}$ (h)	40 [36-43]	41 [37-44]	42 [39-46]
C_{max} ratio	-	3.6 [3.4-3.9]	4.2 [3.9-4.4]
$AUC_{0\text{-}72\ h}$ ratio	-	2.4 [2.3-2.5]	2.9 [2.7-3.1]
DHB			
C_{max} (µM)	-	0.14 [0.11-0.19]	6.4 [5.0-8.1]
$AUC_{0\text{-}72\ h}$ (µM*h)	-	0.61 [0.40-0.94]	15.6 [10.7-22.1]
$t_{1/2}$ (h)	-	6.6 [5.3-8.3]	122 [88-171]

DHB, 6',7'-Dihdyroxybergamottin; C_{max}, maximal plasma concentration; $AUC_{0\text{-}72}$, area under the model predicted plasma-concentration curve from time 0 h to 72 h; C_{max} ratio, the ratio of loperamide C_{max} in the presence to that in the absence of DHB; $AUC_{0\text{-}72\ h}$ ratio, the ratio of loperamide $AUC_{0\text{-}72}$ in the presence to that in the absence of DHB; $t_{1/2}$, terminal half-life. All data are presented as the geometric mean [90% confidence intervals].

APPENDIX H: PHYSIOLOGICALLY-BASED PHARMACOKINETIC/PHARMACODYNAMIC MODEL SIMULATIONS OF ALFENTANIL IN HEALTHY SUBJECTS.

METHODS

Model simulations. Simulations were conducted using an alfentanil PBPK/PD model constructed in Simcyp® and reported in detail in chapter 3, with the modification that E_{max} was set to 100%. Alfentanil induced miosis and plasma concentration time profiles were simulated in 6 virtual healthy volunteers aged 21-32 years following a 4 mg dose of alfentanil in the absence and presence of 6.2 mg DHB (as a marker constituent of whole GFJ).

Data analysis. Non compartmental analysis was reported from Simcyp®. Pharmacokinetic and pharmacodynamic outcomes were reported as either mean, median or as geometric mean values with 95% confidence intervals.

RESULTS AND DISCUSSION

Alfentanil plasma concentrations and pupil miosis were simulated for 6 hours following a 4 mg oral dose and certain pharmacokinetic outcomes were determined (Table H.1) in the presence and absence of DHB. The model predicted less than a 10% increase in alfentanil plasma AUC and C_{max}. This under prediction is likely due to the alfentanil model being constructed using a first order absorption rate instead of the ADAM model. Accordingly, the predicted increase in AUEC was less than 5% in the presence of GFJ/DHB. The model-predicted maximal response (R_{max}) was over predictive of the observed value presented in chapter 4 by ~20%. Model-predicted time to reach R_{max} was approximately equal to the observed values. These results reveal that (1) timelier development of this model may have aided in the clinical study design (chapter 4), and (2) model refinement would be required to accurately apply this alfentanil model to a GFJ/DHB-mediated interaction.

Table H.1. Model-predicted pharmacokinetic and pharmacodynamic outcomes following oral alfentanil administration in healthy volunteers.

Pharmacokinetic Outcomes	Mean	Median	Geometric mean	95% Confidence Interval	
H_2O					
C_{max} (ng/mL)	60.5	60.8	56.2	50.7	62.2
T_{max} (h)	0.49	0.45	0.45	0.41	0.51
$AUC_{0\text{-}6\ h}$ (ng/mL.h)	166	137	135	114	160
GFJ					
C_{max} (ng/mL)	63.5	63.9	58.9	53.2	65.3
T_{max} (h)	0.54	0.5	0.49	0.44	0.55
$AUC_{0\text{-}6\ h}$ (ng/mL.h)	182	148	147	124	174
Ratios					
C_{max} ratio	1.05	1.04	1.05	1.04	1.06
$AUC_{0\text{-}6\ h}$ ratio	1.09	1.08	1.09	1.08	1.10
Pharmacodynamic Outcomes					
H_2O					
R_{max} (%)	65.0	67.1	62.3	57.5	67.5
$t(R_{max})$ (h)	0.67	0.63	0.64	0.6	0.69
$AUEC_{0\text{-}6\ h}$ (%*h)	191	160	153	128	184
DHB					
R_{max} (%)	66.8	68.7	64.4	59.7	69.4
$t(R_{max})$ (h)	0.71	0.65	0.68	0.63	0.73
$AUEC_{0\text{-}6\ h}$ (%*h)	206	172	166	139	199

H_2O, pretreatment with 240 mL water; DHB, pretreatment with 6.2 mg 6',7'-dihydroxybergamottin; C_{max}, maximal observed concentration, T_{max}, time to reach C_{max}; $AUC_{0\text{-}6}$, the area under the plasma concentration-time curve from 0-6 hours; C_{max} ratio, the ratio of C_{max} in the presence to that in the absence of DHB; $AUC_{0\text{-}6\ h}$ ratio, the ratio of $AUC_{0\text{-}6\ h}$ in the presence to that in the absence of DHB; R_{max}, the maximal simulated pupillary response;

REFERENCES

Ainslie GR, Wolf KK, Li Y, Connolly EA, Scarlett YV, Hull JH and Paine MF (2014) Assessment of a Candidate Marker Constituent Predictive of a Dietary Substance-Drug Interaction: Case Study with Grapefruit Juice and CYP3A4 Drug Substrates. *J Pharmacol Exp Ther*.

Di L, Keefer C, Scott DO, Strelevitz TJ, Chang G, Bi YA, Lai Y, Duckworth J, Fenner K, Troutman MD and Obach RS (2012) Mechanistic insights from comparing intrinsic clearance values between human liver microsomes and hepatocytes to guide drug design. *European journal of medicinal chemistry* **57**:441-448.

Goosen TC, Cillie D, Bailey DG, Yu C, He K, Hollenberg PF, Woster PM, Cohen L, Williams JA, Rheeders M and Dijkstra HP (2004) Bergamottin contribution to the grapefruit juice-felodipine interaction and disposition in humans. *Clin Pharmacol Ther* **76**:607-617.

Paine MF, Criss AB and Watkins PB (2004) Two major grapefruit juice components differ in intestinal CYP3A4 inhibition kinetic and binding properties. *Drug Metab Dispos* **32**:1146-1153.

Paine MF, Criss AB and Watkins PB (2005) Two major grapefruit juice components differ in time to onset of intestinal CYP3A4 inhibition. *J Pharmacol Exp Ther* **312**:1151-1160.

Paine MF, Hart HL, Ludington SS, Haining RL, Rettie AE and Zeldin DC (2006) The human intestinal cytochrome P450 "pie". *Drug Metab Dispos* **34**:880-886.

Regueiro J, Vallverdu-Queralt A, Negreira N, Simal-Gandara J and Lamuela-Raventos RM (2014) Identification and quantification of grapefruit juice furanocoumarin metabolites in urine: an approach based on ultraperformance liquid chromatography coupled to linear ion trap-Orbitrap mass spectrometry and solid-phase extraction coupled to ultraperformance liquid chromatography coupled to triple quadrupole-tandem mass spectrometry. *Journal of agricultural and food chemistry* **62**:2134-2140.

US Food and Drug Administration (2013) Draft Guidance: Bioanalytical Method Validation. US Food and Drug Administration, Rockville, MD.

Vandermolen KM, Cech NB, Paine MF and Oberlies NH (2013) Rapid Quantitation of Furanocoumarins and Flavonoids in Grapefruit Juice using Ultra-Performance Liquid Chromatography. *Phytochem Anal* **24**:654-660.

VanderMolen KM, Ainslie GR, Paine MF and Oberlies NH (2014) Labeled content of two furanocoumarins in dietary supplements correlates with neither actual content nor CYP3A inhibitory activity. *J Pharm Biomed Anal* **98**:260-265.